



Steam Explosion Simulation Code JASMINE v.3 User's Guide

Kiyofumi MORIYAMA, Yu MARUYAMA
and Hideo NAKAMURA

Thermohydraulic Safety Research Group
Nuclear Safety Research Center

July 2008

本レポートは独立行政法人日本原子力研究開発機構が不定期に発行する成果報告書です。
本レポートの入手並びに著作権利用に関するお問い合わせは、下記あてにお問い合わせ下さい。
なお、本レポートの全文は日本原子力研究開発機構ホームページ (<http://www.jaea.go.jp>)
より発信されています。

独立行政法人日本原子力研究開発機構 研究技術情報部 研究技術情報課
〒319-1195 茨城県那珂郡東海村白方白根 2 番地 4
電話 029-282-6387, Fax 029-282-5920, E-mail: ird-support@jaea.go.jp

This report is issued irregularly by Japan Atomic Energy Agency
Inquiries about availability and/or copyright of this report should be addressed to
Intellectual Resources Section, Intellectual Resources Department,
Japan Atomic Energy Agency
2-4 Shirakata Shirane, Tokai-mura, Naka-gun, Ibaraki-ken 319-1195 Japan
Tel +81-29-282-6387, Fax +81-29-282-5920, E-mail: ird-support@jaea.go.jp

© Japan Atomic Energy Agency, 2008

Steam Explosion Simulation Code JASMINE v.3 User's Guide

Kiyofumi MORIYAMA, Yu MARUYAMA and Hideo NAKAMURA

Reactor Safety Research Unit
Nuclear Safety Research Center
Japan Atomic Energy Agency
Tokai-mura, Naka-gun, Ibaraki-ken

(Received April 28, 2008)

A steam explosion occurs when hot liquid contacts with cold volatile liquid. In this phenomenon, fine fragmentation of the hot liquid causes extremely rapid heat transfer from the hot liquid to the cold volatile liquid, and explosive vaporization, bringing shock waves and destructive forces. The steam explosion due to the contact of the molten core material and coolant water during severe accidents of light water reactors has been regarded as a potential threat to the integrity of the containment vessel. We developed a mechanistic steam explosion simulation code, JASMINE, that is applicable to plant scale assessment of the steam explosion loads. This document, as a manual for users of JASMINE code, describes the models, numerical solution methods, and also some verification and example calculations, as well as practical instructions for input preparation and usage of the code.

Keywords: Severe Accident, Molten Core, Steam Explosion, Fuel-Coolant Interaction, Premixing, Propagation, Numerical Simulation, Safety Assessment, JASMINE

水蒸気爆発解析コード JASMINE v.3 ユーザーズガイド

日本原子力研究開発機構 安全研究センター
原子炉施設安全評価研究ユニット
森山 清史・丸山 結・中村 秀夫

(2008 年 4 月 28 日 受理)

水蒸気爆発は、高温の液体が低温かつ揮発性の液体に接触するとき、高温液体の細粒化により急激な伝熱と蒸気発生が生じ、衝撃波や破壊力をもたらす現象である。軽水炉シビアアクシデント時の炉心融体と冷却水の接触による水蒸気爆発は、格納容器健全性への脅威となり得る現象として重要視されてきた。著者らは水蒸気爆発の機構論的シミュレーションコード JASMINE を開発した。JASMINE は実機規模の水蒸気爆発負荷の評価に適用可能なコードである。本報告書は、JASMINE コードのユーザーのためのマニュアルとして、モデル、数値解法、コードの検証のための計算、その他の計算例、及び、実地的なコード使用に必要な入力データ作成と計算の実行方法等について解説したものである。

Contents

1	Introduction	1
1.1	Background—Steam Explosion and Safety Assessment	1
1.2	JASMINE Code	2
1.3	Usage of This Manual	4
2	Model Description	5
2.1	Modeling Framework	5
2.2	Melt Model	6
2.2.1	Melt Jet	6
2.2.2	Melt Pool	8
2.2.3	Melt Particles	11
2.2.4	Extension of Melt Particle Model for Explosion Process	18
2.3	Two-Phase Flow Model	21
2.3.1	Basic Equations	21
2.3.2	Constitutive Models	22
3	Numerical Solution Method	28
3.1	Coupling of Melt and Two-Phase Flow Models	28
3.2	Numerical Solution Method for Melt Model	28
3.2.1	Melt Jet	28
3.2.2	Melt Pool	31
3.2.3	Melt Particle	33
3.3	Numerical Solution Method for Two-Phase Flow	34
3.3.1	Overall Scope	34
3.3.2	Finite Difference Form of Basic Equations	34
3.3.3	Boundary Condition Settings	39
3.3.4	Newtonian Iteration	40
3.3.5	Organization of the Pressure Equations	41
3.3.6	Elements of the Jacobian Matrix	42
4	Verification and Example Calculations	47
4.1	Check of the Numerical Behavior of the Models	47
4.1.1	Melt Jet and Pool	47
4.1.2	Melt Particles	51
4.1.3	Shock Wave Propagation in Two-Phase Medium	55
4.2	Simulation of Premixing Experiments	60
4.3	Simulation of Explosion Experiments	64
4.4	Application for Plant Scale Simulation	75
5	Summary	80
	Acknowledgments	82
	Appendix	83

A	Notation	83
B	Particle Heat Conduction Models	86
B.1	Surface Temperature Drop of Melt Particles	86
B.2	Fast Transient Heat Release from Fine Fragments	87
C	Brief Description of CIP Method	90
C.1	Basic Concept of CIP Method	90
C.2	Improvement for Steep Steps—CIP1 Scheme	91
C.3	Non-Linear Equation	91
D	Steam Table Package WRSTEAMTAB	93
E	Input Preparation and Code Usage	97
E.1	Input File Format	97
E.1.1	Preprocessing	97
E.1.2	Input Variables and Their Ordering	97
E.2	Running the Code	110
E.2.1	Normal Run	110
E.2.2	Output Files	111
E.2.3	Restart Run	112
E.2.4	Restart Calculation in “explosion mode”	113
	References	115

目 次

1 はじめに	1
1.1 背景—水蒸気爆発と安全評価	1
1.2 JASMINE コード	2
1.3 本書の用法	4
2 モデル説明	5
2.1 モデルの枠組	5
2.2 メルトモデル	6
2.2.1 メルトジェット	6
2.2.2 メルトプール	8
2.2.3 メルト粒子	11
2.2.4 爆発過程のためのメルト粒子モデル拡張	18
2.3 二相流モデル	21
2.3.1 基礎式	21
2.3.2 構成式	22
3 数値解法	28
3.1 メルトモデルと二相流モデルの連成	28
3.2 メルトモデルの数値解法	28
3.2.1 メルトジェット	28
3.2.2 メルトプール	31
3.2.3 メルト粒子	33
3.3 二相流モデルの数値解法	34
3.3.1 概要	34
3.3.2 基礎式の差分形	34
3.3.3 境界条件の設定	39
3.3.4 Newton 法の反復計算	40
3.3.5 圧力方程式系の構成	41
3.3.6 Jacobi 行列の要素	42
4 検証計算及びその他計算例	47
4.1 各モデルの数値的挙動確認	47
4.1.1 メルトジェット及びプール	47
4.1.2 メルト粒子	51
4.1.3 二相媒体における衝撃波伝播	55
4.2 粗混合実験のシミュレーション	60
4.3 水蒸気爆発実験のシミュレーション	64
4.4 実機規模解析への適用例	75
5 まとめ	80

謝辞	82
付録	83
A 記号表	83
B 粒子内の熱伝導モデル	86
B.1 メルト粒子の表面温度降下	86
B.2 細粒からの急速放熱	87
C CIP 法	90
C.1 CIP 法の概念	90
C.2 急峻な変化がある場合の改良-CIP1	91
C.3 非線型方程式	91
D 蒸気表パッケージ WRSTEAMTAB	93
E 入力データ作成及びコード使用法	97
E.1 入力データの形式	97
E.1.1 プリプロセス	97
E.1.2 入力変数とその順序	97
E.2 コードの実行	110
E.2.1 通常の実行	110
E.2.2 出力ファイル	111
E.2.3 リスタート計算の実行	112
E.2.4 “爆発モード”でのリスタート計算	113
参考文献	115

1 Introduction

1.1 Background—Steam Explosion and Safety Assessment

A steam explosion is a phenomenon in which high temperature liquid contacts with low temperature volatile liquid and transfer heat extremely quickly, causing rapid vaporization and shock wave generation. In other words, a steam explosion is a thermodynamic process which converts a part of the internal energy possessed by the high temperature liquid into mechanical energy, which can produce mechanical damages to the surroundings.

In the field of nuclear safety, the steam explosion due to the contact of the molten core material and coolant water has been recognized as a potential threat to the integrity of the containment vessel during severe accidents of light water reactors. The interaction between the molten fuel and coolant in nuclear power plants is also called fuel-coolant interaction (FCI) in a broad sense, which include both the explosive and mild interactions.

The steam explosion is phenomenologically understood as four stages[1, 2] as shown in Fig. 1.1. The phenomena involved in each stage is described briefly as follows.

- Premixing: coarse break-up and mixing of the high temperature liquid in the low temperature liquid (coolant) while thermally insulated by a vapor film; time scale 0.1–several seconds
- Triggering: destabilization of the vapor film and onset of rapid vaporization and fragmentation of the melt droplets
- Propagation: fine fragmentation of the melt droplets and rapid heat transfer associated with a propagating shock wave; time scale a few milliseconds
- Expansion: vaporization of the coolant and expansion of the mixture potentially causing damages on the surroundings

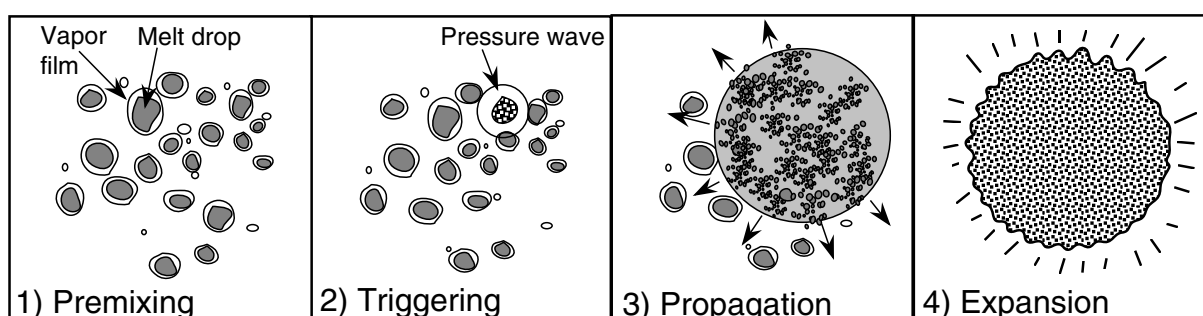


Figure 1.1: Phenomenological four stages of steam explosions.

Plant scale assessment on the steam explosion issue needs a certain analytical approach in order to extrapolate the knowledge obtained from experiments to the scale and conditions relevant to power plant accidents.

Historically, a variety of models and methods were developed ranging from thermodynamic models, which give the bounds of energy conversion efficiency, to multidimensional transient thermohydraulic models, which mechanistically simulates the process.[2, 3]

According to the phenomenology of 4 stages described in the previous section, the assessment of steam explosion energetics is usually done through the following two steps:

- Evaluation of the initial internal energy inventory in the high temperature liquid which is “premixed” with the coolant and ready to participate in the following explosive process, and
- Evaluation of the mechanical energy output through the “propagation” and “expansion” (explosion) processes.

Note that the “triggering” is a tricky process from the view point of safety assessment. It was observed, in some experimental conditions, that the triggering sometimes occurred but sometimes not, depending on even a small uncontrollable change in the condition.[4] While, in the analytical assessment, assuming a triggering or not makes totally different outputs, i.e. explosion loads or nothing.

Considering that, we, at present, recommend to assume a strong enough triggering, and to do the explosion simulation to see the mechanical loads. Actually, it may happen that no significant explosive interaction occurs even if a strong triggering is assumed, depending on the premixture condition, e.g. high void fraction or melt solidification. In such a case, we may say, with some confidence, that at most insignificant damage is predicted in the given condition.

1.2 JASMINE Code

We developed a mechanistic FCI simulation code, JASMINE (**J**AEA **S**imulator for **M**ultiphase **I**nteractions and **E**xplosions).

The first version of JASMINE developed in 1995 [5] was a three-fluid Eulerian model with water, vapor and melt fields aimed at the premixing simulation. This was then called JASMINE-pre and used in the OECD International Standard Problem No.39 (ISP-39) exercise on a large scale melt quenching experiment FARO-L14 [6].

The propagation model was separately developed as JASMINE-pro [7, 8] which was a five-fluid model with additional two fields for the fine fragments of melt generated in the propagation stage and small amount of coolant which interacts with the fine fragments.

A major modification in JASMINE-pre was made in 1997. In the new version, JASMINE-pre v.2, melt droplets generated by coarse break-up was modeled in Lagrangian framework. Finally, in 2003, the propagation related models in JASMINE-pro v.1.1 were merged into JASMINE-pre v.2.2. This change produced JASMINE v.3, which can handle both the premixing and propagation/expansion simulations. JASMINE-pre v.2 and JASMINE v.3 were used in the OECD’s international cooperative research program SERENA Phase-1[9, 10].¹

The structure of the present code is illustrated in Fig. 1.2 in relation to the phenomena expected in the fuel-coolant interaction in a nuclear power plant. JASMINE v.3 consists of two separate parts for the modeling of the molten core behavior and the coolant multiphase flow. The molten core model called MELT includes three sub-models for the melt jet, melt pool and melt particles. The multiphase flow model, which handles the coolant thermohydraulics is a modified version of ACE3D code developed at Japan Atomic Energy Research Institute (JAERI) by Ohnuki et al. [11]. The melt jet and melt pool models are one-dimensional representations of a molten core stream falling into a water pool and a continuous melt body agglomerated on the bottom, respectively. The melt particles generated by the melt jet break-up in the water pool are modeled based on a Lagrangian grouped particle concept.

JASMINE simulates the whole process of the steam explosion in two steps. First, the premixing stage is simulated with the initial/boundary conditions for the flow field and melt inlet. Then, the explosion process—propagation and expansion—is simulated by feeding output

¹The latest version is 3.3a as of April, 2008. The basic structure and functions are the same for versions 3.x.

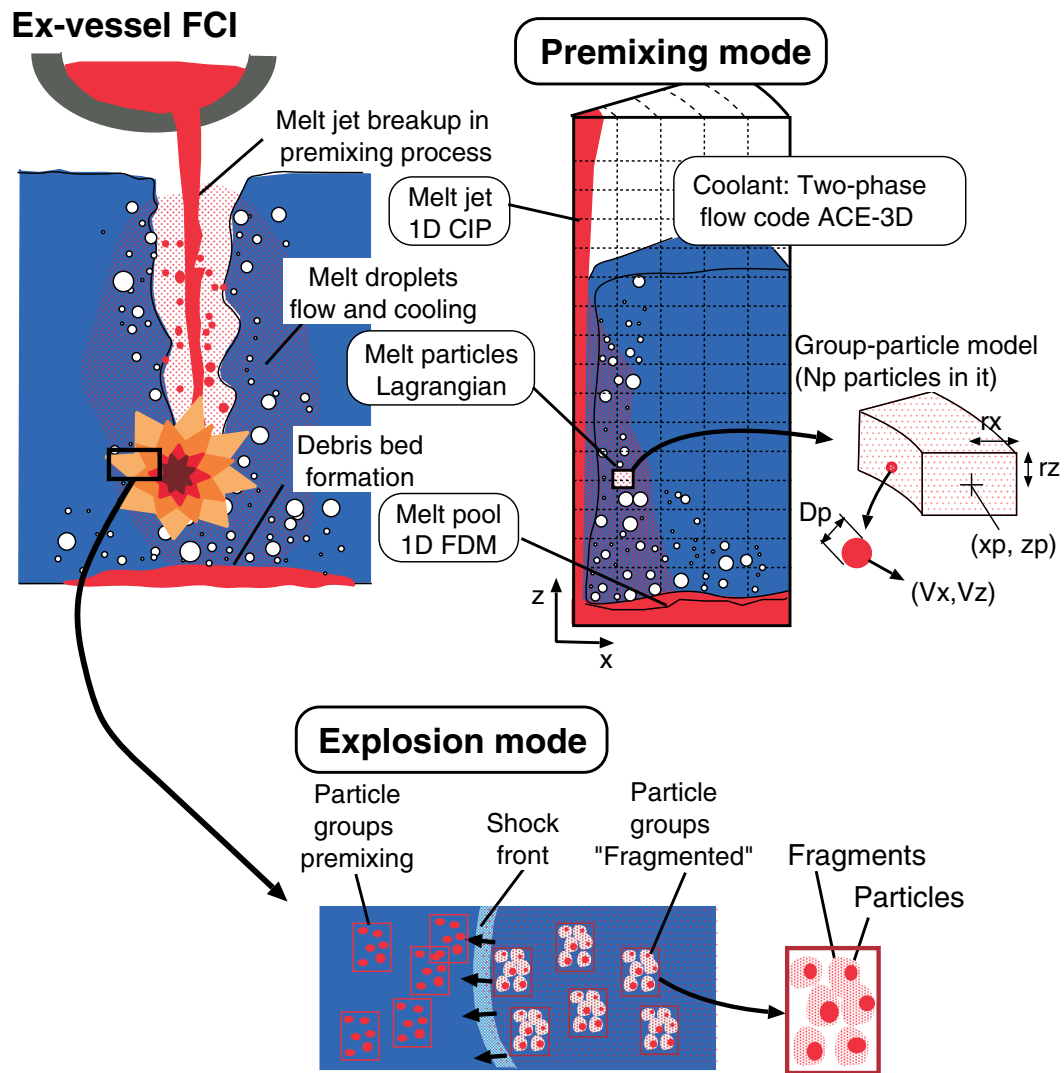


Figure 1.2: Concept and structure of JASMINE code.

Table 1.1: Nature of physics in premixing and explosion processes and related terminology used in this document.

	Premixing	Explosion (propagation & expansion)
Physics		
Dominating physical process	gravity (buoyancy) driven convection	shock wave propagation
Time scale	0.1–10s	0.1–10ms
Melt size scale	1–10mm	1–100 μ m
Terminology		
Name of melt size change process	(coarse) break-up of melt jet or particles (droplets)	(fine) fragmentation of melt particles (droplets)
Name of melt particles	droplets (particles)	(fine) fragments

data from the premixing calculation at a selected time, as an initial condition, and by specifying explosion model options in the input file.

Table 1.1 summarizes the individual features of the premixing and explosion processes and related terminology, that is used in this document.

1.3 Usage of This Manual

The present document describes the models, numerical solution methods, some verification and example calculations, as well as the practical usage of the code.

The instructions on the usage and input preparation, the minimum necessary information to run the code quickly, are given in Appendix E.

It is recommended for the readers, at least, to briefly go through Chapter 2 before running the code, so that they can grab the basic concept of models and definition and meaning of the technical terms.

Chapters 3 and 4 give an explanation of numerical solution methods and verification/example calculations, respectively. Notation of the variables is given in Appendix A. Appendix B–D describes some modeling and numerical method details.

The summary, Chap. 5, includes the information on the limitation and problems in the present model.

2 Model Description

2.1 Modeling Framework

JASMINE consists of a melt model and a two-phase flow model as illustrated in Fig. 1.2. The melt model consists of three components of sub-models: one-dimensional models for melt jet and pool, and Lagrangian grouped-particle model for melt particles. For the explosion calculation, an additional component is attached to the melt particle model for the fine fragments generated by shock wave–melt particle interaction. The coolant flow involving water, vapor and non-condensable gases are handled by a modified version of two-phase flow code ACE3D.

The calculation domain considered is a sector of a cylindrical volume with azimuthal width (angle) Θ . The volume is discretized x - z plane into a finite difference grid. The coolant flow model uses this grid. The melt jet is modeled as a vertical one-dimensional flow accommodated in the central column of the grid. The melt pool is modeled as a horizontal (radial) one-dimensional flow in the bottom layer of the grid. The melt particle groups, modeling the melt droplets, are produced at the jet surface and migrate on the x - z grid as Lagrangian elements.

The basic equations and rules as well as constitutive models are described in the following sections.

In evaluating the constitutive equations, it is often necessary to consider the multi-phase flow regimes of the coolant flow. We constructed the constitutive equations on a basic idea that the melt interacts with the liquid and gas components of the coolant according to the coolant two-phase flow regimes. The flow regimes are defined as follows.

- Bubbly (liquid-continuous): when the total void fraction α (vapor plus non-condensable gases) is less than 0.3.
- Droplet (gas-continuous): when α is more than 0.75, and
- Transition: when α is between 0.3 and 0.75.

Based on the above definition, normally the constitutive equations for melt-coolant interactions are evaluated separately for the gas and liquid components, and averaged with the weighting function:

$$f_{\alpha} = \begin{cases} 0 & (0 \leq \alpha < 0.3) \\ (\alpha - 0.3)/0.45 & (0.3 \leq \alpha \leq 0.75) \\ 1 & (0.75 < \alpha \leq 1) \end{cases} . \quad (2.1)$$

For example, variables X_{liq} and X_{gas} evaluated for the effects of liquid and gas, respectively, are averaged by

$$X_{two-phase} = (1 - f_{\alpha})X_{liq} + f_{\alpha}X_{gas} . \quad (2.2)$$

Hereafter, this averaging scheme is applied if no specific description is given for the composition of two-phase contributions.

2.2 Melt Model

2.2.1 Melt Jet

Basic equations

One-dimensional conservation equations in z -direction for the melt jet are solved. The equations for mass, internal energy and momentum are expressed as follows:

$$\frac{\partial A_J \rho_J}{\partial t} + v_J \frac{\partial A_J \rho_J}{\partial z} = -\sqrt{2\Theta A_J} m_e - A_J \rho_J \frac{\partial v_J}{\partial z} \quad \text{for mass,} \quad (2.3)$$

$$\frac{\partial e_J}{\partial t} + v_J \frac{\partial e_J}{\partial z} = -\sqrt{\frac{2\Theta}{A_J}} \frac{q}{\rho_J} \quad \text{for energy, and} \quad (2.4)$$

$$\frac{\partial v_J}{\partial t} + v_J \frac{\partial v_J}{\partial z} = -\frac{1}{\rho_J} \frac{\partial p_a}{\partial z} + K_f(v_a - v_J) + g \quad \text{for momentum,} \quad (2.5)$$

where A_J , ρ_J , v_J and e_J denote the cross section, density, velocity and internal energy of the melt jet, respectively. Note that the area A_J is for the sector of angle Θ , i.e. $A_J = \Theta D_J^2/8$ where D_J is the jet diameter. The pressure p_a in the momentum equation is given by the outer flow field. Some variables in the source terms: m_e , mass flux due to droplet entrainment from the jet surface, q , heat flux and K_f , friction factor, are to be given by constitutive equations.

Constitutive models

Jet break-up The constitutive equation for the mass entrainment from the jet, i.e. droplet production from the jet surface, was deduced by relating the empirical correlation for jet break-up length and the mass balance of the jet. Figure 2.1 illustrates a situation that a melt jet is eroded in a water pool and reduces its diameter as it proceeds downward. The jet is totally broken up at depth L_{brk} , which is called the break-up length. Empirical correlations are available for this break-up length. By considering the mass balance at a certain depth z , the change of the jet cross section dA , and the volume flux for the droplet entrainment V_e [m/s] are related by

$$V_e = -\frac{V_J}{\pi D_J} \frac{dA}{dz}, \quad (2.6)$$

where $A = \pi D_J^2/4$. This equation connects the jet profile, i.e. the cross section or the diameter as a function of the depth, and the entrainment volume flux. The entrainment volume flux is determined if a profile is assumed. If it is assumed that the jet diameter decreases linearly with the depth, i.e. $dD_J/dz = \text{const.} = D_{Ji}/L_{brk}$, Eq. (2.6) gives

$$V_e = \frac{V_J}{2} \frac{D_{Ji}}{L_{brk}}. \quad (2.7)$$

If it is assumed that the jet cross section decreases linearly with the depth, i.e. $dA/dz = \text{const.} = A_i/L_{brk}$, Eq. (2.6) gives

$$V_e = \frac{V_J}{4D_J} \frac{D_{Ji}^2}{L_{brk}}. \quad (2.8)$$

The variables D_{Ji} and A_i are the jet diameter and cross section at the water surface.

The present version of JASMINE uses Eq. (2.7) when the jet break-up length is shorter than water pool depth H_{pl} . For the case of a shallow water pool where $L_{brk} > H_{pl}$ (incomplete break-up), a correction factor $\sqrt{H_{pl}/L_{brk}}$ is attached to Eq. (2.7) based on a consideration on the strength of the steam upward flow surrounding the melt jet[12].

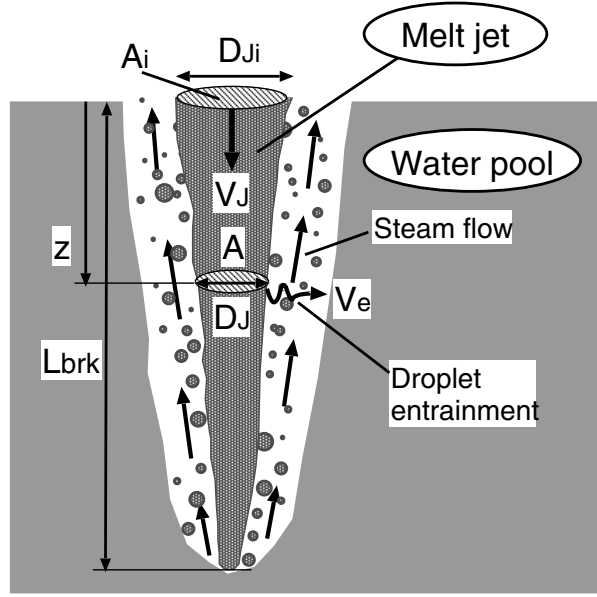


Figure 2.1: Concept of the jet break-up model.

A set of empirical correlation for the jet break-up length was obtained by examination into experimental data by the authors and in the literature[13]. According to a jet diameter-based Bond number,

$$Bo_J = \frac{\rho_J g D_{ji}^2}{\sigma_J}, \quad (2.9)$$

the jet break-up length is given by a Taylor type correlation[14] when $Bo_J \geq 50$,

$$\frac{L_{brk}}{D_{ji}} = 10 \left(\frac{\rho_J}{\rho_l} \right)^{1/2}, \quad (2.10)$$

or otherwise by Saito et al. correlation[15],

$$\frac{L_{brk}}{D_{ji}} = 2.1 \left(\frac{\rho_J}{\rho_l} \right)^{1/2} \left(\frac{V_{ji}^2}{g D_{ji}} \right)^{1/2}, \quad (2.11)$$

where ρ_J and ρ_l are densities of the jet and water, V_{ji} is the jet velocity at the water surface, and g is the gravitational acceleration.

The mass flux of droplet entrainment m_e is given by

$$m_e = C_{ent} \rho_J V_e, \quad (2.12)$$

where C_{ent} is a constant. If the constant C_{ent} is set to be unity, the jet breaks up at the length determined by the empirical correlation. A larger value for C_{ent} shortens the break-up length.

The diameter of the entrained droplet is, right now, left to be given as a constant value by the user. Successive break-up of the droplets are considered in the particle model.

The x and z velocity components of the entrained droplet is given by

$$v_{ex} = C_{vx}(2V_e), \quad \text{and} \quad (2.13)$$

$$v_{ez} = C_{vzwt}v_J + (1 - C_{vzwt})v_c, \quad (2.14)$$

where C_{vx} and C_{vzwt} are parameters which should have the values roughly ~ 5 and ~ 0.5 , respectively.

Friction The friction coefficient is given by considering the relative flow of the coolant in the surrounding boundary layer,

$$K_f = C_{fJ} f \frac{\rho_c}{\rho_J} \sqrt{\frac{\Theta}{2A_J}} v_r . \quad (2.15)$$

The constant C_{fJ} is usually set to be unity. The friction factor f is given as follows:

$$f = \max(16/Re_d, 0.0791/Re_d^{0.25}) , \quad (2.16)$$

$$Re_d = \rho_c d_{bnd} v_r / \mu_c , \quad (2.17)$$

$$d_{bnd} = 0.37 z_{bnd} / Re_z^{0.2} , \text{ and} \quad (2.18)$$

$$Re_z = \rho_c z_{bnd} v_r / \mu_c , \quad (2.19)$$

where Re_d and Re_z are Reynolds numbers based on the boundary layer thickness d_{bnd} and the distance from the jet leading edge z_{bnd} . Equation (2.18) is based on the development of turbulent boundary layer on a flat plate[16].

Heat transfer Heat transfer from the jet is currently not considered, because both the surface area and the duration of travel in the coolant are much smaller than those of the melt particles or the melt pool. Therefore, the heat flux q is simply set 0.

2.2.2 Melt Pool

Basic equations

When the jet column or a particle group reaches the bottom, it may form a continuous melt body. The melt pool model was introduced to contain such a mass. One-dimensional conservation equations for the pool in the radial direction are solved. The conservation equations for the melt pool are given as follows:

$$\frac{\partial w h_P \rho_P}{\partial t} + \frac{\partial (w h_P \rho_P v_P)}{\partial x} = w m_s \quad \text{for mass,} \quad (2.20)$$

$$\frac{\partial e_P}{\partial t} + v_P \frac{\partial e_P}{\partial x} = \frac{q}{h_P \rho_P} + \frac{(e_{ms} - e_P) \max(m_s, 0)}{h_P \rho_P} \quad \text{for energy, and} \quad (2.21)$$

$$\begin{aligned} \frac{\partial v_P}{\partial t} + v_P \frac{\partial v_P}{\partial x} = & -\frac{1}{\rho_P} \left[\frac{\partial p_a}{\partial x} + \frac{g}{2} \frac{\partial (h_P \rho_P)}{\partial x} \right] \\ & + K_{fa}(v_a - v_P) - K_{fw} v_P + \frac{(v_{ms} - v_P) \max(m_s, 0)}{h_P \rho_P} \quad \text{for momentum,} \end{aligned} \quad (2.22)$$

where h_P , $w(x)(\equiv x\Theta)$, ρ_P , e_P and v_P denote the pool height, the sector width of the analysis domain at position x , density, internal energy and velocity, respectively. Variables m_s , q , K_{fa} and K_{fw} denote the mass flux of melt jet and particles falling on to the pool surface, the heat flux at the pool surface, the pool-fluid friction factor and the pool-floor friction factor, respectively.

Constitutive models

Friction The friction is neglected (friction factors are set to be 0) at present. The friction is not important relatively to the heat transfer and mass exchange for the primary purpose of this pool model, i.e. to accommodate the agglomerated mass of melt in a physically reasonable manner.

Heat transfer The surface heat flux is given by considering radiation, film boiling, nucleate boiling and convection heat transfer, with a collection of available correlation equations described in the following. Figure 2.2 shows the boiling curve considered in combining the effects of various modes of heat transfer. Boiling is considered when the temperature of the heat transfer surface is higher than the saturation temperature of the coolant. Convection heat transfer to the coolant liquid and/or gas is considered if it is suitable.

- Convection: natural convection over a horizontal flat surface [17]

$$q_{cvf} = Nu_{cvf}(\lambda/l)(T_w - T_\infty) , \quad (2.23)$$

$$Nu_{cvf} = 0.15Ra^{1/3} , \quad (2.24)$$

$$Ra = GrPr = \{g\beta(T_w - T_\infty)l^3/\nu^2\}Pr , \quad (2.25)$$

where Nu_{cvf} denotes the average Nusselt number over the surface of characteristic scale l ; Ra , Gr and Pr denote Rayleigh, Grashof and Prandtl numbers. The melt pool diameter is taken for the length l . The correlation is valid roughly for $Nu_{cvf} = 50 - 1000$.

- Nucleate boiling: Kutateladze [18]

$$q_{nb} = 3.05 \times 10^{-11} \{\lambda_l(T_w - T_{sat})\}^{10/3} Pr_l^{7/6} \left\{ \frac{\sigma_l}{g(\rho_l - \rho_v)} \right\}^{2/3} \left(\frac{p\rho_l}{\sigma_l \Delta h_{fg} \mu_l \rho_v} \right)^{7/3} . \quad (2.26)$$

- Critical heat flux (CHF): Zuber [19]

$$q_{CHF} = 0.131 \frac{\Delta h_{fg} \rho_v}{\{\rho_v^2 / \sigma_l g(\rho_l - \rho_v)\}^{1/4}} . \quad (2.27)$$

The corresponding temperature is found by substituting q_{CHF} for q_{nb} in the nucleate boiling correlation, Eq. (2.26), and solving it for T_w .

- Film boiling: Berenson [20]

$$q_{fbf} = N_{fbf}(\lambda_{vf}/L)(T_w - T_l) , \quad (2.28)$$

$$Nu_{fbf} = 0.425 \left\{ \frac{g\rho_{vf}(\rho_l - \rho_{vf})L^3/\mu_{vf}^2}{c_{pv}\Delta T_{sat}/\Delta h'_{fg}Pr_{vf}} \right\}^{1/4} , \quad (2.29)$$

$$(2.30)$$

where the Laplace length L and modified latent heat $\Delta h'_{fg}$ are defined by

$$L = \sqrt{\sigma_l/g(\rho_l - \rho_{vf})} , \text{ and} \quad (2.31)$$

$$\Delta h'_{fg} = \Delta h_{fg} + 0.5c_{pvf}\Delta T_{sat} . \quad (2.32)$$

Vapor film properties ρ_{vf} , μ_{vf} , c_{pvf} and Pr_{vf} are evaluated at the film temperature $T_{vf} = 0.5(T_w + T_v)$.

- Minimum film boiling (MFB) heat flux: Berenson [20]

$$q_{mfb} = 0.09 \frac{\Delta h_{fg} \rho_{vf}}{\{\rho_{vf}^2 / \sigma_l g(\rho_l - \rho_{vf})\}^{1/4} \{(\rho_l - \rho_{vf})/\rho_{vf}\}^{1/2}} . \quad (2.33)$$

The corresponding temperature is found by substituting q_{mfb} for q_{fbf} in the film boiling correlation, Eq. (2.28), and solving it for T_w .

- Transition boiling: Linear interpolation is made between the CHF point (T_{CHF}, q_{CHF}) and the MFB point (T_{MFB}, q_{MFB}) on the boiling curve plain. (Fig. 2.2)
- Radiation: Stefan-Boltzmann law

$$q_{rad} = \epsilon_m \sigma_{SB} (T_w^4 - T_l^4) . \quad (2.34)$$

The film boiling and radiation models are combined by

$$q_{sum} = q_{fbf} + (7/8)q_{rad} \quad (2.35)$$

based on Bromley et al. [21] and Liu-Theofanous [22].

The void effect on the boiling and radiation heat transfer is considered by attenuating the heat flux when the flow regime departs from liquid continuous bubbly flow. Also, the boiling and radiation heat transfer is cut off at very high void regime $\alpha > 0.95$ to avoid numerical problems. This is made by multiplying the heat flux by the functions defined as follows.

- For nucleate boiling:

$$f_{\alpha,nb} = \begin{cases} 1 & (0 \leq \alpha < 0.3) \\ 1 - (\alpha - 0.3)/0.2 & (0.3 \leq \alpha \leq 0.5) \\ 0 & (0.5 < \alpha \leq 1) \end{cases} . \quad (2.36)$$

- For film boiling:

$$f_{\alpha,fb} = \begin{cases} 1 & (0 \leq \alpha < 0.3) \\ \{(0.95 - \alpha)/0.65\}^n & (0.3 \leq \alpha \leq 0.95) \\ 0 & (0.95 < \alpha \leq 1) \end{cases} , \quad (2.37)$$

where n is a constant. We set $n = 1$ at present.

- For radiation:

$$f_{\alpha,rd} = \begin{cases} 1 & (0 \leq \alpha < 0.3) \\ \{(0.95 - \alpha)/0.65\}^n & (0.3 \leq \alpha \leq 0.95) \\ 0 & (0.95 < \alpha \leq 1) \end{cases} , \quad (2.38)$$

where n is a constant. We set $n = 1$ at present.

Pool surface temperature The heat transfer at the pool surface depends on the pool surface temperature. Oxide melts, a typical molten core material, has a relatively low thermal conductivity and the surface temperature can be significantly lower than the average temperature. For the melt pool, this aspect is considered by a simple model, based on an assumption of quadratic temperature profile across the melt pool depth. The surface temperature is expressed by

$$T_{sf} = \frac{T_{av} + T_c \frac{h_P H}{6\lambda_P}}{1 + \frac{h_P H}{6\lambda_P}} \quad (2.39)$$

where T_{sf} , T_{av} and T_c denote the pool surface, pool average and coolant temperatures, respectively; H denotes the heat transfer coefficient on the pool surface. Since this model is quite crude, the result is checked to ensure $T_c \leq T_{sf} \leq T_{av}$. If a strange value arises, $T_{sf} = 0.5(T_{av} + T_c)$ is imposed.

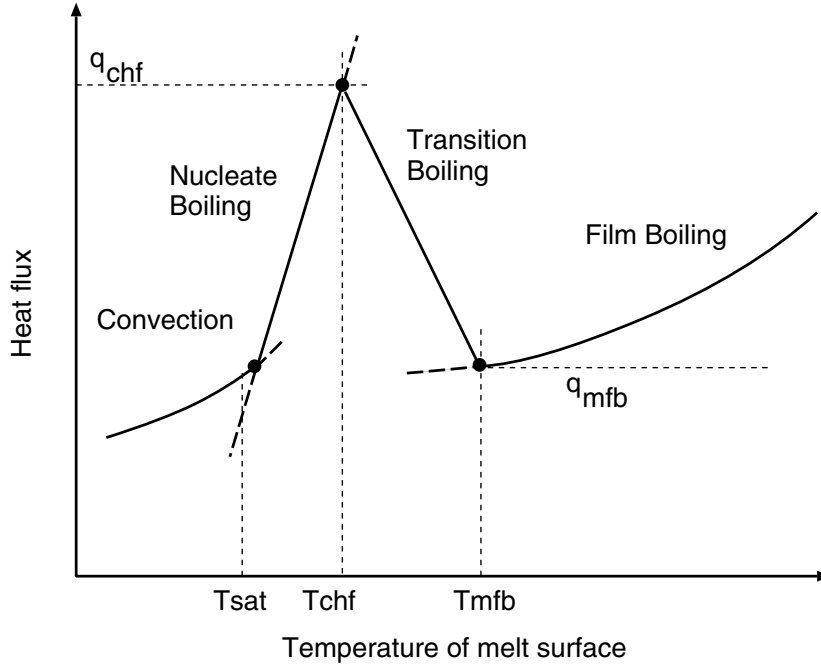


Figure 2.2: Construction of heat transfer model with available heat transfer correlations in various modes according to the boiling curve.

Mass addition When the jet leading edge reaches the bottom of the calculation domain, the mass and energy of the jet is given to the central node of the pool. The momentum of the jet is given to the pool by adding the stagnant impulse due to jet impingement on the central node of the pool. Modeling for the merge of settled particles will be described later in Section 2.2.3.

Freezing of the pool Freezing and melting of the pool is decided according to the average temperature of the whole body of the pool for simplicity. When the average temperature is lower than the melting point, the pool is considered frozen (velocity is set 0 everywhere).

2.2.3 Melt Particles

Concept and basic equations

A concept of grouped particle was developed for two-dimensional cylindrical geometry. It enables a practical use of the code for large systems such as plant scale simulation, in which the number of the real debris particles could be too large to be simulated directly. The grouped particle model has a scalability according to computational resources available, by choosing the size of particle groups adequately.

A “particle group” is a group of N_p particles which are assumed to have the same properties and occupy a finite space, $2r_x$ by $2r_z$ on the x - z plain. (see Fig. 1.2) This assumption of finite size of groups is required to move the melt particle volume, force and heat source smoothly among the two-phase flow cells. If a group is assumed to be a point, the source terms for the two-phase flow model would jump from a cell to another suddenly and might cause numerical problems. Other attributes of the group, i.e. the realistic shape of the group, rotation, diffusive feature etc., were stripped off to simplify the situation and to make this method feasible.

The motion and heat balance of a representative particle in a group are tracked by Lagrangian

equations:

$$\frac{\partial \mathbf{v}_p}{\partial t} = \mathbf{g} - \frac{\nabla p_a}{\rho_p} + \frac{\mathbf{F}_{hy}}{m_p} \quad \text{and} \quad (2.40)$$

$$\frac{\partial \mathbf{x}_p}{\partial t} = \mathbf{v}_p \quad \text{for motion, and} \quad (2.41)$$

$$\frac{\partial e_p}{\partial t} = \frac{q}{m_p} \quad \text{for energy conservation,} \quad (2.42)$$

where \mathbf{v}_p , \mathbf{x}_p , m_p and e_p denote particle velocity (v_{px}, v_{pz}), position (x_p, z_p), mass of a particle and internal energy per unit mass, respectively. The hydrodynamic drag force \mathbf{F}_{hy} and heat exchange rate q are given by constitutive equations.

This method requires other rules to handle the generation and interferences of particle groups as described in the followings.

Rules for generation of particle groups

When particles are generated on the jet surface, the mass, temperature, size and velocity of particles are given in each jet cell at each time step. However, releasing a particle group from every jet cell at every time step makes too many groups. Besides, the mass or number of particles generated in one time step at one cell is usually very few. This is a matter of interfacing between Eulerian and Lagrangian forms of discretization. To workaroud this problem, we introduced a concept of “pre-particle group” as a buffer. (Fig. 2.3) The particles just after the birth are stored in pre-particle groups. They are released as real particle groups after they mature to have enough mass or number of particles. Each pre-particle group is attached to each jet cell and has the same vertical size as the jet cell. ($2r_z = \Delta z_{jet}$) The horizontal size of the pre-particle group develops as the particles inside travels outward. Pre-particle groups do not exchange momentum and heat with the coolant until they are released as real-particle groups. The criteria of release are defined as follows.

1. Total mass of pre-particle group is larger than 0, and
2. one of the conditions below is satisfied;
 - the number of particles $N_p > N_{pcr}$,
 - x -direction size $r_x > r_{xcr} (\equiv \Delta x_{min}/4)$,
 - x outer edge position exceeds the first cell boundary, or
 - the age exceeds a time limit (n_{hist} time steps),

where N_{pcr} and n_{hist} are the criteria given by the user and Δx_{min} is the minimum x -direction grid width in the system.

When a pre-particle group is released as a real-particle group, the x -direction velocity that was given by Eq. (2.13) is multiplied by a stochastic function

$$f_r = 0.02 + 0.98\phi_r, \quad (2.43)$$

where ϕ_r is a random number distributed uniformly between 0 and 1. This stochastic function is a trial model to express stochastic nature of the initial velocity of melt droplets emitted through turbulence surrounding the melt jet.

Rules for interference of particle groups with other particle groups or boundaries

Some rules are required to avoid the occurrence of physically unreasonable situation upon the interference between particle groups or between a particle group and a boundary. The following rules were defined for this purpose.

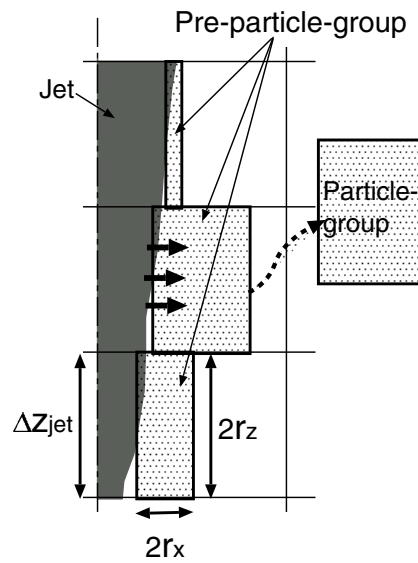


Figure 2.3: Pre-particle group concept.

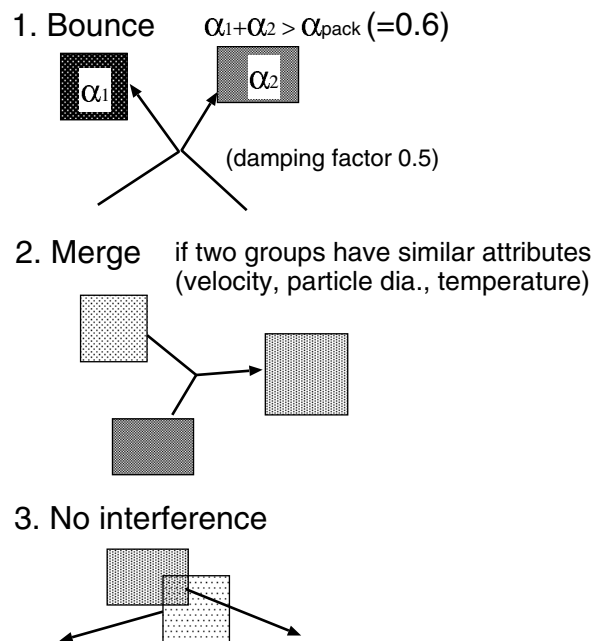


Figure 2.4: Rules for the interference between particle groups.

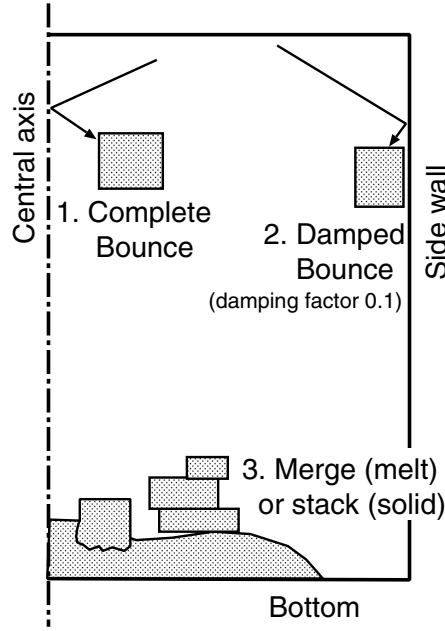


Figure 2.5: Rules for the interference between a particle group and boundary.

(a) Between particle groups (Fig. 2.4)

1. If the sum of the particle volume fractions of two groups in contact is more than the packing limit $\alpha_{pack}(= 0.6)$, the two groups bounce apart with a damping factor $C_{damppar}(= 0.5)$,
2. else if the two groups in contact have similar attributes: temperature, particle size and velocity, matching within 20%, they merge into one group,
3. otherwise, the two groups have no interference, but just go through each other.

(b) With boundaries (Fig. 2.5)

1. If a group reaches the central boundary, it is bounced back inside.
2. If a group reaches the top or the side boundary, it is bounced back inside with a damping factor $C_{dampwal}(= 0.1)$.
3. If a group reaches the bottom, it merges into the pool if the pool or the particle group is molten, otherwise the group piles up on the frozen pool making a debris bed. When a group joins into the debris bed, the group is vertically collapsed so that its particle volume fraction becomes the packing limit or the group height becomes the same as the particle size (the height of a single particle layer).

Constitutive models

Hydrodynamic drag The drag is evaluated by a correlation for a sphere subjected to flow [23]:

$$\mathbf{F}_{hy} = C_{fp} f \frac{\pi}{4} D_p^2 \frac{1}{2} \rho v_r \mathbf{v}_r, \quad (2.44)$$

$$f = \max \left(24/Re_p, 18.5/Re_p^{0.6}, 0.44 \right), \quad (2.45)$$

$$Re_p = \rho D_p v_r / \mu, \quad (2.46)$$

where C_{fp} is a correction parameter to consider deformation and irregular shape of particles. Variables D_p , \mathbf{v}_r , v_r , ρ and μ are the melt particle diameter, relative velocity between the melt particle and the coolant and its absolute value, density and viscosity of the coolant, respectively. The drag force \mathbf{F}_{hy} is calculated for the liquid and gas components of the coolant separately, and the effects are combined with the method described by Eqs. (2.1) and (2.2).

Heat transfer The surface heat transfer coefficients are evaluated by a set of correlations for radiation, film boiling, nucleate boiling and convection around a sphere as described in the following. Those various modes of heat transfer are combined by considering the boiling regimes as shown in Fig. 2.2. Boiling is considered when the temperature of the heat transfer surface is higher than the saturation temperature of the coolant. Convection heat transfer to the coolant liquid and/or gas is considered if it is suitable.

- Convection: forced convection around a sphere [24]

$$q_{cvp} = Nu_{cvp}(\lambda/D_p)(T_w - T_\infty) , \quad (2.47)$$

$$Nu_{cvp} = 2 + 0.6Re_p^{1/2}Pr^{1/3} , \quad (2.48)$$

$$Re_p = \rho_p D_p v_r / \mu , \quad (2.49)$$

where Nu_{cvp} denotes the average Nusselt number for a particle of diameter D_p exposed to flow with relative velocity v_r ; Re_p and Pr denote Reynolds and Prandtl numbers.

- Nucleate boiling: Kutateladze [18], Eq.(2.26).
- Critical heat flux (CHF): Zuber [19], Eq.(2.27).
- Film boiling: Liu-Theofanous [22]

$$q_{fbp} = Nu_{fbp}(\lambda_{vf}/D_p)(T_w - T_l) , \quad (2.50)$$

$$Nu_{fbp} = \{Nu_p^5 + (F_f Nu_f)^5\}^{1/5} , \quad (2.51)$$

$$F_f = 1 - 0.2/\{1 + (Fr^{1/2} - 1)\} , \quad (2.52)$$

$$Fr = v_{rl}^2 / g D_p , \quad (2.53)$$

$$Nu_f = Nu_s + 0.072 Re_l^{0.77} Pr_l^{1/2} (\mu_l / \mu_{vf}) (Sc' / Sp') , \quad (2.54)$$

$$Nu_s = 0.5 Re_l^{1/2} (\mu_l / \mu_{vf}) (KR^4 / Sp')^{1/4} , \quad (2.55)$$

$$Re_l = \rho_l D_p v_{rl} / \mu_l , \quad (2.56)$$

$$Nu_p / (1 + 2/Nu_p) = kc(Ar / Sp')^{1/4} Mc^{1/4} , \quad (2.57)$$

$$Mc = E^3 / \{(1 + E/Sp'Pr_l)(RPr_lSp')^2\} , \quad (2.58)$$

$$E = (A + CB^{1/2})^{1/3} + (A - CB^{1/2})^{1/3} + (1/3)Sc' , \quad (2.59)$$

$$A = (1/27)Sc'^3 + (1/3)R^2 Sp'Pr_l Sc' + (1/4)R^2 Sp'^2 Pr_l^2 , \quad (2.60)$$

$$B = -(4/27)Sc'^2 + (2/3)Sp'Pr_l Sc' - (32/27)R^2 Sp'Pr_l + (1/4)Sp'^2 Pr_l^2 + (2/27)Sc'^3 / R^2 , \quad (2.61)$$

$$C = (1/2)R^2 Sp'Pr_l , \quad (2.62)$$

$$K = \rho_l / \rho_{vf} , \quad (2.63)$$

$$R = (\mu_{vf} \rho_{vf} / \mu_l \rho_l)^{1/2} , \quad (2.64)$$

$$Ar = g(\rho_l - \rho_{vf})D_p^3 / (\mu_{vf}^2 / \rho_{vf}) , \quad (2.65)$$

$$D' = D_p / \{\sigma_l / g(\rho_l - \rho_{vf})\}^{1/2} , \quad (2.66)$$

$$Sc' = c_{pl} \Delta T_{sub} / \Delta h'_{fg} Pr_l , \quad (2.67)$$

$$Sp' = c_{pvf}\Delta T_{sup}/\Delta h'_{fg}Pr_{vf}, \quad (2.68)$$

$$\Delta h'_{fg} = \Delta h_{fg} + 0.5c_{pvf}\Delta T_{sup}, \quad (2.69)$$

$$kc = \begin{cases} 0.5/D'^{1/4} & (D' \leq 0.14) \\ 0.86/(1 + 0.28D') & (0.14 < D' \leq 1.25) \\ 2.4D'/(1 + 3.0D') & (1.25 < D' \leq 6.6) \\ 0.47D'^{1/4} & (6.6 < D') \end{cases}. \quad (2.70)$$

The relative velocity v_{rl} is the one between water and melt particles. The liquid temperature T_l is used in the superheat term, i.e. $(T_w - T_l)$, instead of the saturation temperature because it is favorable for the numerical stability. The physical properties of vapor with suffix vf is evaluated at the film temperature $T_{vf} = 0.5(T_w + T_v)$. In the original correlation, the void effect is considered in Nu_s . However, we consider it by multiplying the heat flux q_{fbp} with a function as described later. Our method gives a result close to the original expression.

- Minimum film boiling (MFB) temperature: Kondo et al. [25]

$$T_{mfb} = T_{sat} + C \left(\frac{27}{32} T_{cr} - T_{sat} \right) + \left(\frac{\lambda_l}{\lambda_{vf}} \right) \frac{Nu_c \Delta T_{sub}}{D_p / \delta_{min} + Nu_r}, \quad (2.71)$$

where C is a constant ($= 0.6$); T_{cr} is the critical temperature of the coolant; δ_{min} is the minimum limit of the vapor film thickness, practically 0.1mm. The Nusselt number for convection around the vapor film which envelopes the hot particle, Nu_c , is given by Eq.(2.48). The Nusselt number for radiation heat transfer, Nu_r , is given based on the Stefan-Boltzmann law Eq.(2.34) and by taking account of $T_{mfb} \gg T_l$,

$$Nu_r = \epsilon_m \sigma_{SB} T_{mfb}^3 (D_p / \lambda_{vf}). \quad (2.72)$$

The corresponding heat flux q_{mfb} is found by substituting T_{mfb} for T_w in the film boiling correlation, Eq. (2.50).

- Transition boiling: linear interpolation is made between the CHF point (T_{CHF}, q_{CHF}) and the MFB point (T_{mfb}, q_{mfb}) on the boiling curve plain. (Fig. 2.2)
- Radiation: Stefan-Boltzmann law, Eq.(2.34). It is combined with the film boiling correlation by Eq. (2.35).

The void effect on the boiling and radiation heat transfer is considered by attenuating the heat flux when the flow regime departs from liquid continuous bubbly flow. Also, the boiling and radiation heat transfer is cut off at very high void regime $\alpha > 0.95$ to avoid numerical problems. The functions are the same as defined for the melt pool model, Eq.(2.36)–(2.38), except that the power n is 0.3 for film boiling to fit the behavior of the original Liu-Theofanous correlation, and that n is left tunable through the user input for radiation because it may have a strong influence and it is not easy to give a precise value with a simple model.

When the particles travel downward and finally settle on the floor making a debris bed, the particle groups are vertically collapsed. In such a case, the heat transfer is degraded due to ineffectiveness in the contact with the liquid coolant and in the emission of radiation. This heat transfer degradation is simulated by putting a reduction factor to the heat transfer coefficient. The reduction factor is given as an input parameter (typically ~ 0.1). When the collapsed group consists of more than one particle layers, further reduction factor, $D_p / (2r_z)$, is attached, with which groups containing more layers of particles have more ineffective heat transfer.

Secondary break-up of particles The secondary break-up of particles are modeled based on total break-up time τ_{brk} and maximum stable size of liquid droplets D_{smx} evaluated by the correlations by Pilch & Erdman [26],

$$D_{smx} = \frac{We_{cr}\sigma_d}{\rho_c v_0^2} \left(1 - \frac{v^*}{v_0}\right)^{-2}, \quad (2.73)$$

$$\tau_{brk} = \tau^* \frac{D_0}{v_0 \epsilon^{0.5}}, \quad (2.74)$$

$$v^* = v_0 \epsilon^{0.5} \left(\frac{0.75 C_d \tau^*}{1 + 0.75 C_d \epsilon^{0.5} \tau^*} \right), \quad (2.75)$$

$$\tau^* = \begin{cases} 6(We - 12)^{-0.25} & (12 \leq We < 18) \\ 2.45(We - 12)^{0.25} & (18 \leq We < 45) \\ 14.1(We - 12)^{-0.25} & (45 \leq We < 351) \\ 0.766(We - 12)^{0.25} & (351 \leq We < 2670) \\ 5.5 & (2670 \leq We) \end{cases}, \text{ and} \quad (2.76)$$

$$C_d = \begin{cases} 5.6 & (Re < 4 \times 10^4) \\ 3.3 & (4 \times 10^4 \leq Re < 10^5) \\ 1.4 & (10^5 \leq Re) \end{cases}, \quad (2.77)$$

where C_d : friction factor,
 D_0 : original droplet diameter,
 Re : Reynolds number ($\equiv \rho_c v_0 D_0 / \mu_c$),
 v_0 : original relative velocity between the droplet and coolant,
 v^* : relative velocity decrease during droplet break-up,
 We : Weber number ($\equiv \rho_c v_0^2 D_0 / \sigma_d$),
 We_{cr} : critical Weber number ($\equiv 12$),
 ϵ : density ratio ($\equiv \rho_c / \rho_d$),
 μ_c : viscosity of the continuous fluid ($\equiv 1 / \{\alpha / \mu_g + (1 - \alpha) / \mu_l\}$),
 ρ_c : density of the continuous fluid ($\equiv \alpha \rho_g + (1 - \alpha) \rho_l$),
 ρ_d : density of the droplet,
 σ_d : surface tension of droplet, and
 τ^* : non-dimensional break-up time.

The decrease rate of the droplet diameter is evaluated by

$$\frac{dD_p}{dt} = \frac{D_{med} - D_p}{\tau_{brk}}, \quad (2.78)$$

where the mass median diameter of droplets after the break-up, D_{med} , is simply considered to be the half of the maximum stable diameter, i.e. $D_{med} = D_{smx}/2$. Note that the relative velocity v_0 is evaluated by using the two-phase mixture velocity for the coolant, $v_c = \{\alpha \rho_g v_g + (1 - \alpha) \rho_l v_l\} / \rho_c$.

Strictly according to the original meaning of Pilch-Erdman correlation, the relative velocity, v_0 , should be the one before the break-up process begins. However, because of the difficulty of finding the start and end of the break-up for each droplet (particle group) in the present framework of the code, we use the relative velocity at the start of each time step to obtain the diameter decrease rate due to break-up, dD_p/dt , for that time step. This model is let in effect when the droplets are molten.

However, usage of this model is not recommended for practical purpose, i.e. safety evaluation, because this model is strongly affected by two-phase flow velocity that sometimes shows unstable feature in calculations. This model may cause unexpectedly small particle sizes, that significantly affects the heat transfer, void generation, and all the phenomena calculated. So, we recommend to turn off this model and do a parameter study on the droplet size given as an input constant.

Surface temperature of particles The surface temperature is required for the evaluation of heat transfer and as a criterion of the droplet break-up. It is important especially for oxide melts which have much smaller thermal conductivity than metals, and tend to have large difference between the inside and surface temperatures.

It is not easy to fully model the temperature distribution inside the particle with consideration on the development of solid layer at the surface even if a temperature profile is assumed. Therefore, a simple approach was adopted, that is, a quadratic temperature profile is assumed inside a particle and the difference of surface and average temperatures were evaluated from the time passed from the particle generation.

Based on the consideration detailed in Appendix B.1, the following formula is obtained. Development of the thermal boundary layer thickness δ inside a particle surface is expressed by

$$\delta \left\{ 1 - \frac{3}{4} \frac{\delta}{R} + \frac{1}{5} \left(\frac{\delta}{R} \right)^2 \right\} d\delta = 3\kappa dt \quad (2.79)$$

where κ is the thermal diffusion coefficient and R is the particle radius. At the first time step (in numerical integration) after particle generation, δ is obtained by the first order approximation

$$\delta = \sqrt{6\kappa\Delta t}. \quad (2.80)$$

After that, Eq. (2.79) is integrated numerically to get updated δ successively. The difference of the surface and average temperatures is obtained by

$$T_{av} - T_{sf} = \frac{q\delta}{2\lambda} \left[1 - \frac{\delta}{R} \left\{ 1 - \frac{1}{2} \frac{\delta}{R} + \frac{1}{10} \left(\frac{\delta}{R} \right)^2 \right\} \right], \quad (2.81)$$

where q is the surface heat flux evaluated by heat transfer models, λ is the thermal conductivity of melt.

Neglect of phase change (crust formation) does nothing until the surface temperature drops to the melting point, though it will make separation from the reality after that. Therefore, the timing of surface solidification should be adequately predicted. Besides, the surface temperature plateau near the phase change point is practically simulated through the average temperature and the material property model that expresses the latent heat through an artificial specific heat peak around the melting point.

2.2.4 Extension of Melt Particle Model for Explosion Process

Framework and basic equations

The explosion process is modeled based on the following concept on the primary physics included.

- When the melt particles are exposed to shock wave, i.e. an intense relative velocity of the surrounding coolant, very fine fragments are produced from the surface of the particles by hydrodynamic force.
- The fine fragments have sizes of micrometer order and the heat release from them is extremely quick, so that it vaporizes water quick enough to support high pressure to propel and escalate the shock wave. The heat release is dominated by the generation rate of fine fragments.

An additional component of the melt model, “fragment group”, is attached to the particle group model (Fig. 2.6) for implementation of the above described concept. A fragment group is a swarm of fragments which is generated from a particle group. Fragment groups behave as follows.

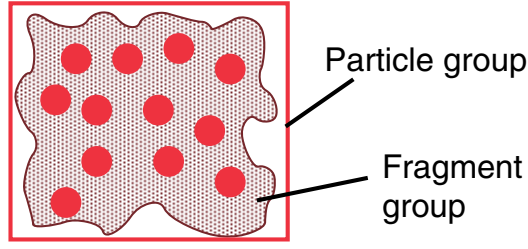


Figure 2.6: Particle group and fragment group.

- Generation: The fragment mass is separated from the “mother” particle group by hydrodynamic interaction. The mass conservation law is expressed by

$$\frac{dm_p}{dt} = -\dot{m}_f, \text{ and} \quad (2.82)$$

$$\frac{dM_f}{dt} = n_p \dot{m}_f \quad (2.83)$$

where m_p is the mass of one particle in the particle group, M_f is the mass of fragments in the fragment group and n_p is the number of particles in the particle group. The mass fragmentation rate for a particle, \dot{m}_f , is given by a constitutive model, Eq. (2.85).

- Heat transfer and energy conservation: The limiting process of the heat transfer is the heat conduction inside the fragment. The heat transfer coefficient outside the fragment is considered to be quite large and any steady state heat transfer correlation is not reliable in this highly transient situation. With a given heat release rate per unit mass of fragments \dot{q}_f , the energy conservation of the fragments is expressed by

$$\frac{de_f}{dt} = e_p \frac{n_p \dot{m}_f}{M_f} - \dot{q}_f \quad (2.84)$$

where e_f and e_p are the specific internal energies of fragments and particles. The specific internal energy of the mother particle is assumed constant during the explosion process.

- Size: Size of the fragment is given in the input as a constant, d_f . When the heat release time of the fragment is comparable to the numerical time step, the size does not affect much.
- Movement: No kinetic equation is solved for fragments. Instead, they are just assumed to accompany the mother particle group. The primary function of the fragments is the quick heat release and the kinetic aspect is regarded not important.

Since the primary physical process relevant to the melt in the propagation phase is the generation of fine fragments and quick heat release from them, there is no need of keeping the melt components of jet and pool. Therefore, the jet and pool components are re-casted into particle groups with equivalent surface area and volume at the start of an explosion calculation. Normally, the jet and pool have much less surface area to volume ratio than particles, and relatively small contribution in the heat release in the explosion process.

Constitutive models for propagation simulation

Fine fragmentation model The mass fragmentation rate from one melt particle \dot{m}_f [kg/s] is given by

$$\dot{m}_f = C_{frag} \frac{1}{t_b^*} \frac{\pi}{6} D_p^2 v_r (\rho_c \rho_p)^{1/2}, \quad (2.85)$$

$$t_b^* = \begin{cases} 1 & : \text{Caracharios et al. model[27], or} \\ 13.7/Bo^{1/4} & : \text{Yuen et al. model[28],} \end{cases} \quad (2.86)$$

$$Bo = \frac{3}{16} \frac{C_D \rho_c D_p v_r^2}{\sigma_p}, \quad (2.87)$$

where t_b^* is a non-dimensional time of break-up [26]; D_p is the particle diameter; v_r is the relative velocity between the particle and coolant; ρ_c and ρ_p denote the coolant and particle densities, respectively; σ_p is the surface tension of the melt particle. For the drag coefficient, C_D , the value for Newtonian regime, 0.44, is used.[23] An empirical constant C_{frag} is put in the equation for tuning.

Equation (2.85) means a simple fact that the whole volume of a particle $(\pi/6)D_p^3$ is stripped away in a characteristic period of break-up

$$t_b = t_b^* \sqrt{\frac{\rho_p}{\rho_c}} \frac{D_p}{v_r}. \quad (2.88)$$

Caracharios et al.[27] model gives the non-dimensional time t_b^* as a constant, and Yuen et al.[28] model includes the influence of Bond number Bo .

The coolant density, ρ_c , and the relative velocity, v_r , can be evaluated in several ways. Those in the Bond number, Bo , are evaluated simply by averaging for gas and liquid phases by

$$\rho_c = \alpha \rho_g + (1 - \alpha) \rho_l, \quad (2.89)$$

$$\mathbf{v}_c = \frac{\alpha \rho_g \mathbf{v}_g + (1 - \alpha) \rho_l \mathbf{v}_l}{\rho_c} \quad \text{and} \quad (2.90)$$

$$v_r = |\mathbf{v}_p - \mathbf{v}_c|. \quad (2.91)$$

Note that the Bond number is included with the power of 1/4 and the definition of these variables does not affect the result strongly. Those included in the expression of \dot{m}_f , however, have stronger influences and are given more carefully by the following three options. By default, the liquid density and velocity is used,

$$\rho_c = \rho_l \quad \text{and} \quad v_r = |\mathbf{v}_p - \mathbf{v}_l|, \quad (2.92)$$

and the evaluated \dot{m}_f is attenuated in case of high void fractions with a factor defined by

$$f_{\alpha,frag} = \begin{cases} 1 & (0 \leq \alpha < 0.3) \\ (0.75 - \alpha)/0.45 & (0.3 \leq \alpha \leq 0.75) \\ 0 & (0.75 < \alpha \leq 1) \end{cases}. \quad (2.93)$$

The second option is to use liquid density and velocity as in Eq. (2.92) and put a factor $(1 - \alpha)$, and the last option is to use the average as in Eqs. (2.89)–(2.91).

There is another model parameter for the usage of this fragmentation model. It is the duration to keep the fragmentation model active after the passage of the shock front, $\tau_{trigliffe}$. So far, we tested the model with alumina steam explosion experiments KROTOS[29] and found that JASMINE reproduces the experimentally observed pressure pulse and kinetic energy fairly well by $C_{frag} \sim 0.35$ with Caracharios et al.[27] model, with $\tau_{trigliffe} \sim 1\text{ms}$. (see Section 4.3)

Heat release model Heat release rate from a unit mass of the fragment \dot{q}_f [J/kg] is given by

$$\dot{q}_f = C_{qf} \frac{f_{rel}}{t_{rel}} (E_{ini} - E_{low}), \quad (2.94)$$

$$t_{rel} = \frac{1}{4} \frac{d_f^2}{\kappa_f} \tau_f,$$

where E_{ini} and E_{low} denote the internal energy of fragments at the initial high and the final low temperatures, κ_f is the thermal diffusion coefficient of fragments. The two temperatures are set to be the melt particle and the water temperatures, respectively. Equation (2.94) means the fraction f_{rel} of the heat possessed by the fragment is released in time t_{rel} . Based on an analysis of transient heat conduction inside a spherical fragment (see Appendix B.2 for the detail), the constants are $f_{rel} = 0.632$ and $\tau_f = 0.045$. An empirical constant C_{qf} is put for tuning.

An attenuation factor referring the void fraction

$$f = (1 - \alpha)^{0.2} \quad (2.95)$$

is put to Eq. (2.94) to avoid numerical difficulty which might be caused by depositing large amount of heat to a cell which contains little water.

With typical oxide melt properties ($\kappa_f \sim 1 \times 10^{-6}$ m²/s) and the fragment diameter in the order of 10 μ m, the heat release time t_{rel} is in the order of micro seconds. This is practically comparable to the numerical time step for propagation calculations. Thus, conceptually instant release of heat from the fragments holds. Therefore, the fragment diameter d_f does not significantly affect the result as long as a small enough value in the above mentioned range is given.

2.3 Two-Phase Flow Model

2.3.1 Basic Equations

Extensions to the two-phase flow model

The two-phase flow code ACE3D developed by Ohnuki et al. [11], which solves a two-fluid model for steam-water or air-water system in three-dimensional coordinates, was extended to include the following models required for the present purpose.

1. Convecting non-fluid volume model to accommodate the melt model components among the two-phase flow cells
2. Momentum and heat exchange schemes between the two-phase flow and the melt models
3. Non-condensable gas components to handle highly subcooled (non-condensable gas rich) conditions

Thus, the present coolant flow model in JASMINE has steam, water and non-condensable gas components. Mass and energy equations are solved individually for these components, while momentum equations are solved for two-phases, gas mixture and water, based on an assumption of mechanic equilibrium among gas components.

Definition of volume fractions

As usual in the conventional multi-fluid modeling, we express the conservation equations with volume fractions of each component. The relationship among the volume fractions: α_s , steam; α_a ($a = a_1, a_2, \dots, a_{ng}$), non-condensable gases; α_l , water; α , total void fraction, is defined by the following equations.

$$\alpha = \alpha_s + \sum \alpha_a \quad (2.96)$$

$$\alpha_l = 1 - \alpha \quad (2.97)$$

This multi-fluid modeling has a deviation from the reality that the gas components are actually mixed together: each component occupies the total gas volume and has a partial pressure.

However, from the mass account point of view, the mass of each gas component are equivalent between the model and the reality, as long as the ideal gas assumption is valid. This aspect is discussed again later in Section 2.3.2

Note that the volume fractions of fluids defined above are based on the fluid volume in cells after subtracting the melt volume. This fluid volume in a cell is denoted by V in the followings.

Conservation equations

Conservation equations for mass and energy of each component are formulated as follows:

$$\frac{\partial}{\partial t}(V\alpha_k\rho_k) + \nabla \cdot (V\alpha_k\rho_k\mathbf{v}_k) = \Gamma_k \quad \text{for mass, and} \quad (2.98)$$

$$\begin{aligned} \frac{\partial}{\partial t}(V\alpha_k\rho_k e_k) + \nabla \cdot (V\alpha_k\rho_k e_k\mathbf{v}_k) = & -Vp \left[\frac{\partial\alpha_k}{\partial t} + \nabla \cdot (\alpha_k\mathbf{v}_k) \right] \\ & + q_{ik} + q_{mk} + q_{wk} + \sum_{j \neq k} q_{jk} + \Gamma_k h_k \quad \text{for energy,} \end{aligned} \quad (2.99)$$

where ρ , e , p and \mathbf{v} denote the density, internal energy, pressure and velocity, respectively. The subscript k specifies a component s , l or a . The variable Γ_k denotes the mass generation rate in a cell. Source terms q_{ik} , q_{mk} , q_{wk} and q_{jk} are the heat input from the gas-liquid interface (for water and steam), from the melt, from the wall, and from other components, respectively.

The momentum equation is formulated by

$$\frac{\partial\mathbf{v}_k}{\partial t} + \mathbf{v}_k \cdot \nabla\mathbf{v}_k = -\frac{1}{\rho_k}\nabla p - [K_{ik}(\mathbf{v}_k - \mathbf{v}_i)]_{i \neq k} - \frac{\Gamma_k^+}{V\alpha_k\rho_k}(\mathbf{v}_k - \mathbf{v}_i)_{i \neq k} + \frac{F_{mk}}{V\alpha_k\rho_k} + \mathbf{g} \quad (2.100)$$

The suffix k is either g (gas) or l (liquid water). The total void fraction α and averaged gas properties are used for the phase g . The variables K_{ik} and F_{mk} are the interface friction coefficient and the body force exerted by the melt, respectively. The phase generation term Γ_k^+ equals Γ_k if $\Gamma_k \geq 0$, or otherwise 0.

2.3.2 Constitutive Models

Phase equilibrium under the existence of non-condensable gases

As described above, non-condensable gases are handled in a multi-fluid model, where each component is assumed to occupy a volume fraction α_k , and to be compressed by the total pressure p . While, in the physical reality, the gas components are mixed together extending to the total gas volume fraction (void fraction) α , having lower density corresponding to the partial pressures p_k ($k = s, a_1, a_2, \dots, a_{ng}$). This gap makes, however, no difference in the mass if the gases can be treated as uniformly mixed ideal gases. Besides, the present method has an advantage in easiness of coding because it is a natural extension of the two-fluid model in the original ACE3D code.

The saturation temperature of water is evaluated at the “pseudo partial pressure” of steam defined by

$$p_s = p \frac{\alpha_s}{\alpha}. \quad (2.101)$$

As a result, the saturation temperature becomes a function of α_s and α as well as pressure. Density and internal energy of vapor are also evaluated at the pseudo partial pressure of steam, and the density is converted to the value at the total pressure by

$$\rho_s(p) = \frac{p}{p_s} \rho_s(p_s). \quad (2.102)$$

Evaporation and condensation

The amount of phase change in a cell is defined by

$$\Gamma_s = -\Gamma_l = \frac{-(q_{is} + q_{il}) + q_{int}}{h_s - h_l}, \quad (2.103)$$

$$q_{is} = A_i h_{is} (T_{sat} - T_s), \text{ and} \quad (2.104)$$

$$q_{il} = A_i h_{il} (T_{sat} - T_l), \quad (2.105)$$

where q_{is} and q_{il} are heat exchange rates from the interface to steam and liquid water; q_{int} is the direct heat input to the interface from the melt; h_{is} and h_{il} are interface heat transfer coefficients on the gas side and liquid side, respectively; A_i is the interface area in a cell. Note that the saturation temperature T_{sat} is evaluated at the pseudo partial pressure of steam, p_s .

Exchange among components

Dispersed flow model The interface exchange terms are given based on the dispersed flow model in which either of gas or liquid is considered to be continuous and the other to be dispersed. The regimes are selected according to the void fraction as described in Section 2.1, i.e. bubbly for $\alpha < 0.3$, droplet for $\alpha > 0.75$ and transition in-between.

The averaging scheme for the transition zone, $0.3 \geq \alpha \geq 0.75$, is defined by

$$X_{trans} = (1 - f_\alpha) X_{bubbly}(\alpha = 0.3) + f_\alpha X_{droplet}(\alpha = 0.75) \quad (2.106)$$

with the interpolation function f_α defined by Eq.(2.1).

Following models were used for the exchange coefficients.

- Friction coefficient: dispersed flow friction factor based on correlations used in TRAC-PF1 code[30]

$$K_{ik} = \frac{3}{4} \frac{\alpha_d C_d \rho_c}{d_d} \frac{|\mathbf{v}_k - \mathbf{v}_i|}{\alpha_k \rho_k}, \quad (2.107)$$

$$C_d = \begin{cases} 240 & (Re_d \leq 0.1031) \\ \frac{24}{Re_d} (1 + 0.15 Re_d^{0.687}) & (0.1031 \leq Re_d < 989) \\ 0.44 & (Re_d \geq 989) \end{cases}, \quad (2.108)$$

$$Re_d = \frac{\rho_c d_d V_r}{\mu_c}, \quad (2.109)$$

$$d_d = \frac{We_{cr} \sigma}{\rho_c V_r^2}, \quad (2.110)$$

where suffixes c and d mean continuous and dispersed phases. The critical Weber number to evaluate the diameter of the dispersed phase is set 4.0 for droplets and 7.5 for bubbles. The relative velocity between the dispersed and continuous phases, V_r , that is specifically used for evaluation of the friction factor, C_d , is evaluated either by directly applying the relative velocity $|\mathbf{v}_k - \mathbf{v}_i|$, or by force balance of buoyancy and drag on a bubble or droplet in a steady state (at terminal velocity) given by

$$\frac{\pi}{6} d_d^3 (\rho_l - \rho_g) g = C_d \frac{\pi}{4} d_d^2 \frac{1}{2} \rho_c V_r^2. \quad (2.111)$$

The latter is recommended to avoid troubles caused by numerical (not physical) disturbances in the velocities.

- Heat transfer coefficient: dispersed flow heat transfer coefficient based on correlations used in TRAC-PF1 code[30]

– Bubbly flow, liquid side

$$h_{il} = 0.02\rho_l c_{pl} |\mathbf{v}_l - \mathbf{v}_g| , \quad (2.112)$$

– Bubbly flow, gas side

$$h_{is} = 200 \frac{\lambda_g}{d_d} , \quad (2.113)$$

– Droplet flow, liquid side

$$h_{il} = 0.02\rho_l c_{pl} v_{circ} , \quad (2.114)$$

$$v_{circ} = \min \left\{ 0.5 \frac{\mu_g}{\mu_g + \mu_l} |\mathbf{v}_l - \mathbf{v}_g| , 1.4 \left(\frac{\sigma}{d_d \rho_l} \right)^{1/2} \right\} , \quad (2.115)$$

– Droplet flow, gas side

$$h_{ig} = (2 + 0.74 Re_d^{1/2}) \frac{\lambda_g}{d_d} , \quad (2.116)$$

$$Re_d = \frac{\rho_g d_d |\mathbf{v}_l - \mathbf{v}_g|}{\mu_g} . \quad (2.117)$$

The size of the dispersed phase, d_d , is determined by the same method as that used for the friction factor, i.e. Eqs. (2.110) and (2.111). Once the size is determined, the interface area is given by

$$A_i = \frac{6V\alpha_d}{d_d} . \quad (2.118)$$

Equilibration approach In some cases, heat transfer coefficients to force the system to approach thermal equilibrium state in a certain period might be more effective than the one deduced from a geometrical model. This type of method is used for the heat exchange between steam and non-condensable gases to keep them in close temperatures.

Heat exchange rate [W/K] is given by

$$R_{sa} = \frac{V(\alpha \rho c_p)_m}{\tau_{rsa}} . \quad (2.119)$$

The suffix m means one of two components having less internal energy deviation from the equilibrium state. With this formulation, excess heat in the component of less energy deviation is given up to the other roughly in the order of time τ_{rsa} at temperature difference of 1 K. The time constant is set $\tau_{rsa} \sim 0.1$ s.

Diffusion of steam in gas phase Diffusion of steam in the gas phase is considered by an auxiliary model. Because the basic conservation equations (Eq. (2.98)~(2.100)) do not include the diffusion term between gas components, it may happen that physically unrealistic gaps in steam concentration in the gas field develops, which cause abrupt change of saturation temperature and affect numerical stability. Thus, this diffusion model is implemented not to develop such steam concentration gaps by enhancing intermixing of gas components. Diffusion of steam against the mixture of non-condensable gases is expressed by

$$\frac{\partial V \alpha_s \rho_s}{\partial t} + \nabla \cdot (V \mathbf{j}_s) = 0 \quad (2.120)$$

where \mathbf{j}_s denotes diffusional mass flux of steam, and it is expressed by

$$\mathbf{j}_s = - \left(\frac{c_g^2}{\rho_g} \right) M_s M_{nc} \mathcal{D} \nabla \left(\frac{\alpha_s}{\alpha} \right) , \quad (2.121)$$

where c_g and ρ_g are total molar concentration and total mass concentration of gas mixture, respectively; M_s and M_{nc} are molecular weight of steam and average molecular weight of non-condensable gases, respectively; \mathcal{D} is the diffusion coefficient. The concentrations and the average molecular weight are defined by

$$c_g = \frac{1}{\alpha} \left(\frac{\alpha_s \rho_s}{M_s} + \sum \frac{\alpha_a \rho_a}{M_a} \right) , \quad (2.122)$$

$$\rho_g = \frac{1}{\alpha} (\alpha_s \rho_s + \sum \alpha_a \rho_a) , \text{ and} \quad (2.123)$$

$$M_{nc} = \frac{\sum \alpha_a M_a}{\alpha - \alpha_s} . \quad (2.124)$$

The subscript a denotes non-condensable gas components, $a = a_1, a_2, \dots, a_{ng}$. The diffusion coefficient is given with a large enough value, $\mathcal{D} = 0.01 - 0.1$ [m²/s], that ensures the effect of the model.

This auxiliary model is solved outside of the solution of basic equations. Preceding the solution of the basic equations, volume fraction of steam, α_s , in each cell is modified by equations (2.120) and (2.121). Then, non-condensable gases are moved to compensate the volume (molarity) change of steam in each cell, to keep the consistency of total pressure and total gas volume (molarity). The correction of non-condensable gas volume fractions are given by

$$\frac{\partial V \alpha_a \rho_a}{\partial t} + \nabla \cdot (V \mathbf{j}_a) = 0 , \text{ and} \quad (2.125)$$

$$\mathbf{j}_a = - \mathbf{j}_s \frac{\rho_a}{\rho_s} \frac{\alpha_a}{\alpha - \alpha_s} . \quad (2.126)$$

Exchange with melt

As described later in Section 3.1, melt calculation is done preceding the two-phase flow calculation, and it gives the melt volume, heat exchanged and force exerted in each cell to the two-phase flow model.

Volume The fluid volume in each cell V are obtained as a result of melt calculation. The mass and energy equations have dV/dt term derived from the transient term. The new time and the old time values of V are passed to evaluate them.

Force The force exerted from the melt in a cell is distributed into steam, water and non-condensable gases so that all these components get a same acceleration. Though this treatment is not precise in view of physics, it is a simple and numerically stable method that also gives a physically reasonable result.

Heat The heat release from the melt in a cell is distributed into steam, water, steam-water interface and non-condensable gases. The heat deposited on the interface is used directly for evaporation. Rules for the partition of heat is as follows.

- Cells not including melt heat source (Fig. 2.7): Heat transfer between bulk water/gas is considered. The heat deposited/removed at the gas-liquid interface is used for evaporation/condensation. (Eq. (2.103))

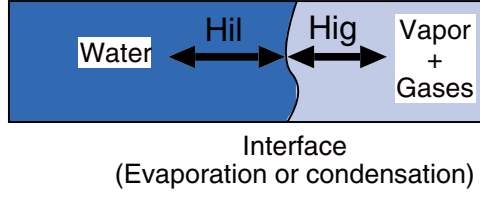
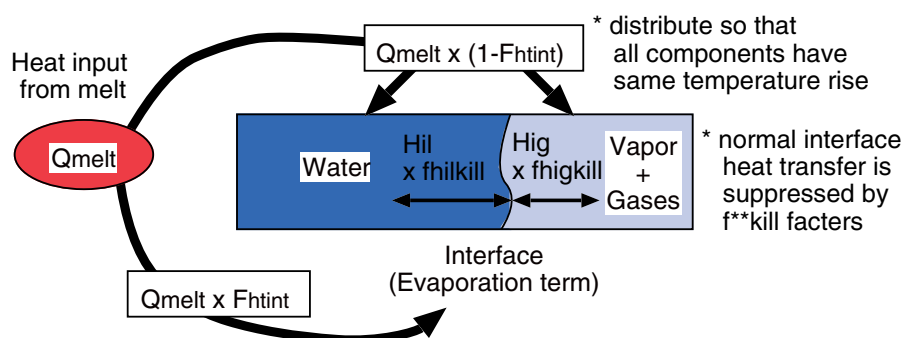


Figure 2.7: Heat partition scheme for cells not including melt heat source.

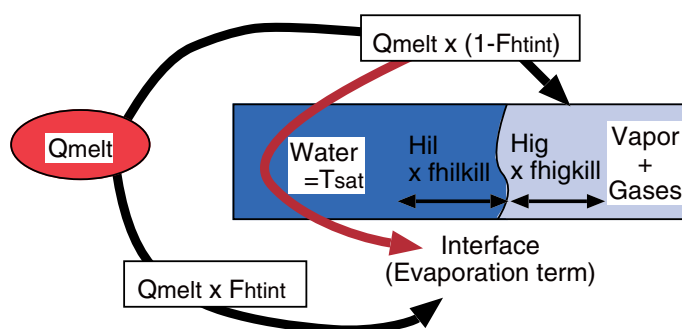
- Cells including melt heat source (premixing) (Fig. 2.8):
 1. Basic concept: A fraction F_{htint} (~ 0.02 is recommended at present) of the heat input from the melt is deposited at the interface for evaporation. The rest of the heat is distributed to water, steam and non-condensable gases so that every component has same temperature rise. Normal gas-liquid interface heat transfer is suppressed with factors $f_{higkill}$ and $f_{hilkill}$, typically 0.1 and 0.001, respectively, so that the effect of the melt becomes dominant.
 2. Water at T_{sat} : If water temperature reaches saturation temperature, the heat to bulk water is assigned to the gas-liquid interface in stead.
 3. No water: If there is no water (no latent heat capacity), the heat to the interface is assigned to the gas phase in stead.
- Cells including melt heat source (explosion) (Fig. 2.9): A fraction K_{ev} (~ 0.7 is recommended at present) of the heat from melt (fine fragments) is deposited at the gas-liquid interface for evaporation. The rest is assigned to bulk water. Normal heat transfer between the interface and bulk water/gas is suppressed, unless physically unstable conditions of superheated water or supercooled steam, or too high gas temperature arises.

In the above scheme, the method distributing heat to water, steam and non-condensable gases so that they have same temperature rise, is not a physically accurate one. However, we adopted this method due to its simplicity and numerical stability, and experiences that we did not have significant problem with this.

1. Basic heat partition concept



2. If water temperature reaches T_{sat} , the heat to "water" is assigned to the "interface".



3. If there is no water (no-evaporation heat capacity), the heat to "interface" is assigned to the "vapor+gases".

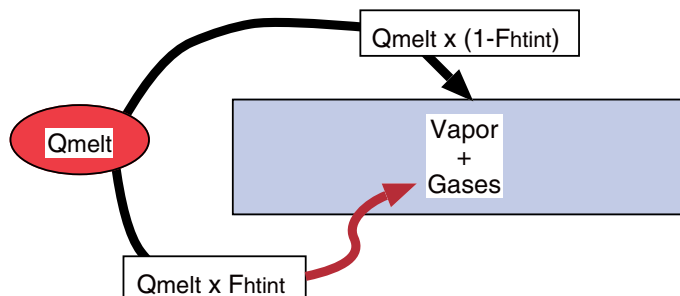


Figure 2.8: Heat partition scheme for cells including melt heat source (premixing).

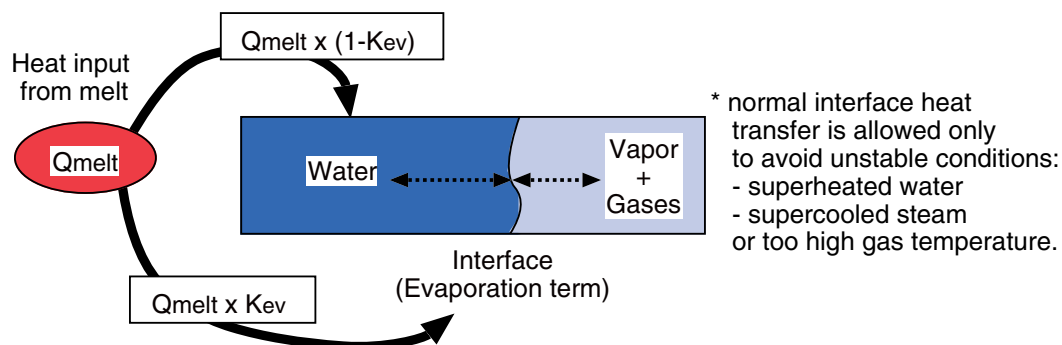


Figure 2.9: Heat partition scheme for cells including melt heat source (explosion).

3 Numerical Solution Method

3.1 Coupling of Melt and Two-Phase Flow Models

Coupling of the melt and two-phase models are made explicitly in time as illustrated in Fig. 3.1. The melt model is called at the beginning of a new time step, referring the two-phase flow variables obtained in the previous step. After interpolating the two-phase flow variables to the melt jet and melt pool grids, and to the location of each particle group, the three melt model components, i.e. jet, particles and pool, are calculated successively, with necessary information exchanges among them: jet out-flow to the pool, jet break-up to the particle, and particle settlement to the pool.

The exchange terms from the melt models, i.e. melt volume, heat transfer and force, are summed for two-phase flow cells and given back to the two-phase flow calculation for update to the next time step.

Figure 3.2 shows the grid that is used for the numerical solution. Melt jet and pool grids are accommodated in the two-phase grid on x - z plain.

In the following sections (Sections 3.2 and 3.3), solution methods for the sub-models are described.

3.2 Numerical Solution Method for Melt Model

3.2.1 Melt Jet

The conservation equations, Eqs. (2.3)–(2.5), were solved by CIP (cubic-interpolated pseudo-particle) method [31], which is known as a high resolution scheme. Conceptually it is free from numerical diffusion that is caused by finite difference of the advection term. The detail of this method is described in Appendix C.

The grid for the melt jet is fit in the z -direction grid of two-phase flow model, with a manner that one two-phase flow cell is subdivided into $N_{sub}(\sim 5)$ jet cells to give the jet finer resolution than the coolant flow field. A staggered grid is adopted where scalar variables are defined at the cell center and vector variables are defined at the cell boundary. Figure 3.3 shows the geometry of the grid for the melt jet model.

In the CIP method, basic equations are solved simultaneously with their derivatives. A general form of the conservation equations and their derivatives are expressed by

$$\frac{\partial f}{\partial t} + v_J \frac{\partial f}{\partial z} = G, \text{ and} \quad (3.1)$$

$$\frac{\partial f'}{\partial t} + v_J \frac{\partial f'}{\partial z} = G' - f' \frac{\partial v_J}{\partial z}, \quad (3.2)$$

where f and G denote the advected variable and source term, respectively. For the mass, energy and momentum equations, they are expressed as follows.

$$\text{Mass} : f_i = [A_J \rho_J]_i, \quad G_i = -[\sqrt{2\Theta A_J} m_e]_i - [A_J \rho_J]_i \left[\frac{\partial v_J}{\partial z} \right]_i \quad (3.3)$$

$$\text{Energy} : f_i = [e_J]_i, \quad G_i = - \left[\sqrt{\frac{2\Theta}{A_J}} \frac{q}{\rho_J} \right]_i \quad (3.4)$$

$$\text{Momentum} : f_{i+\frac{1}{2}} = [v_J]_{i+\frac{1}{2}},$$

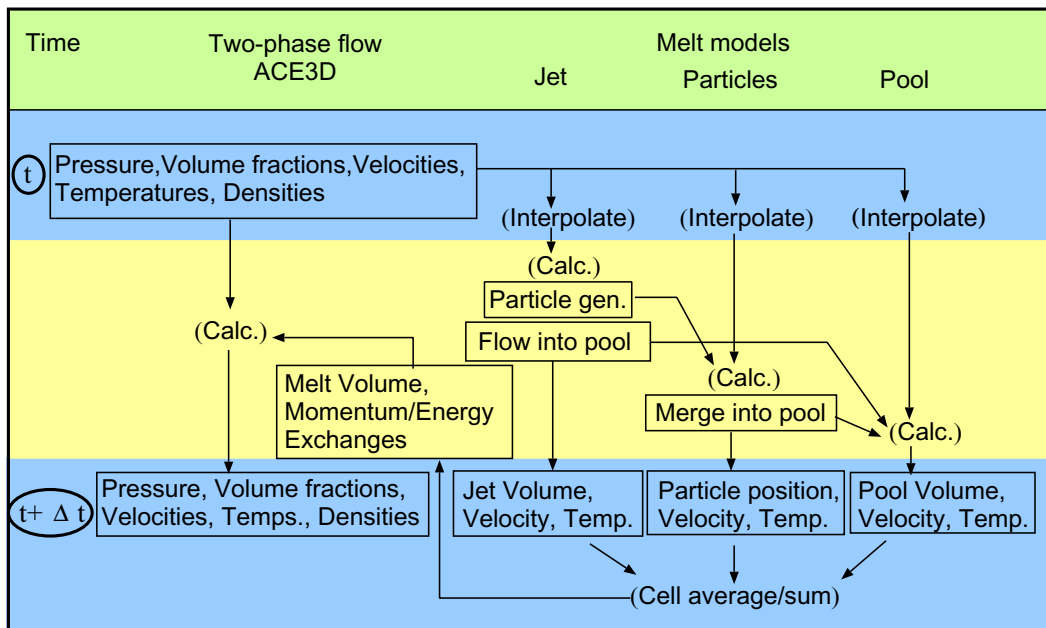


Figure 3.1: Coupling algorithm of melt and two-phase flow models.

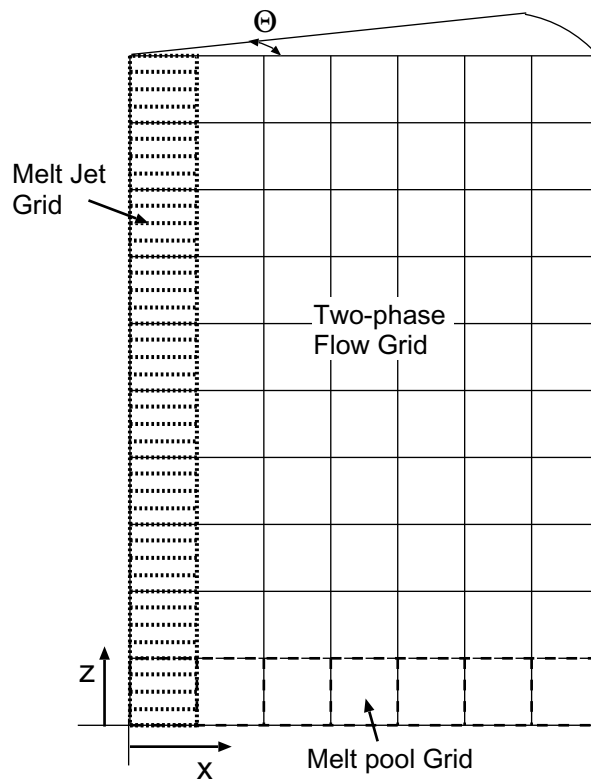


Figure 3.2: Grid for two-phase flow, melt jet and melt pool.

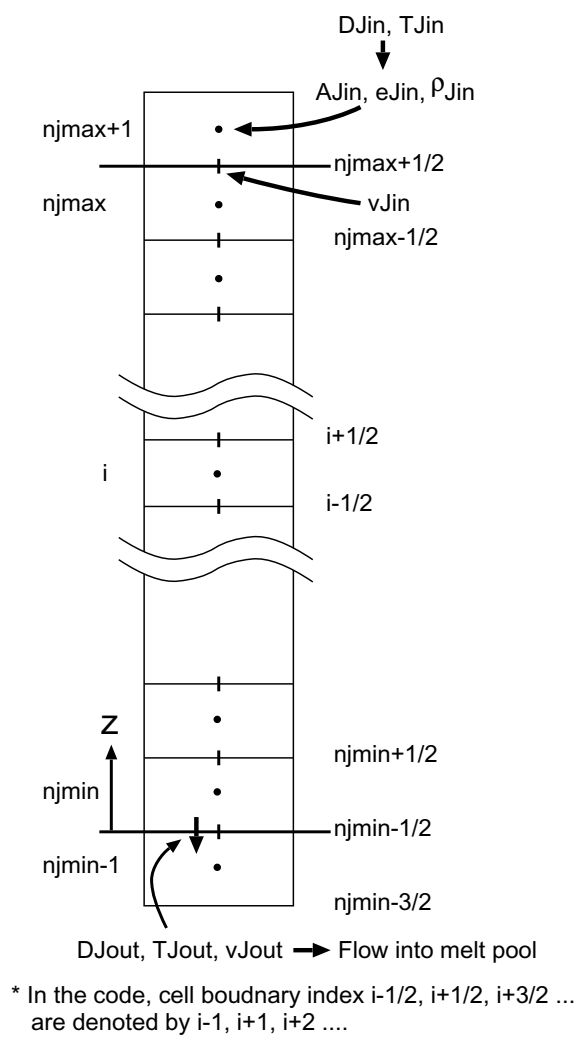


Figure 3.3: Grid geometry and boundary conditions for melt jet model.

$$G_{i+\frac{1}{2}} = - \left[\frac{1}{\rho_J} \frac{\partial p_a}{\partial z} \right]_{i+\frac{1}{2}} + [K_f(v_a - v_J)]_{i+\frac{1}{2}} + g_{i+\frac{1}{2}} \quad (3.5)$$

The suffix i or $i + \frac{1}{2}$ denotes the location of the variable definition. The center of a cell i is represented by i , and its both ends are represented by $i - \frac{1}{2}$ and $i + \frac{1}{2}$.

Because of this difference of the definition points between velocity and other variables we need a scheme for averaging velocities. Interpolation of the velocity and its derivative is given by the followings. It is third-order by taking advantage of having the values of derivatives.

$$[v_J]_i = \frac{1}{2}(v_{J,i+\frac{1}{2}} + v_{J,i-\frac{1}{2}}) - \frac{z_{i+\frac{1}{2}} - z_{i-\frac{1}{2}}}{8}(v'_{J,i+\frac{1}{2}} - v'_{J,i-\frac{1}{2}}), \text{ and} \quad (3.6)$$

$$\left[\frac{\partial v_J}{\partial z} \right]_i = \frac{3}{2(z_{i+\frac{1}{2}} - z_{i-\frac{1}{2}})}(v_{J,i+\frac{1}{2}} - v_{J,i-\frac{1}{2}}) - \frac{1}{4}(v'_{J,i+\frac{1}{2}} + v'_{J,i-\frac{1}{2}}). \quad (3.7)$$

In the momentum equation, the pressure gradient term was discretized as follows.

$$\left[\frac{1}{\rho_J} \frac{\partial p_a}{\partial z} \right]_{i+\frac{1}{2}} = \frac{2}{\rho_{i+1} - \rho_i} \frac{p_{a,i+1} - p_{a,i}}{z_{i+1} - z_i} \quad (3.8)$$

As described in Appendix C in detail, the conservation equations are solved in two steps, i.e. advection and non-advection phases. Starting from the old time step value, f^n , first, the advection phase is calculated with so called CIP1 scheme, and the intermediate value, f^* , is obtained. Then, the non-advection phase is solved by ordinary finite difference scheme and the updated value, f^{n+1} , is obtained.

Boundary conditions are given as follows. (Fig. 3.3)

- At the inlet: velocity, diameter and temperature (internal energy) is given.

$$v_{J,njmax+\frac{1}{2}} = v_{Jin}, D_{J,njmax+1} = D_{Jin}, e_{J,njmax+1} = e_{Jin}$$

Corresponding advected variables are calculated from them. Derivatives are set 0.

- At the bottom: Free flow-out condition is given, i.e. $v_{J,njmin-\frac{3}{2}}$ and $f_{njmin-1}$ ($f = A_J \rho_J$ or e_J) are calculated from advection of linear interpolated profiles for $[njmin - \frac{3}{2}, njmin - \frac{1}{2}]$ and $[njmin - 1, njmin]$, respectively. Derivatives are also obtained from the linear profiles.

Evaluation of the flow out mass needs high accuracy because a large part of the jet mass is passed to the melt pool through it, and the accuracy is directly reflected on the total melt mass conservation. So, the cell centered variables are 3rd order interpolated to the bottom end, $njmin - \frac{1}{2}$, by

$$f_{njmin-\frac{1}{2}} = \frac{1}{2}(f_{njmin} + f_{njmin-1}) + \frac{\Delta}{4}(f'_{njmin-1} - f'_{njmin}), \text{ where} \quad (3.9)$$

$$\Delta = \frac{1}{2}(z_{njmin+\frac{1}{2}} - z_{njmin-\frac{1}{2}}). \quad (3.10)$$

Then, the variables passed to the pool, i.e. jet diameter D_{Jout} , velocity v_{Jout} and temperature T_{Jout} , are evaluated by averaging the new and old time step values.

3.2.2 Melt Pool

The one-dimensional (radial direction) grid for the melt pool resides in a single layer of the two-phase flow grid on the bottom. The pool model uses the same x -direction grid with the two-phase flow model. Figure 3.4 shows the grid geometry for the melt pool model. A conventional upwind scheme with a staggered mesh, i.e. velocities defined at cell boundaries $i - \frac{1}{2}$ and $i + \frac{1}{2}$, and

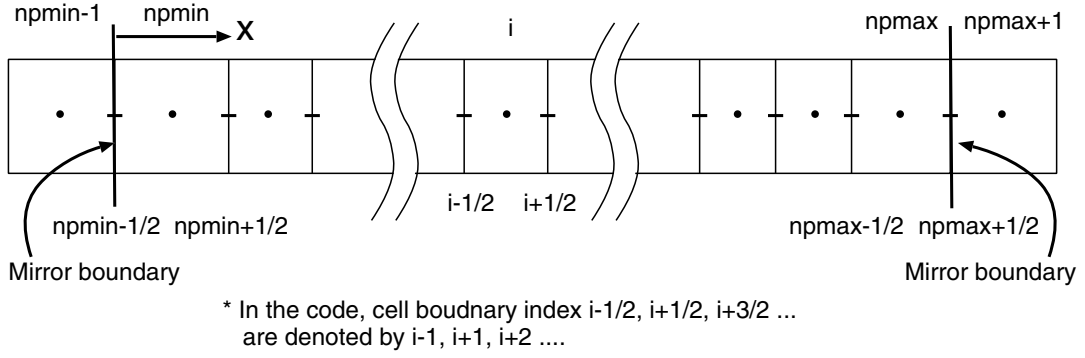


Figure 3.4: Grid geometry and boundary conditions for melt pool model.

other variables at the cell center i , and the SIMPLE algorithm [32] were applied for numerical solution.

The finite difference form of the conservation equations Eqs. (2.20)–(2.22) are expressed as follows.

$$\begin{aligned} \frac{f_i^{n+1} - f_i^n}{\Delta t} = & - \frac{1}{x_{i+\frac{1}{2}} - x_{i-\frac{1}{2}}} \left[\{ \max(v_{i+\frac{1}{2}}, 0) f_i^{n+1} + \min(v_{i+\frac{1}{2}}, 0) f_{i+1}^{n+1} \} \right. \\ & \left. - \{ \max(v_{i-\frac{1}{2}}, 0) f_{i-1}^{n+1} + \min(v_{i-\frac{1}{2}}, 0) f_i^{n+1} \} \right] + [wm_s]_i \end{aligned} \quad (3.11)$$

for mass, where $f = wh_P \rho_P$,

$$\begin{aligned} \frac{e_{P,i}^{n+1} - e_{P,i}^n}{\Delta t} = & - \left[\max(v_{P,i}, 0) \frac{e_{P,i}^{n+1} - e_{P,i-1}^{n+1}}{x_i - x_{i-1}} + \min(v_{P,i}, 0) \frac{e_{P,i+1}^{n+1} - e_{P,i}^{n+1}}{x_{i+1} - x_i} \right] \\ & + \left[\frac{q}{h_P \rho_P} + \frac{(e_{ms} - e_P) \max(m_s, 0)}{h_P \rho_P} \right]_i \end{aligned} \quad (3.12)$$

for energy, and

$$\begin{aligned} \frac{v_{P,i+\frac{1}{2}}^{n+1} - v_{P,i+\frac{1}{2}}^n}{\Delta t} = & - \left[\max(v_{P,i+\frac{1}{2}}, 0) \frac{v_{P,i+\frac{1}{2}}^{n+1} - v_{P,i-\frac{1}{2}}^{n+1}}{x_{i+\frac{1}{2}} - x_{i-\frac{1}{2}}} + \min(v_{P,i+\frac{1}{2}}, 0) \frac{v_{P,i+\frac{3}{2}}^{n+1} - v_{P,i+\frac{1}{2}}^{n+1}}{x_{i+\frac{3}{2}} - x_{i+\frac{1}{2}}} \right] \\ & - \frac{1}{\rho_{P,i+\frac{1}{2}}} \left[\frac{p_{a,i+1} - p_{a,i}}{x_{i+1} - x_i} + \frac{g}{2} \frac{[h_P \rho_P]_{i+1} - [h_P \rho_P]_i}{x_{i+1} - x_i} \right] \\ & + \left[K_{fa}(v_a - v_P) - K_{fw} v_P + \frac{(v_{ms} - v_P) \max(m_s, 0)}{h_P \rho_P} \right]_{i+\frac{1}{2}} \end{aligned} \quad (3.13)$$

for momentum.

The mass and momentum equations are solved by the SIMPLE method, first, to obtain the updated velocity and mass fields. Then, the energy equation is solved.

At the center of the melt pool where the melt jet drops into, the pressure by jet impingement,

$$p_{Jin} = \frac{1}{2} \frac{\rho_J v_J^2 D_J^2}{4x_1^2} \quad (3.14)$$

is added to the pool surface pressure p_a , where x_1 is the size of the central cell for the melt pool.

When the melt jet comes into the center of the melt pool, it gives sudden increase of the pool height and velocity, and easily causes numerical instability. To suppress this problem, an artificial viscosity term

$$\frac{\mu_a}{\rho_P} \frac{\partial^2 v_P}{\partial x^2} \quad (3.15)$$

is added to the right hand side of the momentum equation. The artificial viscosity by Fletcher[33]

$$\frac{\mu_a}{\rho_P} = \begin{cases} (b_0 \Delta x)^2 \left| \frac{\partial v_P}{\partial x} \right| & \text{if } \frac{\partial v_P}{\partial x} v_P < 0, \text{ or} \\ 0 & \text{otherwise} \end{cases} \quad (3.16)$$

is used with the constant $b_0 \sim 10$. The discretized form of the artificial viscosity term, when it is not zero, is given by

$$\left[\frac{\mu_a}{\rho_P} \frac{\partial^2 v_P}{\partial x^2} \right]_{i+\frac{1}{2}} = b_0^2 (x_{i+1} - x_i) \left| \frac{\partial v_P}{\partial x} \right|_{DW} \left\{ \frac{v_{P,i+\frac{3}{2}}^{n+1} - v_{P,i+\frac{1}{2}}^{n+1}}{x_{i+\frac{3}{2}} - x_{i+\frac{1}{2}}} - \frac{v_{P,i+\frac{1}{2}}^{n+1} - v_{P,i-\frac{1}{2}}^{n+1}}{x_{i+\frac{1}{2}} - x_{i-\frac{1}{2}}} \right\}, \quad (3.17)$$

where the velocity gradient with suffix DW means down-wind finite difference, given by

$$\left| \frac{\partial v_P}{\partial x} \right|_{DW} = \begin{cases} \left| \frac{v_{P,i+\frac{3}{2}} - v_{P,i+\frac{1}{2}}}{x_{i+\frac{3}{2}} - x_{i+\frac{1}{2}}} \right| & \text{if } v_{P,i+\frac{1}{2}} > 0, \text{ or} \\ \left| \frac{v_{P,i+\frac{1}{2}} - v_{P,i-\frac{1}{2}}}{x_{i+\frac{1}{2}} - x_{i-\frac{1}{2}}} \right| & \text{otherwise.} \end{cases} \quad (3.18)$$

Boundary conditions at both ends of the grid are given as mirror conditions. (Fig. 3.4) The velocity is set 0 at $npmin - \frac{1}{2}$ and $npmax + \frac{1}{2}$. Cell centered variables, i.e. pool hight and internal energy, in the boundary cells are given by

$$f_{npmin-1} = f_{npmin} \frac{w_{npmin-1}}{w_{npmin}}, \quad (3.19)$$

$$f_{npmax+1} = f_{npmax} \frac{w_{npmax+1}}{w_{npmax}}. \quad (3.20)$$

3.2.3 Melt Particle

The kinetic and energy conservation equations for a particle in a particle group, Eq. (2.40)–(2.42), are solved by a simple explicit scheme for time advancement,

$$\frac{\mathbf{v}_p^{n+1} - \mathbf{v}_p^n}{\Delta t} = \mathbf{g} - \frac{\nabla p_a}{\rho_p} + \frac{\mathbf{F}_{hy}}{m_p}, \quad (3.21)$$

$$\frac{\mathbf{x}_p^{n+1} - \mathbf{x}_p^n}{\Delta t} = \mathbf{v}_p^{n+1}, \text{ and} \quad (3.22)$$

$$\frac{e_p^{n+1} - e_p^n}{\Delta t} = \frac{q}{m_p}. \quad (3.23)$$

Additional equations for the explosion process, Eqs. (2.82)–(2.84), are also solved in the same way.

$$\frac{m_p^{n+1} - m_p^n}{\Delta t} = -\dot{m}_f \quad (3.24)$$

$$\frac{M_f^{n+1} - M_f^n}{\Delta t} = n_p \dot{m}_f, \text{ and} \quad (3.25)$$

$$\frac{e_f^{n+1} - e_f^n}{\Delta t} = e_p \frac{n_p \dot{m}_f}{M_f} - \dot{q}_f. \quad (3.26)$$

Evaluation of the variables ∇p_a , \mathbf{F}_{hy} , q , \dot{m}_f and \dot{q}_f needs interpolation of two-phase flow variables to the location of particle groups. For this purpose, the indexes, i and k , of two-phase flow cells in which particle groups exist are searched by bi-section algorithm, and the interpolation of two-phase flow variables is done at the start of the calculation of the melt particle model.

During the calculation, the melt volume, force and heat exchanged with the two-phase flow are summed and stored for every two-phase flow cell and passed to the two-phase flow model.

3.3 Numerical Solution Method for Two-Phase Flow

3.3.1 Overall Scope

Figure 3.5 shows the geometry of the grid for two-phase flow model. The ACE3D code is originally a 3D two-phase flow code, capable of solving a 3D basic equation set on Cartesian or cylindrical coordinate. JASMINE uses the code, however, with limitation of the geometry to 2D cylindrical coordinate. In the followings, equations are expressed in 3D Cartesian system for brevity.

Numerical solutions are obtained by a conventional finite difference method, i.e. semi-implicit scheme for time advancement, staggered grid and upwind scheme for spatial discretization. Practically, the following $10 + 2n_g$ discretized equations are solved.

- Mass: steam, steam+water, non-condensable gases ($2 + n_g$)
- Energy: steam, steam+water, non-condensable gases ($2 + n_g$)
- Momentum: gas (steam and non-condensable gases), water ($2 \text{ phases} \times 3 \text{ directions} = 6$)

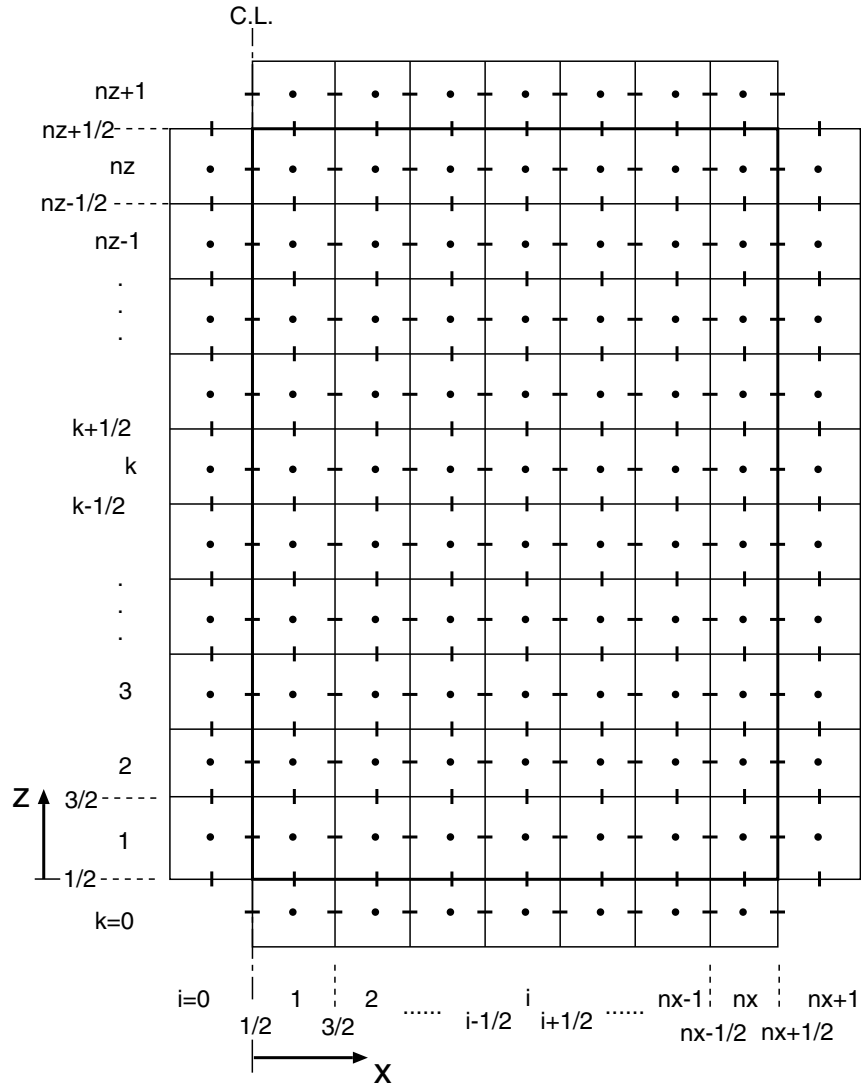
Independent variables solved for are the total pressure, $2 + n_g$ temperatures, $1 + n_g$ volume fractions (water volume fraction is known if others are obtained), and 3 velocity components for 2 phases— $10 + 2n_g$ variables in total.

The mass and energy equations of the water-steam mixture are included so that at least one of the two equations is kept significant when either of water or steam is vanished. Also, a variable conversion, $T \rightarrow \alpha T$, is done in constructing the innermost system equation set which is solved by matrix inversion and Newtonian iteration, not to have singularity for vanished components.

The overall solution method is briefly as follows. The velocities at the new time step can be expressed by pressures in the adjacent cells by transforming momentum equations. By using these expressions, velocities are eliminated from mass and energy equations. The mass and energy equations are, then, linearized for the variance of independent variables, i.e. pressure, volume fractions of steam and non-condensable gases, and αT of all the components. Thus, a system of linear equations for Newtonian iteration is obtained. A set of pressure equation, that only includes pressure at adjacent cells, is picked from the linear system. In solving the linear system, pressure correction is obtained first by the pressure equation, then correction of other variables are obtained by substituting the pressure correction into the rest of the equations in the linear system. This process is iterated until residual becomes small enough, then all the variables except velocities at the new time step are obtained. Finally, velocities are calculated from pressure distribution by the momentum equations.

3.3.2 Finite Difference Form of Basic Equations

In the following expressions, suffix i , j and k denote $x(r)$, $y(\theta)$ and z direction indexes of the coordinates, respectively. When the coordinate index is omitted, that means the location where the equation is defined. (e.g. $p_{i,j,k} \rightarrow p$, $u_{i+\frac{1}{2},j,k} \rightarrow u$) Suffix m denotes a component either s (steam), l (water) or a ($= a_1, a_2, \dots, a_{n_g}$) (non-condensable gas) for the mass and energy equations.



- * Only x-z plain is shown. JASMINE uses only $j=1$ layer in $y(\text{theta})$ -direction of 3D field supported by ACE3D.
- * In the code, cell boudnary index $i-1/2$, $i+1/2$, $i+3/2$... are denoted by $i-1$, $i+1$, $i+2$

Figure 3.5: Grid geometry for two-phase flow model.

In the momentum equation, m denotes either of g (gas mixture) or l (water). Superscripts n and $n+1$ denote the old and new time step values. An expression $v \langle X \rangle$ means that the variable X is taken at the upwind side of the velocity definition point for v . For example, if $u_{i+\frac{1}{2}} > 0$, $u \langle X \rangle = u_{i+\frac{1}{2}} X_i$.

Mass at (i, j, k) :

$$\begin{aligned}
 M_m = & V \{ (\alpha_m \rho_m)^{n+1} - (\alpha_m \rho_m)^n \} + \Delta t \frac{dV}{dt} (\alpha_m \rho_m)^n \\
 & + \Delta t V \frac{\langle \alpha_m \rho_m \rangle_{i+\frac{1}{2},j,k}^n u_{m,i+\frac{1}{2},j,k}^{n+1} - \langle \alpha_m \rho_m \rangle_{i-\frac{1}{2},j,k}^n u_{m,i-\frac{1}{2},j,k}^{n+1}}{x_{i+\frac{1}{2}} - x_{i-\frac{1}{2}}} \\
 & + \Delta t V \frac{\langle \alpha_m \rho_m \rangle_{i,j+\frac{1}{2},k}^n v_{m,i,j+\frac{1}{2},k}^{n+1} - \langle \alpha_m \rho_m \rangle_{i,j-\frac{1}{2},k}^n v_{m,i,j-\frac{1}{2},k}^{n+1}}{y_{j+\frac{1}{2}} - y_{j-\frac{1}{2}}} \\
 & + \Delta t V \frac{\langle \alpha_m \rho_m \rangle_{i,j,k+\frac{1}{2}}^n w_{m,i,j,k+\frac{1}{2}}^{n+1} - \langle \alpha_m \rho_m \rangle_{i,j,k-\frac{1}{2}}^n w_{m,i,j,k-\frac{1}{2}}^{n+1}}{z_{k+\frac{1}{2}} - z_{k-\frac{1}{2}}} \\
 & - \Delta t \Gamma_m^{n+1} = 0
 \end{aligned} \tag{3.27}$$

Energy at (i, j, k) :

$$\begin{aligned}
 E_m = & V \{ (\alpha_m \rho_m e_m)^{n+1} - (\alpha_m \rho_m e_m)^n \} + \Delta t \frac{dV}{dt} (\alpha_m \rho_m e_m)^n \\
 & + \Delta t V \frac{\langle \alpha_m \rho_m e_m \rangle_{i+\frac{1}{2},j,k}^n u_{m,i+\frac{1}{2},j,k}^{n+1} - \langle \alpha_m \rho_m e_m \rangle_{i-\frac{1}{2},j,k}^n u_{m,i-\frac{1}{2},j,k}^{n+1}}{x_{i+\frac{1}{2}} - x_{i-\frac{1}{2}}} \\
 & + \Delta t V \frac{\langle \alpha_m \rho_m e_m \rangle_{i,j+\frac{1}{2},k}^n v_{m,i,j+\frac{1}{2},k}^{n+1} - \langle \alpha_m \rho_m e_m \rangle_{i,j-\frac{1}{2},k}^n v_{m,i,j-\frac{1}{2},k}^{n+1}}{y_{j+\frac{1}{2}} - y_{j-\frac{1}{2}}} \\
 & + \Delta t V \frac{\langle \alpha_m \rho_m e_m \rangle_{i,j,k+\frac{1}{2}}^n w_{m,i,j,k+\frac{1}{2}}^{n+1} - \langle \alpha_m \rho_m e_m \rangle_{i,j,k-\frac{1}{2}}^n w_{m,i,j,k-\frac{1}{2}}^{n+1}}{z_{k+\frac{1}{2}} - z_{k-\frac{1}{2}}} \\
 & + \Delta t V p \left[\frac{\alpha_m^{n+1} - \alpha_m^n}{\Delta t} + \frac{\langle \alpha_m \rangle_{i+\frac{1}{2},j,k}^n u_{m,i+\frac{1}{2},j,k}^{n+1} - \langle \alpha_m \rangle_{i-\frac{1}{2},j,k}^n u_{m,i-\frac{1}{2},j,k}^{n+1}}{x_{i+\frac{1}{2}} - x_{i-\frac{1}{2}}} \right. \\
 & + \frac{\langle \alpha_m \rangle_{i,j+\frac{1}{2},k}^n v_{m,i,j+\frac{1}{2},k}^{n+1} - \langle \alpha_m \rangle_{i,j-\frac{1}{2},k}^n v_{m,i,j-\frac{1}{2},k}^{n+1}}{y_{j+\frac{1}{2}} - y_{j-\frac{1}{2}}} \\
 & \left. + \frac{\langle \alpha_m \rangle_{i,j,k+\frac{1}{2}}^n w_{m,i,j,k+\frac{1}{2}}^{n+1} - \langle \alpha_m \rangle_{i,j,k-\frac{1}{2}}^n w_{m,i,j,k-\frac{1}{2}}^{n+1}}{z_{k+\frac{1}{2}} - z_{k-\frac{1}{2}}} \right] \\
 & - \Delta t \left\{ q_{im}^{n+1} + q_m^n + q_w^n + \sum_{j \neq m} q_{jm}^{n+1} + \Gamma_m^{n+1} h_m^{n+1} \right\} = 0
 \end{aligned} \tag{3.28}$$

Momentum, x -direction at $(i + \frac{1}{2}, j, k)$:

$$\begin{aligned}
 & \frac{u_m^{n+1} - u_m^n}{\Delta t} + u_m^n \left\langle \frac{\partial u_m}{\partial x} \right\rangle_{i+\frac{1}{2},j,k} + v_m^n \left\langle \frac{\partial u_m}{\partial y} \right\rangle_{i+\frac{1}{2},j,k} + w_m^n \left\langle \frac{\partial u_m}{\partial z} \right\rangle_{i+\frac{1}{2},j,k} \\
 & + \frac{1}{\rho_m} \frac{p_{i+1}^{n+1} - p_i^{n+1}}{x_{i+1} - x_i} + \left[K_{im} + \frac{\Gamma_m^+}{V \alpha_m \rho_m} \right] (u_m^{n+1} - u_i^{n+1})_{i \neq m}
 \end{aligned}$$

$$- \frac{F_{mk}}{V\alpha_m\rho_m} - g_x = 0 \quad (3.29)$$

The momentum equations constitute simultaneous equations of u_g and u_l . By solving them analytically, we obtain expressions of u_g and u_l at the new time step in terms of pressure at new time step,

$$u_{g,i+\frac{1}{2}}^{n+1} = C_{gx,i+\frac{1}{2}} + D_{gx,i+\frac{1}{2}}(p_{i+1}^{n+1} - p_i^n), \quad (3.30)$$

$$u_{l,i+\frac{1}{2}}^{n+1} = C_{lx,i+\frac{1}{2}} + D_{lx,i+\frac{1}{2}}(p_{i+1}^{n+1} - p_i^n), \quad (3.31)$$

where C_{gx} , D_{gx} , C_{lx} , D_{lx} are constants (including only old time step variables). In the same way, expression of every component of gas and liquid velocities in terms of pressure is obtained.

$$v_{g,j+\frac{1}{2}}^{n+1} = C_{gy,j+\frac{1}{2}} + D_{gy,j+\frac{1}{2}}(p_{j+1}^{n+1} - p_j^n), \quad (3.32)$$

$$v_{l,j+\frac{1}{2}}^{n+1} = C_{ly,j+\frac{1}{2}} + D_{ly,j+\frac{1}{2}}(p_{j+1}^{n+1} - p_j^n), \quad (3.33)$$

$$w_{g,k+\frac{1}{2}}^{n+1} = C_{gz,k+\frac{1}{2}} + D_{gz,k+\frac{1}{2}}(p_{k+1}^{n+1} - p_k^n), \quad (3.34)$$

$$w_{l,k+\frac{1}{2}}^{n+1} = C_{lz,k+\frac{1}{2}} + D_{lz,k+\frac{1}{2}}(p_{k+1}^{n+1} - p_k^n). \quad (3.35)$$

These equations are substituted into mass and energy equations to eliminate velocities at the new time step.

After eliminating velocities, Eqs. (3.27) and (3.28) are expressed in the following form,

$$\begin{aligned} & M_m(p^{n+1}, p_{adj}^{n+1}, \alpha_m^{n+1}, T_m^{n+1}) \\ &= V(\alpha_m\rho_m)^{n+1} + V \sum_{adj} \tilde{m}_{m,adj}(p_{adj}^{n+1} - p^{n+1}) - \Delta t \Gamma_m^{n+1} \\ &+ (\alpha_m\rho_m)^n \frac{dV}{dt} \Delta t - V \tilde{M}_m = 0 \\ & E_m(p^{n+1}, p_{adj}^{n+1}, \alpha_m^{n+1}, T_m^{n+1}) \\ &= V(\alpha_m\rho_m e_m)^{n+1} + V \sum_{adj} (\tilde{e}_{m,adj}^{(1)} + \tilde{e}_{m,adj}^{(2)} p^{n+1})(p_{adj}^{n+1} - p^{n+1}) \\ &+ V p^{n+1} \alpha_m^{n+1} + V p^{n+1} \tilde{D}_m - \Delta t (q_{im}^{n+1} + \Gamma_m^{n+1} h_m^{n+1}) - \Delta t \sum_{j \neq m} q_{jm}^{n+1} \\ &- V \tilde{E}_m + (\alpha_m\rho_m e_m)^n \frac{dV}{dt} \Delta t = 0. \end{aligned} \quad (3.36)$$

The suffix *adj* means adjacent cells; m denotes either of s (steam), l (water) or a_i (i -th element of non-condensable gases). Symbols $\tilde{m}_{m,adj}$, \tilde{M}_m , $\tilde{e}_{m,adj}^{(n)}$, \tilde{D}_m and \tilde{E}_m are constants including only old time values, and are derived from the advection terms. The summation in the second term of the right hand side of mass equation, Eq. (3.36), is expanded as

$$\begin{aligned} \sum_{adj} \tilde{m}_{m,adj}(p_{adj}^{n+1} - p^{n+1}) &= \frac{\Delta t}{x_{i+\frac{1}{2}} - x_{i-\frac{1}{2}}} D_{mx,i+\frac{1}{2}} \langle \alpha_m\rho_m \rangle_{i+\frac{1}{2}} (p_{i+1}^{n+1} - p^{n+1}) \\ &+ \frac{\Delta t}{x_{i+\frac{1}{2}} - x_{i-\frac{1}{2}}} D_{mx,i-\frac{1}{2}} \langle \alpha_m\rho_m \rangle_{i-\frac{1}{2}} (p_{i-1}^{n+1} - p^{n+1}) \\ &+ \frac{\Delta t}{y_{j+\frac{1}{2}} - y_{j-\frac{1}{2}}} D_{my,j+\frac{1}{2}} \langle \alpha_m\rho_m \rangle_{j+\frac{1}{2}} (p_{j+1}^{n+1} - p^{n+1}) \\ &+ \frac{\Delta t}{y_{j+\frac{1}{2}} - y_{j-\frac{1}{2}}} D_{my,j-\frac{1}{2}} \langle \alpha_m\rho_m \rangle_{j-\frac{1}{2}} (p_{j-1}^{n+1} - p^{n+1}) \end{aligned}$$

$$\begin{aligned}
 & + \frac{\Delta t}{z_{k+\frac{1}{2}} - z_{k-\frac{1}{2}}} D_{mz,k+\frac{1}{2}} \langle \alpha_m \rho_m \rangle_{k+\frac{1}{2}} (p_{k+1}^{n+1} - p^{n+1}) \\
 & + \frac{\Delta t}{z_{k+\frac{1}{2}} - z_{k-\frac{1}{2}}} D_{mz,k-\frac{1}{2}} \langle \alpha_m \rho_m \rangle_{k-\frac{1}{2}} (p_{k-1}^{n+1} - p^{n+1}) . \quad (3.38)
 \end{aligned}$$

The constant \widetilde{M}_m is expressed by

$$\begin{aligned}
 \widetilde{M}_m & = \alpha_m \rho_m \\
 & + \Delta t \frac{\langle \alpha_m \rho_m \rangle_{i+\frac{1}{2}} C_{mx,i+\frac{1}{2}} - \langle \alpha_m \rho_m \rangle_{i-\frac{1}{2}} C_{mx,i-\frac{1}{2}}}{x_{i+\frac{1}{2}} - x_{i-\frac{1}{2}}} \\
 & + \Delta t \frac{\langle \alpha_m \rho_m \rangle_{j+\frac{1}{2}} C_{my,j+\frac{1}{2}} - \langle \alpha_m \rho_m \rangle_{j-\frac{1}{2}} C_{my,j-\frac{1}{2}}}{y_{j+\frac{1}{2}} - y_{j-\frac{1}{2}}} \\
 & + \Delta t \frac{\langle \alpha_m \rho_m \rangle_{k+\frac{1}{2}} C_{mz,k+\frac{1}{2}} - \langle \alpha_m \rho_m \rangle_{k-\frac{1}{2}} C_{mz,k-\frac{1}{2}}}{z_{k+\frac{1}{2}} - z_{k-\frac{1}{2}}} . \quad (3.40)
 \end{aligned}$$

The summation in the second term of the right hand side of energy equation, Eq. (3.37), is expanded as

$$\begin{aligned}
 \sum_{adj} (\tilde{e}_{m,adj}^{(1)} + \tilde{e}_{m,adj}^{(2)} p^{n+1}) (p_{adj}^{n+1} - p^{n+1}) = \\
 \frac{\Delta t}{x_{i+\frac{1}{2}} - x_{i-\frac{1}{2}}} D_{mx,i+\frac{1}{2}} (\langle \alpha_m \rho_m e_m \rangle_{i+\frac{1}{2}} + \langle \alpha_m \rangle_{i+\frac{1}{2}} p^{n+1}) (p_{i+1}^{n+1} - p^{n+1}) \\
 \frac{\Delta t}{x_{i+\frac{1}{2}} - x_{i-\frac{1}{2}}} D_{mx,i-\frac{1}{2}} (\langle \alpha_m \rho_m e_m \rangle_{i-\frac{1}{2}} + \langle \alpha_m \rangle_{i-\frac{1}{2}} p^{n+1}) (p_{i-1}^{n+1} - p^{n+1}) \\
 \frac{\Delta t}{y_{j+\frac{1}{2}} - y_{j-\frac{1}{2}}} D_{my,j+\frac{1}{2}} (\langle \alpha_m \rho_m e_m \rangle_{j+\frac{1}{2}} + \langle \alpha_m \rangle_{j+\frac{1}{2}} p^{n+1}) (p_{j+1}^{n+1} - p^{n+1}) \\
 \frac{\Delta t}{y_{j+\frac{1}{2}} - y_{j-\frac{1}{2}}} D_{my,j-\frac{1}{2}} (\langle \alpha_m \rho_m e_m \rangle_{j-\frac{1}{2}} + \langle \alpha_m \rangle_{j-\frac{1}{2}} p^{n+1}) (p_{j-1}^{n+1} - p^{n+1}) \\
 \frac{\Delta t}{z_{k+\frac{1}{2}} - z_{k-\frac{1}{2}}} D_{mz,k+\frac{1}{2}} (\langle \alpha_m \rho_m e_m \rangle_{k+\frac{1}{2}} + \langle \alpha_m \rangle_{k+\frac{1}{2}} p^{n+1}) (p_{k+1}^{n+1} - p^{n+1}) \\
 \frac{\Delta t}{z_{k+\frac{1}{2}} - z_{k-\frac{1}{2}}} D_{mz,k-\frac{1}{2}} (\langle \alpha_m \rho_m e_m \rangle_{k-\frac{1}{2}} + \langle \alpha_m \rangle_{k-\frac{1}{2}} p^{n+1}) (p_{k-1}^{n+1} - p^{n+1}) . \quad (3.41)
 \end{aligned}$$

The constant \widetilde{D}_m and \widetilde{E}_m are expressed by

$$\begin{aligned}
 \widetilde{D}_m & = -\alpha_m \\
 & + \frac{\Delta t}{x_{i+\frac{1}{2}} - x_{i-\frac{1}{2}}} (\langle \alpha_m \rangle_{i+\frac{1}{2}} C_{mx,i+\frac{1}{2}} - \langle \alpha_m \rangle_{i-\frac{1}{2}} C_{mx,i-\frac{1}{2}}) \\
 & + \frac{\Delta t}{y_{j+\frac{1}{2}} - y_{j-\frac{1}{2}}} (\langle \alpha_m \rangle_{j+\frac{1}{2}} C_{my,j+\frac{1}{2}} - \langle \alpha_m \rangle_{j-\frac{1}{2}} C_{my,j-\frac{1}{2}}) \\
 & + \frac{\Delta t}{z_{k+\frac{1}{2}} - z_{k-\frac{1}{2}}} (\langle \alpha_m \rangle_{k+\frac{1}{2}} C_{mz,k+\frac{1}{2}} - \langle \alpha_m \rangle_{k-\frac{1}{2}} C_{mz,k-\frac{1}{2}}) , \text{ and} \quad (3.42)
 \end{aligned}$$

$$\widetilde{E}_m = \alpha_m \rho_m e_m + \Delta t \frac{q_{melt,m}}{V}$$

$$\begin{aligned}
 & - \frac{\Delta t}{x_{i+\frac{1}{2}} - x_{i-\frac{1}{2}}} (\langle \alpha_m \rho_m e_m \rangle_{i+\frac{1}{2}} C_{mx,i+\frac{1}{2}} - \langle \alpha_m \rho_m e_m \rangle_{i-\frac{1}{2}} C_{mx,i-\frac{1}{2}}) \\
 & - \frac{\Delta t}{y_{j+\frac{1}{2}} - y_{j-\frac{1}{2}}} (\langle \alpha_m \rho_m e_m \rangle_{j+\frac{1}{2}} C_{my,j+\frac{1}{2}} - \langle \alpha_m \rho_m e_m \rangle_{j-\frac{1}{2}} C_{my,j-\frac{1}{2}}) \\
 & - \frac{\Delta t}{z_{k+\frac{1}{2}} - z_{k-\frac{1}{2}}} (\langle \alpha_m \rho_m e_m \rangle_{k+\frac{1}{2}} C_{mz,k+\frac{1}{2}} - \langle \alpha_m \rho_m e_m \rangle_{k-\frac{1}{2}} C_{mz,k-\frac{1}{2}}) . \quad (3.43)
 \end{aligned}$$

Now, the mass and energy equations at a cell (i, j, k) include pressure, volume fractions and temperatures at the local cell and pressure at adjacent cells $(i \pm 1, j \pm 1 \text{ and } k \pm 1)$ as unknown variables. In other words, the equations for a cell is connected with those of adjacent cells only through pressure, and the dependence is linear. The dependence on the variables in the local cell is, however, non-linear, through the phase change term and physical properties.

So, the mass and energy equations are solved by Newtonian iteration as described later in Section 3.3.4.

3.3.3 Boundary Condition Settings

Boundary condition for velocities

Boundary conditions for velocities are categorized and given by the followings. Expressions are given at the cell $(i, 1, 1)$ as an example (See Fig. 3.5).

Normal velocity The normal velocity is defined on the wall surface. Therefore, the condition is given by setting it adequately through Eqs. (3.30)~(3.35).

- Fill: given velocity at the wall surface; $w_{i,1,\frac{1}{2}} = w_{in}$, that is satisfied by setting $C_{mz,\frac{1}{2}} = w_{in}$ and $D_{mz,\frac{1}{2}} = 0$ ($m = g$ or l)
- Break: given pressure at the boundary cell $(p_{i,1,0})$ (outside of the system), solution of the momentum equation to obtain $w_{i,1,\frac{1}{2}}$

Tangential velocity Since the tangential velocity is not defined just on the wall surface, the velocity in the boundary cell $u_{i+\frac{1}{2},1,0}$ (outside of the system) is given in terms of that inside of the system $u_{i+\frac{1}{2},1,1}$ so that the condition on the surface is satisfied.

- Slip: zero shear force at wall surface, i.e. derivative of the tangential velocity in the normal direction $(\partial u / \partial z) = 0$;
 $u_{i+\frac{1}{2},1,0} = u_{i+\frac{1}{2},1,1}$
- Non-slip: zero tangential velocity at wall surface,
 $u_{i+\frac{1}{2},1,\frac{1}{2}} \simeq \frac{\Delta z_1 u_{i+\frac{1}{2},1,0} + \Delta z_0 u_{i+\frac{1}{2},1,1}}{\Delta z_0 + \Delta z_1} = 0 \quad (\Delta z_0 = z_{\frac{1}{2}} - z_{-\frac{1}{2}}, \Delta z_1 = z_{\frac{3}{2}} - z_{\frac{1}{2}});$
 therefore, $u_{i+\frac{1}{2},1,0} = -\frac{\Delta z_0}{\Delta z_1} u_{i+\frac{1}{2},1,1}$

Velocity boundary conditions on other wall surfaces are given in the same manner.

Boundary condition for cell-centered variables

Cell-centered variables, pressure, volume fractions and temperatures, should be given at the boundary with “fill” condition, where inlet velocity is given. Values of those variables are set at the boundary cell so that they are used for the fluid flowing into the system. As an example, when $k = 1/2$ boundary is a “fill” boundary, $p_{i,1,0}$, $\alpha_{m,i,1,0}$ and $T_{m,i,1,0}$ should be given (suffix m denotes a component).

3.3.4 Newtonian Iteration

General method

The solution of a set of non-linear equations

$$F_k(x_1, x_2, \dots, x_i, \dots, x_n) = 0 \quad (3.44)$$

where $k = 1, \dots, n$ is obtained iteratively as follows. Assume that the unknown variables x_i has initial values that give non-zero values of F_k (residual errors). The desired correction of F_k is

$$\delta F_k = -F_k . \quad (3.45)$$

On the other hand, the variation of F_k is approximated in terms of variation of x_i by Taylor expansion

$$\delta F_k \simeq \frac{\partial F_k}{\partial x_1} \delta x_1 + \frac{\partial F_k}{\partial x_2} \delta x_2 + \dots + \frac{\partial F_k}{\partial x_n} \delta x_n . \quad (3.46)$$

Equations (3.45) and (3.46) gives a linear equation set to give correction values of x_i ,

$$J \begin{pmatrix} \delta x_1 \\ \vdots \\ \delta x_n \end{pmatrix} = - \begin{pmatrix} F_1 \\ \vdots \\ F_n \end{pmatrix} , \quad (3.47)$$

where J denote Jacobian matrix,

$$J = \begin{pmatrix} \partial F_1/\partial x_1 & \partial F_1/\partial x_2 & \dots & \partial F_1/\partial x_n \\ \partial F_2/\partial x_1 & \partial F_2/\partial x_2 & \dots & \partial F_2/\partial x_n \\ \vdots & & & \vdots \\ \partial F_n/\partial x_1 & \partial F_n/\partial x_2 & \dots & \partial F_n/\partial x_n \end{pmatrix} . \quad (3.48)$$

Obtaining the correction values δx_i by solving Eq. (3.47) and doing correction by

$$x_i^{next} = x_i^{current} + \delta x_i \quad (3.49)$$

until the residual errors F_k become close enough to zero makes conversion of the solution (x_1, \dots, x_n) .

Application to the present case

The above method is applied for the mass and energy equations. However, the pressure field is treated differently as follows because it includes connection to adjacent cells. In the present case, the equation for correction, Eq. (3.47), for a cell (i, j, k) is given by

$$J \begin{pmatrix} \delta p \\ \delta \alpha_s \\ \delta \beta_s \\ \delta \beta_l \\ \delta \alpha_{a_1} \\ \delta \beta_{a_1} \\ \vdots \\ \delta \alpha_{a_{ng}} \\ \delta \beta_{a_{ng}} \end{pmatrix} = - \begin{pmatrix} M_{sl} \\ M_s \\ E_s \\ E_{sl} \\ M_{a_1} \\ E_{a_1} \\ \vdots \\ M_{a_{ng}} \\ E_{a_{ng}} \end{pmatrix} - \sum_{adj} \begin{pmatrix} \partial M_{sl}/\partial P_{adj} \\ \partial M_s/\partial P_{adj} \\ \partial E_s/\partial P_{adj} \\ \partial E_{sl}/\partial P_{adj} \\ \partial M_{a_1}/\partial P_{adj} \\ \partial E_{a_1}/\partial P_{adj} \\ \vdots \\ \partial M_{a_{ng}}/\partial P_{adj} \\ \partial E_{a_{ng}}/\partial P_{adj} \end{pmatrix} \delta P_{adj} , \quad (3.50)$$

where suffix sl means sum of the steam and water equations, i.e. $M_{sl} = M_s + M_l$, $E_{sl} = E_s + E_l$; $\beta_m \equiv \alpha_m T_m$ is used as an independent variable instead of T_m to avoid trouble in getting T_m for missing components ($\alpha_m = 0$). The Jacobian matrix J is, for the present case, a matrix of partial derivatives of the variables in the first term in the right hand side by p , α_s , β_s , β_l , α_{a_1} , β_{a_1} , \dots , $\alpha_{a_{ng}}$ and $\beta_{a_{ng}}$.

Note that the pressures in adjacent cells are kept out of the Jacobian matrix and they are solved separately together with all the pressures in the system. By matrix inversion, Eq. (3.50) becomes

$$\begin{pmatrix} \delta p \\ \delta \alpha_s \\ \delta \beta_s \\ \delta \beta_l \\ \delta \alpha_{a_1} \\ \delta \beta_{a_1} \\ \vdots \\ \delta \alpha_{a_{ng}} \\ \delta \beta_{a_{ng}} \end{pmatrix} = -J^{-1} \begin{pmatrix} M_{sl} \\ M_s \\ E_s \\ E_{sl} \\ M_{a_1} \\ E_{a_1} \\ \vdots \\ M_{a_{ng}} \\ E_{a_{ng}} \end{pmatrix} - J^{-1} \sum_{adj} \begin{pmatrix} \partial M_{sl} / \partial p_{adj} \\ \partial M_s / \partial p_{adj} \\ \partial E_s / \partial p_{adj} \\ \partial E_{sl} / \partial p_{adj} \\ \partial M_{a_1} / \partial p_{adj} \\ \partial E_{a_1} / \partial p_{adj} \\ \vdots \\ \partial M_{a_{ng}} / \partial p_{adj} \\ \partial E_{a_{ng}} / \partial p_{adj} \end{pmatrix} \delta p_{adj} . \quad (3.51)$$

This equation can be rewritten by

$$\begin{pmatrix} \delta p \\ \delta \alpha_s \\ \delta \beta_s \\ \delta \beta_l \\ \vdots \\ \delta \alpha_{a_{ng}} \\ \delta \beta_{a_{ng}} \end{pmatrix} = - \begin{pmatrix} f_1 \\ f_2 \\ f_3 \\ f_4 \\ \vdots \\ f_{4+2n_g-1} \\ f_{4+2n_g} \end{pmatrix} - \sum_{adj} \begin{pmatrix} g_1 \\ g_2 \\ g_3 \\ g_4 \\ \vdots \\ g_{4+2n_g-1} \\ g_{4+2n_g} \end{pmatrix} \delta p_{adj} . \quad (3.52)$$

The first line of this equation

$$\delta p = f_1 - \sum_{adj} g_1 \delta p_{adj} \quad (3.53)$$

includes only pressures of the cell and adjacent cells as unknown variables, and can be solved as a system wide pressure equation set. After obtaining the correction values of all the pressures in the system by Eq. (3.53), correction values for other variables are obtained cell by cell, by applying the rest of the lines in Eq. (3.52),

$$\begin{pmatrix} \delta \alpha_s \\ \delta \beta_s \\ \delta \beta_l \\ \vdots \\ \delta \alpha_{a_{ng}} \\ \delta \beta_{a_{ng}} \end{pmatrix} = - \begin{pmatrix} f_2 \\ f_3 \\ f_4 \\ \vdots \\ f_{4+2n_g-1} \\ f_{4+2n_g} \end{pmatrix} - \sum_{adj} \begin{pmatrix} g_2 \\ g_3 \\ g_4 \\ \vdots \\ g_{4+2n_g-1} \\ g_{4+2n_g} \end{pmatrix} \delta p_{adj} . \quad (3.54)$$

3.3.5 Organization of the Pressure Equations

The pressure equation, Eq. (3.53) include the pressures in cell (i, j, k) and six adjacent cells. To solve this system wide set of equations, it is convenient to have a one dimensional index (one dimensional array), and it is defined by

$$m(i, j, k) = i + n_x(j - 1) + n_x n_y(k - 1) , \quad (3.55)$$

where n_x and n_y denote the number of cells in $x(r)$ and $y(\theta)$ directions. The matrix for the coefficients of the system wide pressure equation set becomes a multi-band coarse matrix of $n_x n_y n_z$ dimensions which has non-zero elements in the diagonal (i, j, k) , both sides of the diagonal $(i \pm 1, j, k)$, and in the distances $n_x (i, j \pm 1, k)$ and $n_x n_y (i, j, k \pm 1)$ from the diagonal, i.e. seven non-zero bands. The mapping scheme by Eq. (3.55) is advantageous when the number of cells in z direction is larger than that in x or y directions.

The pressure equation is solved by ILUBCG (Incomplete LU decomposition BiConjugate Gradient) method[34].

3.3.6 Elements of the Jacobian Matrix

Full description of the mass and energy equations

A full description of the mass and energy equations that is solved, and derivatives for the Jacobian matrix are given as follows. Note that the derivatives are given here in terms of the original independent variables p , α_m and T_m . A variable transformation to avoid numerical problem with temperatures of missing components is described later.

Mass (steam):

$$M_s = V(\alpha_s \rho_s)^{n+1} + V \sum_{adj} \tilde{m}_{s,adj} (p_{adj}^{n+1} - p^{n+1}) - \Delta t \Gamma_s + (\alpha_s \rho_s)^n \frac{dV}{dt} \Delta t - V \tilde{M}_s \quad (3.56)$$

$$\frac{\partial M_s}{\partial p} = V \alpha_s \frac{\partial \rho_s}{\partial p} - \Delta t \frac{\partial \Gamma_s}{\partial p} - V \sum_{adj} m_{s,adj} \quad (3.57)$$

$$\frac{\partial M_s}{\partial \alpha_s} = V \rho_s - \Delta t \frac{\partial \Gamma_s}{\partial \alpha_s} \quad (3.58)$$

$$\frac{\partial M_s}{\partial T_s} = V \alpha_s \frac{\partial \rho_s}{\partial T_s} - \Delta t \frac{\partial \Gamma_s}{\partial T_s} \quad (3.59)$$

$$\frac{\partial M_s}{\partial T_l} = -\Delta t \frac{\partial \Gamma_s}{\partial T_l} \quad (3.60)$$

$$\frac{\partial M_s}{\partial \alpha_a} = -\Delta t \frac{\partial \Gamma_s}{\partial \alpha_a} \quad (3.61)$$

$$\frac{\partial M_s}{\partial T_a} = 0 \quad (3.62)$$

Mass (steam+water):

$$M_{sl} = V \left\{ \alpha_s \rho_s + \left(1 - \alpha_s - \sum_a \alpha_a \right) \rho_l \right\}^{n+1} + V \sum_{adj} (\tilde{m}_{s,adj} + \tilde{m}_{l,adj}) (p_{adj}^{n+1} - p^{n+1}) + (\alpha_s \rho_s + \alpha_l \rho_l)^n \frac{dV}{dt} \Delta t - V (\tilde{M}_s + \tilde{M}_l) \quad (3.63)$$

$$\frac{\partial M_{sl}}{\partial p} = V \left\{ \alpha_s \rho_s + \left(1 - \alpha_s - \sum_a \alpha_a \right) \rho_l \right\} - V \sum_{adj} (\tilde{m}_{s,adj} + \tilde{m}_{l,adj}) \quad (3.64)$$

$$\frac{\partial M_{sl}}{\partial \alpha_s} = V (\rho_s - \rho_l) \quad (3.65)$$

$$\frac{\partial M_{sl}}{\partial T_s} = V \alpha_s \frac{\partial \rho_s}{\partial T_s} \quad (3.66)$$

$$\frac{\partial M_{sl}}{\partial T_l} = V \alpha_l \frac{\partial \rho_l}{\partial T_l} \quad (3.67)$$

$$\frac{\partial M_{sl}}{\partial \alpha_a} = -V \rho_l \quad (3.68)$$

$$\frac{\partial M_{sl}}{\partial T_a} = 0 \quad (3.69)$$

Mass (non-condensable gases):

$$\begin{aligned} M_a = & V(\alpha_a \rho_a)^{n+1} + V \sum_{adj} \tilde{m}_{a,adj} (p_{adj}^{n+1} - p^{n+1}) \\ & + (\alpha_a \rho_a)^n \frac{dV}{dt} \Delta t - V \tilde{M}_a \end{aligned} \quad (3.70)$$

$$\frac{\partial M_a}{\partial p} = V \alpha_a \frac{\partial \rho_a}{\partial p} - V \sum_{adj} \tilde{m}_{a,adj} \quad (3.71)$$

$$\frac{\partial M_a}{\partial \alpha_s} = 0 \quad (3.72)$$

$$\frac{\partial M_a}{\partial T_s} = 0 \quad (3.73)$$

$$\frac{\partial M_a}{\partial T_l} = 0 \quad (3.74)$$

$$\frac{\partial M_a}{\partial \alpha_a} = V \rho_a \quad (3.75)$$

$$\frac{\partial M_a}{\partial T_a} = V \alpha_a \frac{\partial \rho_a}{\partial T_a} \quad (3.76)$$

Energy (steam):

$$\begin{aligned} E_s = & V(\alpha_s \rho_s e_s)^{n+1} + V \sum_{adj} (\tilde{e}_{s,adj}^{(1)} + \tilde{e}_{s,adj}^{(2)} p^{n+1}) (p_{adj}^{n+1} - p^{n+1}) \\ & + V p^{n+1} \alpha_s^{n+1} + V p^{n+1} \tilde{D}_s - \Delta t (q_{is}^{n+1} + \Gamma_s^{n+1} h_s^{n+1}) - \Delta t \sum_a q_{sa}^{n+1} \\ & - V \tilde{E}_s + (\alpha_s \rho_s e_s)^n \frac{dV}{dt} \Delta t \end{aligned} \quad (3.77)$$

$$\begin{aligned} \frac{\partial E_s}{\partial p} = & V \alpha_s \left(\frac{\partial \rho_s}{\partial p} e_s + \rho_s \frac{\partial e_s}{\partial p} \right) - V \sum_{adj} \{ \tilde{e}_{s,adj}^{(1)} + \tilde{e}_{s,adj}^{(2)} (2p - p_{adj}) \} \\ & + V \alpha_s + V \tilde{D}_s - \Delta t \left(\frac{\partial q_{is}}{\partial p} + \frac{\partial \Gamma_s}{\partial p} h_s + \Gamma_s \frac{\partial h_s}{\partial p} \right) \end{aligned} \quad (3.78)$$

$$\frac{\partial E_s}{\partial \alpha_s} = V \rho_s e_s + V p - \Delta t \left(\frac{\partial q_{is}}{\partial \alpha_s} + \frac{\partial \Gamma_s}{\partial \alpha_s} h_s \right) \quad (3.79)$$

$$\frac{\partial E_s}{\partial T_s} = V \alpha_s \left(\frac{\partial \rho_s}{\partial T_s} e_s + \rho_s \frac{\partial e_s}{\partial T_s} \right) - \Delta t \left(\frac{\partial q_{is}}{\partial T_s} + \frac{\partial \Gamma_s}{\partial T_s} h_s + \Gamma_s \frac{\partial h_s}{\partial T_s} \right) - \Delta t \sum_a R_{sa} \quad (3.80)$$

$$\frac{\partial E_s}{\partial T_l} = -\Delta t \frac{\partial \Gamma_s}{\partial T_l} h_s \quad (3.81)$$

$$\frac{\partial E_s}{\partial \alpha_a} = -\Delta t \left(\frac{\partial q_{is}}{\partial \alpha_a} + \frac{\partial \Gamma_s}{\partial \alpha_a} h_s \right) \quad (3.82)$$

$$\frac{\partial E_s}{\partial T_a} = \Delta t R_{sa} \quad (3.83)$$

Energy (steam+water):

$$\begin{aligned}
 E_{sl} = & V \left\{ \alpha_s \rho_s e_s + \left(1 - \alpha_s - \sum_a \alpha_a \right) \rho_l e_l \right\}^{n+1} \\
 & + V \sum_{adj} (\tilde{e}_{s,adj}^{(1)} + \tilde{e}_{l,adj}^{(1)} + \tilde{e}_{s,adj}^{(2)} p^{n+1} + \tilde{e}_{l,adj}^{(2)} p^{n+1}) (p_{adj}^{n+1} - p^{n+1}) \\
 & + V p^{n+1} \left(1 - \sum_a \alpha_a \right)^{n+1} + V p^{n+1} (\tilde{D}_s + \tilde{D}_l) - \Delta t \left(\sum_a q_{sa}^{n+1} + q_{int} \right) \\
 & - V (\tilde{E}_s + \tilde{E}_l) + \left\{ \alpha_s \rho_s e_s + \left(1 - \alpha_s - \sum_a \alpha_a \right) \rho_l e_l \right\}^n \frac{dV}{dt} \Delta t
 \end{aligned} \tag{3.84}$$

$$\begin{aligned}
 \frac{\partial E_{sl}}{\partial p} = & V \left\{ \alpha_s \left(\frac{\partial \rho_s}{\partial p} e_s + \rho_s \frac{\partial e_s}{\partial p} \right) + \alpha_l \left(\frac{\partial \rho_l}{\partial p} e_l + \rho_l \frac{\partial e_l}{\partial p} \right) \right\} \\
 & - V \sum_{adj} \{ \tilde{e}_{s,adj}^{(1)} + \tilde{e}_{l,adj}^{(1)} + (\tilde{e}_{s,adj}^{(2)} + \tilde{e}_{l,adj}^{(2)}) (2p - p_{adj}) \} \\
 & + V(\alpha_s + \alpha_l) + V(\tilde{D}_s + \tilde{D}_l)
 \end{aligned} \tag{3.85}$$

$$\frac{\partial E_{sl}}{\partial \alpha_s} = V(\rho_s e_s - \rho_l e_l) \tag{3.86}$$

$$\frac{\partial E_{sl}}{\partial T_s} = V \alpha_s \left(\frac{\partial \rho_s}{\partial T_s} e_s + \rho_s \frac{\partial e_s}{\partial T_s} \right) - \Delta t \sum_a R_{sa} \tag{3.87}$$

$$\frac{\partial E_{sl}}{\partial T_l} = V \alpha_l \left(\frac{\partial \rho_l}{\partial T_l} e_l + \rho_l \frac{\partial e_l}{\partial T_l} \right) \tag{3.88}$$

$$\frac{\partial E_{sl}}{\partial \alpha_a} = -V \rho_l e_l - V p \tag{3.89}$$

$$\frac{\partial E_{sl}}{\partial T_a} = \Delta t R_{sa} \tag{3.90}$$

Energy (non-condensable gases):

$$\begin{aligned}
 E_a = & V(\alpha_a \rho_a e_a)^{n+1} + V \sum_{adj} (\tilde{e}_{a,adj}^{(1)} + \tilde{e}_{a,adj}^{(2)} p^{n+1}) (p_{adj}^{n+1} - p^{n+1}) \\
 & + V p^{n+1} \alpha_a^{n+1} + V p^{n+1} \tilde{D}_a + \Delta t \sum_a q_{sa}^{n+1} \\
 & - V \tilde{E}_a + (\alpha_a \rho_a e_a)^n \frac{dV}{dt} \Delta t
 \end{aligned} \tag{3.91}$$

$$\begin{aligned}
 \frac{\partial E_a}{\partial p} = & V \alpha_a \left(\frac{\partial \rho_a}{\partial p} e_a + \rho_a \frac{\partial e_a}{\partial p} \right) - V \sum_{adj} \{ \tilde{e}_{a,adj}^{(1)} + \tilde{e}_{a,adj}^{(2)} (2p - p_{adj}) \} \\
 & + V \alpha_a + V \tilde{D}_a
 \end{aligned} \tag{3.92}$$

$$\frac{\partial E_a}{\partial \alpha_s} = 0 \tag{3.93}$$

$$\frac{\partial E_a}{\partial T_s} = \Delta t R_{sa} \tag{3.94}$$

$$\frac{\partial E_a}{\partial T_l} = 0 \tag{3.95}$$

$$\frac{\partial E_a}{\partial \alpha_a} = V \rho_a e_a - V p \tag{3.96}$$

$$\frac{\partial E_a}{\partial T_a} = V \alpha_a \left(\frac{\partial \rho_a}{\partial T_a} e_a + \rho_a \frac{\partial e_a}{\partial T_a} \right) - \Delta t R_{sa} \tag{3.97}$$

Derivatives of the phase change and heat transfer terms

The phase change (evaporation, condensation) term given by Eq. (2.103) is dependent on steam and water temperatures and also on the pressure and volume fractions through the saturation temperature at steam partial pressure. Derivatives for those variables necessary for the Jacobian matrix are given as follows.

$$\frac{\partial \Gamma_s}{\partial p} = -A_i \frac{h_{is} + h_{il}}{h_s - h_l} \frac{\partial T_{sat}}{\partial p_s} \frac{\partial p_s}{\partial p} - A_i \frac{\Gamma_s}{h_s - h_l} \left(\frac{\partial h_s}{\partial p} - \frac{\partial h_l}{\partial p} \right) \quad (3.98)$$

$$\frac{\partial \Gamma_s}{\partial \alpha_s} = -A_i \frac{h_{is} + h_{il}}{h_s - h_l} \frac{\partial T_{sat}}{\partial p_s} \frac{\partial p_s}{\partial \alpha_s} \quad (3.99)$$

$$\frac{\partial \Gamma_s}{\partial T_s} = A_i \frac{h_{is}}{h_s - h_l} - A_i \frac{\Gamma_s}{h_s - h_l} \frac{\partial h_s}{\partial T_s} \quad (3.100)$$

$$\frac{\partial \Gamma_s}{\partial T_l} = A_i \frac{h_{il}}{h_s - h_l} + A_i \frac{\Gamma_s}{h_s - h_l} \frac{\partial h_l}{\partial T_l} \quad (3.101)$$

$$\frac{\partial \Gamma_s}{\partial \alpha_a} = -A_i \frac{h_{is} + h_{il}}{h_s - h_l} \frac{\partial T_{sat}}{\partial p_s} \frac{\partial p_s}{\partial \alpha_a} \quad (3.102)$$

$$\frac{\partial q_{is}}{\partial p} = A_i h_{is} \frac{\partial T_{sat}}{\partial p_s} \frac{\partial p_s}{\partial p} \quad (3.103)$$

$$\frac{\partial q_{is}}{\partial \alpha_s} = A_i h_{is} \frac{\partial T_{sat}}{\partial p_s} \frac{\partial p_s}{\partial \alpha_s} \quad (3.104)$$

$$\frac{\partial q_{is}}{\partial T_s} = -A_i h_{is} \quad (3.105)$$

$$\frac{\partial q_{is}}{\partial \alpha_a} = A_i h_{is} \frac{\partial T_{sat}}{\partial p_s} \frac{\partial p_s}{\partial \alpha_a} \quad (3.106)$$

The derivatives of pseudo partial pressure of steam (Eq. (2.101)) are given as follows.

$$\frac{\partial p_s}{\partial p} = \frac{\alpha_s}{\alpha} \quad (3.107)$$

$$\frac{\partial p_s}{\partial \alpha_s} = p \frac{\alpha - \alpha_s}{\alpha^2} \quad (3.108)$$

$$\frac{\partial p_s}{\partial \alpha_a} = -p \frac{\alpha_s}{\alpha^2} \quad (3.109)$$

Variable transformation

To avoid the singularity for T_m of missing components, a variable transformation $T \rightarrow \alpha T$ is done before constructing the Jacobian matrix. The transformation is expressed by

$$f(p, \alpha_s, T_s, \alpha_a, T_a(a = a_1, \dots, a_{n_g})) \rightarrow f(P, A_s, \beta_s, A_a, \beta_a(a = a_1, \dots, a_{n_g})) \quad (3.110)$$

where the new set of independent variables are defined as follows.

$$P = p \quad (3.111)$$

$$A_s = \alpha_s \quad (3.112)$$

$$\beta_s = \alpha_s T_s \quad (3.113)$$

$$\beta_l = \alpha_l T_l = (1 - \alpha_s - \sum \alpha_{a_i}) T_l \quad (3.114)$$

$$A_a = \alpha_a, \quad (3.115)$$

$$\beta_a = \alpha_a T_a \quad (3.116)$$

The relation between partial derivatives are given as follows.

$$\frac{\partial f}{\partial P} = \frac{\partial f}{\partial p} \quad (3.117)$$

$$\frac{\partial f}{\partial A_s} = \frac{\partial f}{\partial \alpha_s} - \frac{\partial f}{\partial T_s} \frac{T_s}{\alpha_s} + \frac{\partial f}{\partial T_l} \frac{T_l}{\alpha_l} \quad (3.118)$$

$$\frac{\partial f}{\partial \beta_s} = \frac{\partial f}{\partial T_s} \frac{1}{\alpha_s} \quad (3.119)$$

$$\frac{\partial f}{\partial \beta_l} = \frac{\partial f}{\partial T_l} \frac{1}{\alpha_l} \quad (3.120)$$

$$\frac{\partial f}{\partial A_a} = \frac{\partial f}{\partial \alpha_a} + \frac{\partial f}{\partial T_l} \frac{T_l}{\alpha_l} - \frac{\partial f}{\partial T_a} \frac{T_a}{\alpha_a} \quad (3.121)$$

$$\frac{\partial f}{\partial \beta_a} = \frac{\partial f}{\partial T_a} \frac{1}{\alpha_a} \quad (3.122)$$

4 Verification and Example Calculations

4.1 Check of the Numerical Behavior of the Models

4.1.1 Melt Jet and Pool

Purpose

Free fall and spreading of a column of liquid was simulated for confirmation of physically proper behavior of the melt jet and pool models and their mass conservation accuracy.

Calculation conditions

Figure 4.1 shows the geometric condition. A liquid column, diameter 90mm and initial velocity 0.5m/s at inlet, flows into a closed chamber of radius 0.2m and height 1m filled with gas. The liquid column is subjected to the gravitational acceleration. The chamber is discretized into 0.1m cells in vertical direction, and each vertical cell is sub-divided into finer cells for the melt jet. The base case condition and some variations are defined as follows.

- Base case: jet cell size 2cm, time step 1ms
- “dz” case: jet cell size 5mm ($\times 0.25$)
- “dt” case: time step 0.1ms ($\times 0.1$)

Also, the result is compared with theoretical solution (“Theoretical” in figures) and the up-wind finite difference solution (“FDM up-wind” in figures).

Calculation results

The leading edge profile and trailing edge profile are shown in Figs. 4.2 and 4.3, respectively. The base case solution shows a reasonable agreement with the theoretical solution, and that is much better than the up-wind finite difference because of the usage of CIP method. The calculation with a finer mesh showed a result closer to the theoretical solution. The case with a smaller time step showed a result almost identical to the base case.

Figure 4.4 shows the comparison of the results with the free fall curve. Admitting that the plotted leading edge position by calculation is affected by the criterion with which the existence of the jet is detected in cells, the leading edge position agrees with the progress by free fall.

Figure 4.5 shows the evolution of jet and pool profiles in the base case. The mass conservation accuracy is checked during the mass transfer from the jet model to the pool model. Figure 4.6 shows the model has a good mass conservation. The total liquid mass conservation error through the simulation was $< 0.2\%$.

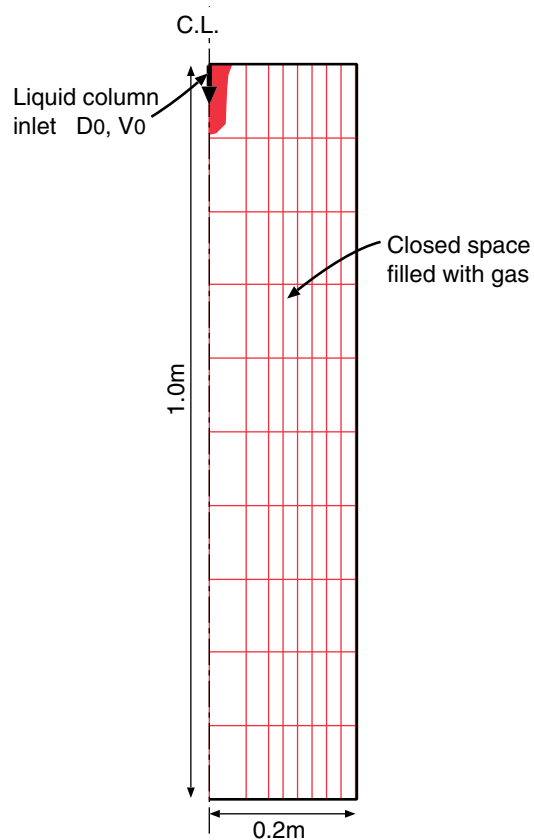


Figure 4.1: Melt jet and pool test calculation geometry.

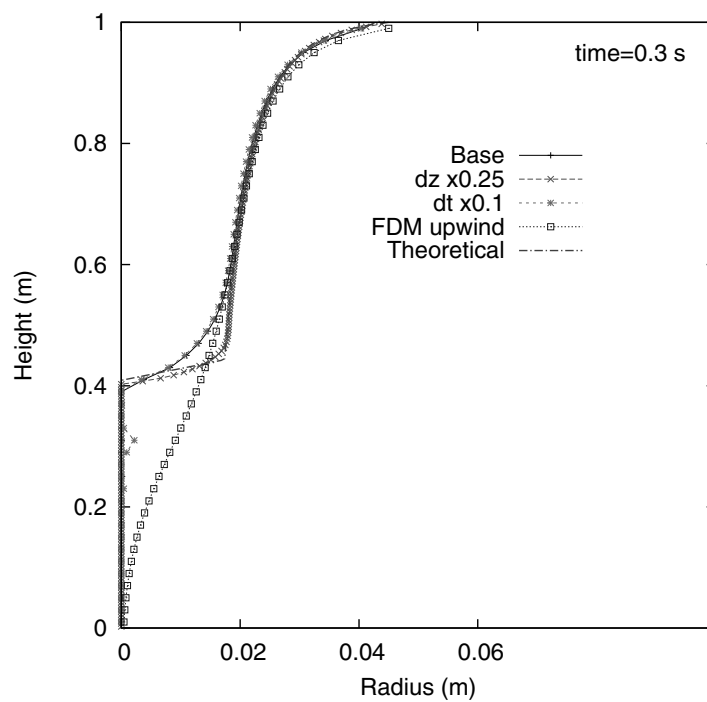


Figure 4.2: The jet leading edge profile at 0.3s.

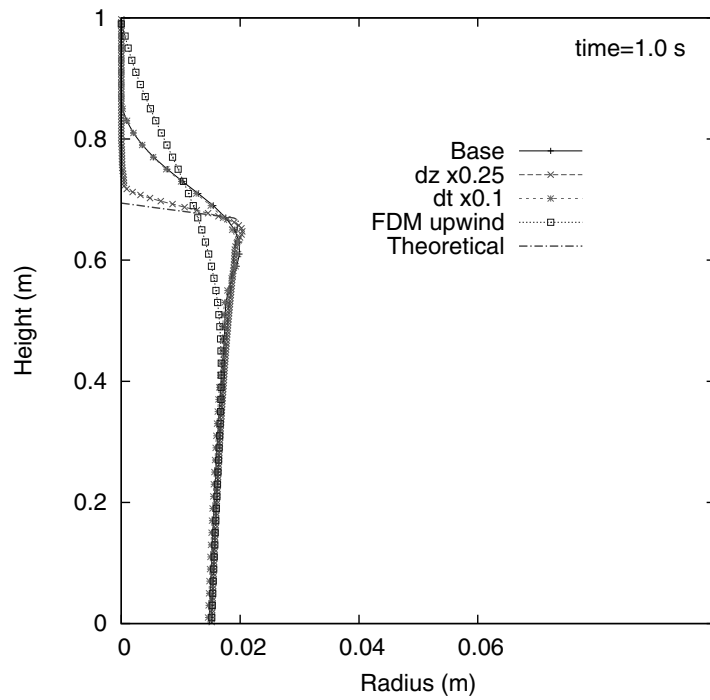


Figure 4.3: The jet trailing edge profile at 1.0s.

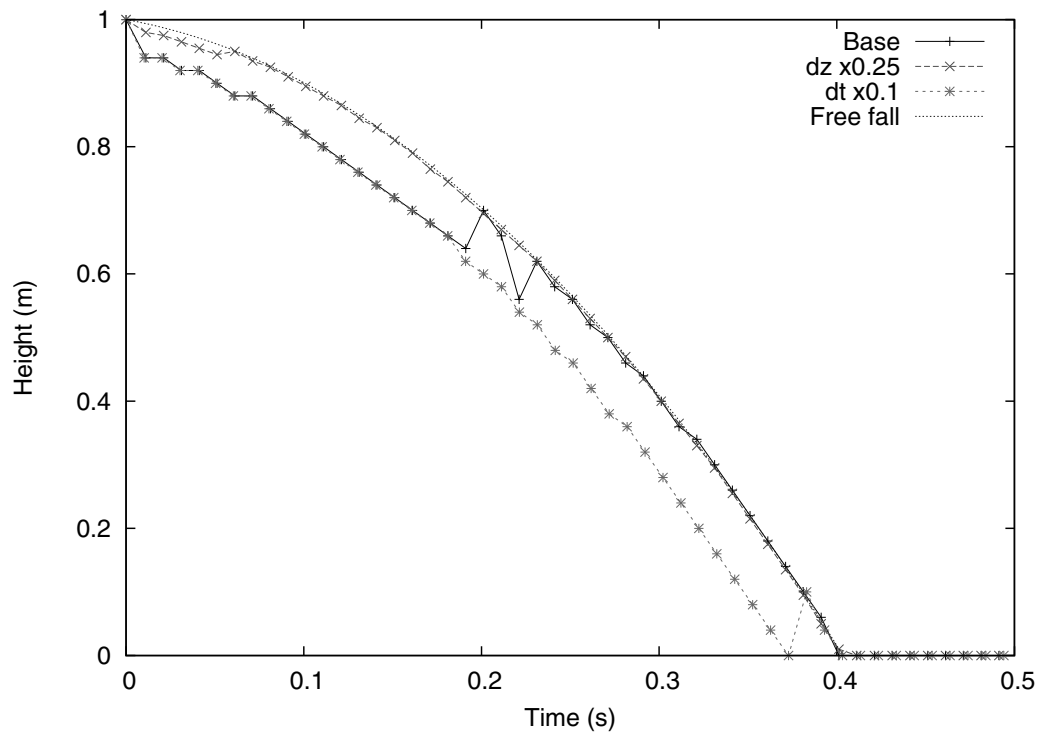


Figure 4.4: Comparison of the jet leading edge progress with the free fall curve.

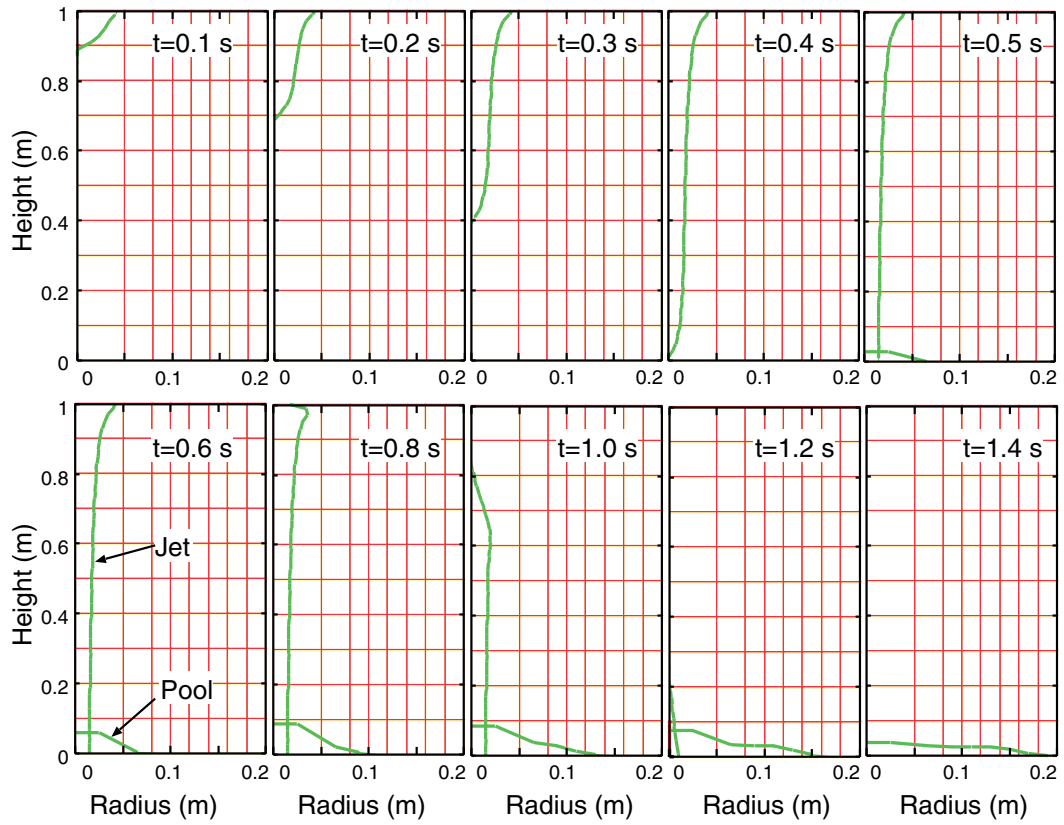


Figure 4.5: Overall profiles of the melt jet/pool evolution.

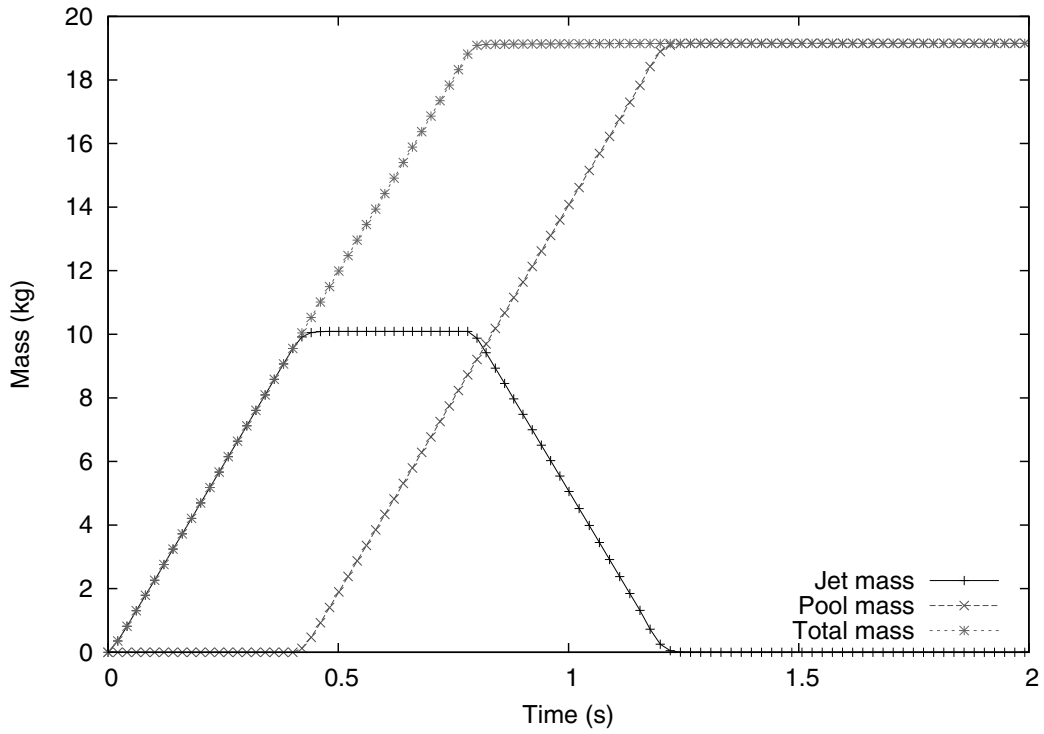


Figure 4.6: Plot of the jet, pool and total melt mass for the check of mass conservation.

4.1.2 Melt Particles

Purpose

Free fall of the melt particles and their merging into the melt pool, or stacking on the floor was simulated for confirmation of physically proper behavior of the melt particles and pool models and their mass conservation accuracy.

Calculation conditions

Figure 4.7 shows the geometric condition. Melt particle groups are initially distributed in the upper area of the calculation field that is a cylinder of radius 0.2m and height 1m filled with steam, with constant radial and vertical intervals. The diameter of the individual particle in the groups is 1mm and the number of the particles in each group is given so that their particle volume fraction becomes 0.2. The initial vertical velocity of the particle groups is set 0 and they are subjected to the free fall. The base case condition and some variations are defined as follows.

- Base case: particles are molten, initial x -direction velocity 0, time step 1ms
- “dt” case: time step 0.1ms ($\times 0.1$)
- “Slid” case: particles are solid
- “Solid-rand” case: particles are solid and have initial x -direction velocity randomly given in the range $-0.2 < v_x < 0.2\text{m/s}$

Calculation results

The evolution of the particle group distribution is shown in Figs 4.8–4.10, by the positions of the centers of particle groups. In the base case, the particle groups fall on to the floor and make a melt pool. In “Solid” and “Solid-rand” cases, the particle groups stack on the floor and make a debris bed. In the “Solid-rand” case, the randomly given horizontal initial velocities make a difference from the “Solid” case.

Figure 4.11 shows a comparison between the leading edge progress obtained in the calculation and the free fall curve. They agreed well.

Figure 4.12 shows that a good mass conservation accuracy is kept during the mass transfer from the particle group model to the pool model. The total melt mass conservation error through the simulation was $< 0.01\%$.

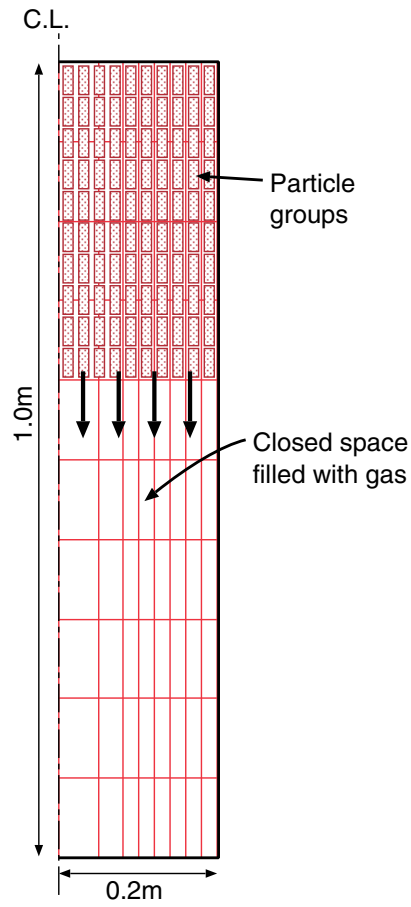


Figure 4.7: Melt particles and pool calculation geometry.

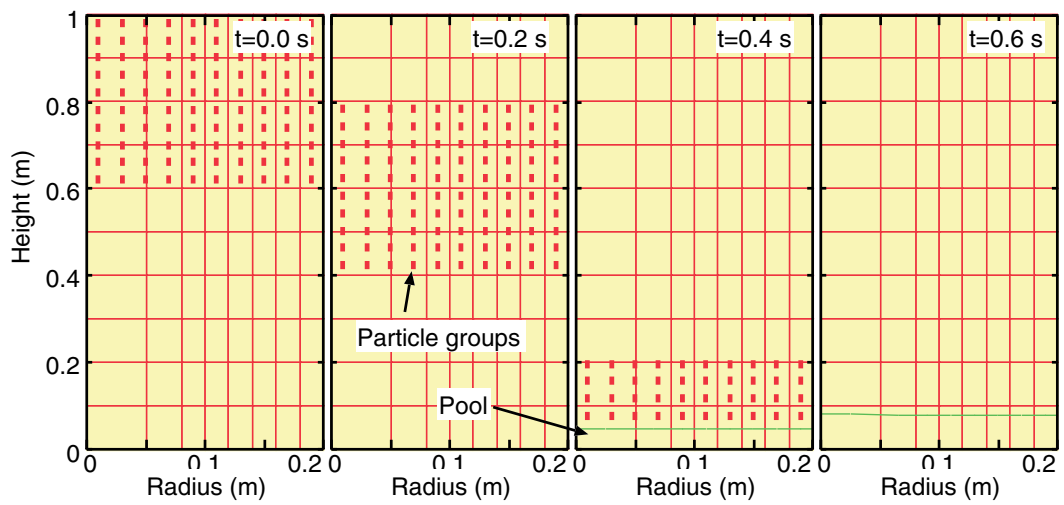


Figure 4.8: Evolution of particle group distribution: Base case.

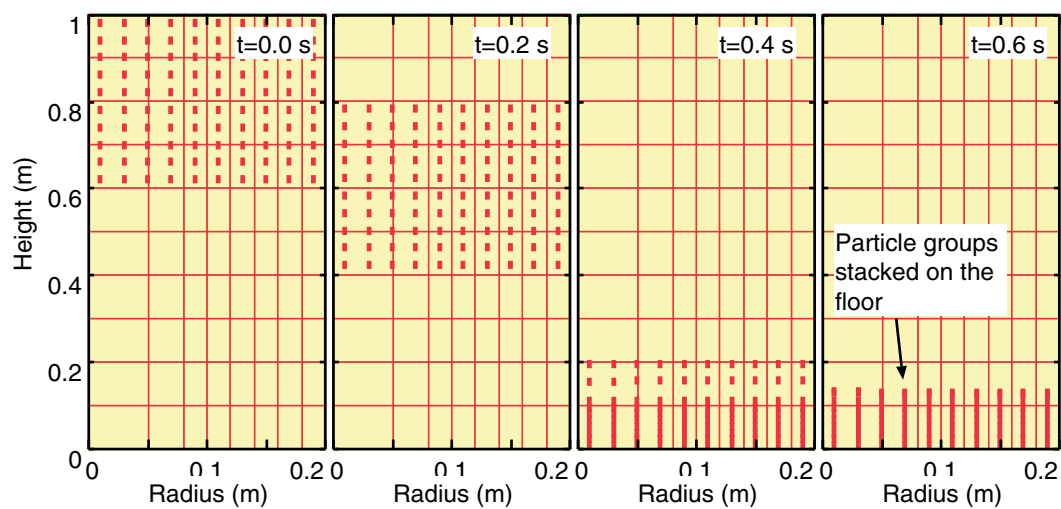


Figure 4.9: Evolution of particle group distribution: "Solid" case.

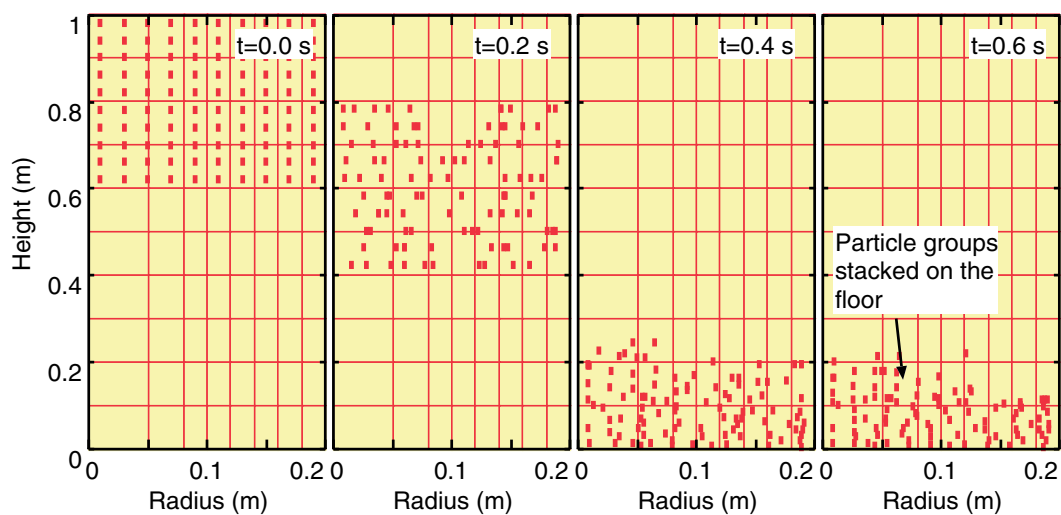


Figure 4.10: Evolution of particle group distribution: "Solid-rand" case.

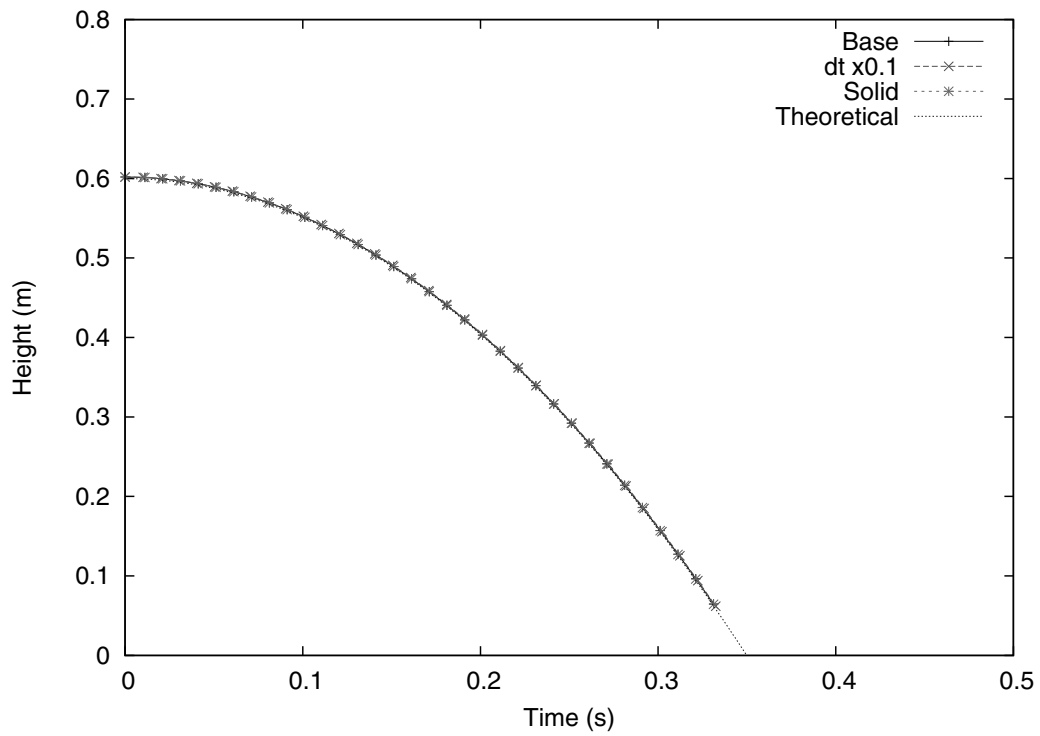


Figure 4.11: Comparison of the particle leading edge progress with the free fall curve.

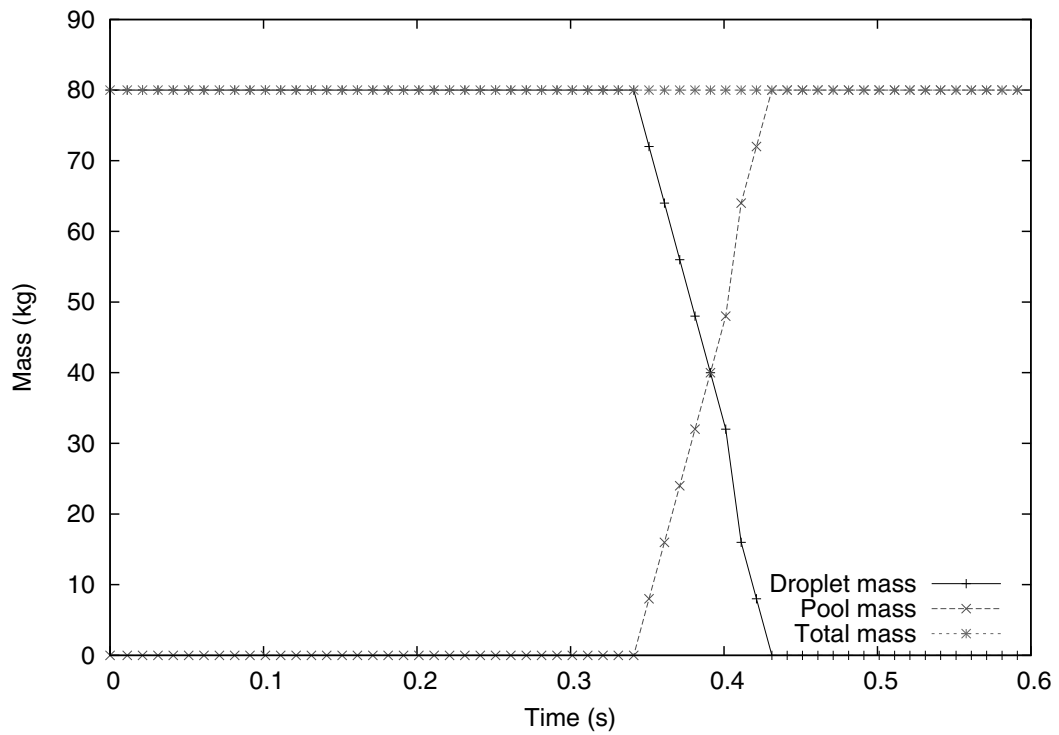


Figure 4.12: Plot of the droplet, pool and total melt mass for the check of mass conservation.

4.1.3 Shock Wave Propagation in Two-Phase Medium

Purpose

Because the shock wave propagation in a two-phase medium is a primary physical process to be captured by the two-phase flow model in a steam explosion simulation, the ability of the two-phase flow model in this aspect was checked by simple simulations.

First, dependence of the sonic velocity on the void fraction was checked by a nearly one-dimensional geometry. Then, spherical wave propagation was tested in a two-dimensional (cylindrical) geometry.

Two-phase sonic velocity

Calculation conditions Figure 4.13 shows the geometric condition. A cylindrical chamber of radius 0.2m and height 2.5m, filled with water up to the level 2.05m was considered. A pressure source was initially placed in the center bottom cell, where void fraction 0.5 and pressure 0.12MPa is given. The initial system pressure was set 0.1MPa.

The sonic velocity was evaluated by tracing the propagation of the pressure front, and compared with theoretical values evaluated for homogeneous bubbly medium given by

$$c_{tphm}(\alpha) = \left\{ \alpha^2 + \alpha(1 - \alpha) \frac{\rho_l}{\rho_g} + \left((1 - \alpha)^2 + \alpha(1 - \alpha) \frac{\rho_g}{\rho_l} \right) \left(\frac{c_g}{c_l} \right)^2 \right\}^{-1/2}. \quad (4.1)$$

The void fraction in the water column was changed as a parameter.

Calculation results Figures 4.14–4.16 show the pressure histories at height 0.475m, 0.975m and 1.95m with void fractions 10^{-5} , 10^{-3} and 0.1 as a parameter. The time of the arrival of the shock front was read at the half value of the first peak. It was observed that the shock front propagation delayed with increase of the void fraction, and that the shock wave was rapidly damped when the void fraction was 0.1.

The sonic velocity was calculated from the shock arrival time, and plotted with the theoretical value (Eq. (4.1)) in Fig. 4.17. The sonic velocity evaluated by the calculation results agreed well with the theoretical values.

Spherical shock wave propagation

Calculation conditions Figure 4.18 shows the geometric condition. A cylindrical chamber of radius 1m and height 2m, filled with water up to the level 1.78m was considered. A pressure source was initially placed in the center bottom cell, where void fraction 0.5 and pressure 1MPa is given. The initial system pressure was set 0.1MPa. The void fraction in the water pool was set 10^{-4} .

Calculation results Figure 4.19 shows the pressure profiles obtained by the calculation. The plots show that the shock front propagates spherically from the pressure source, and reflects at the side wall and the floor. Thus, it is demonstrated that the wave dynamics is reasonably captured by the present two-phase flow model.

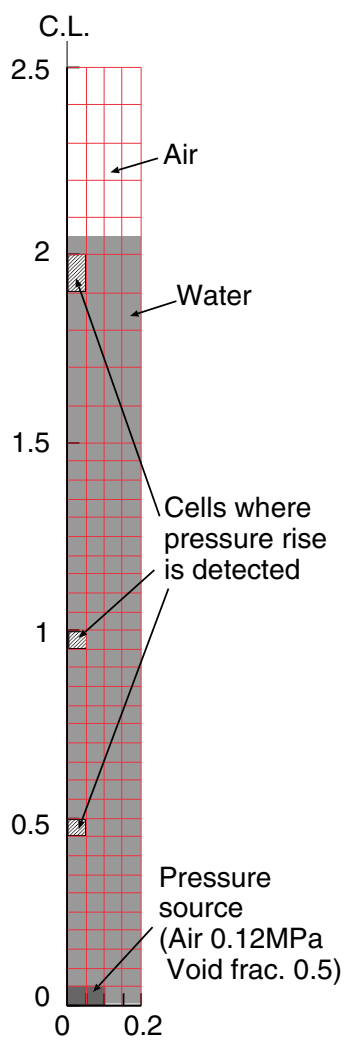
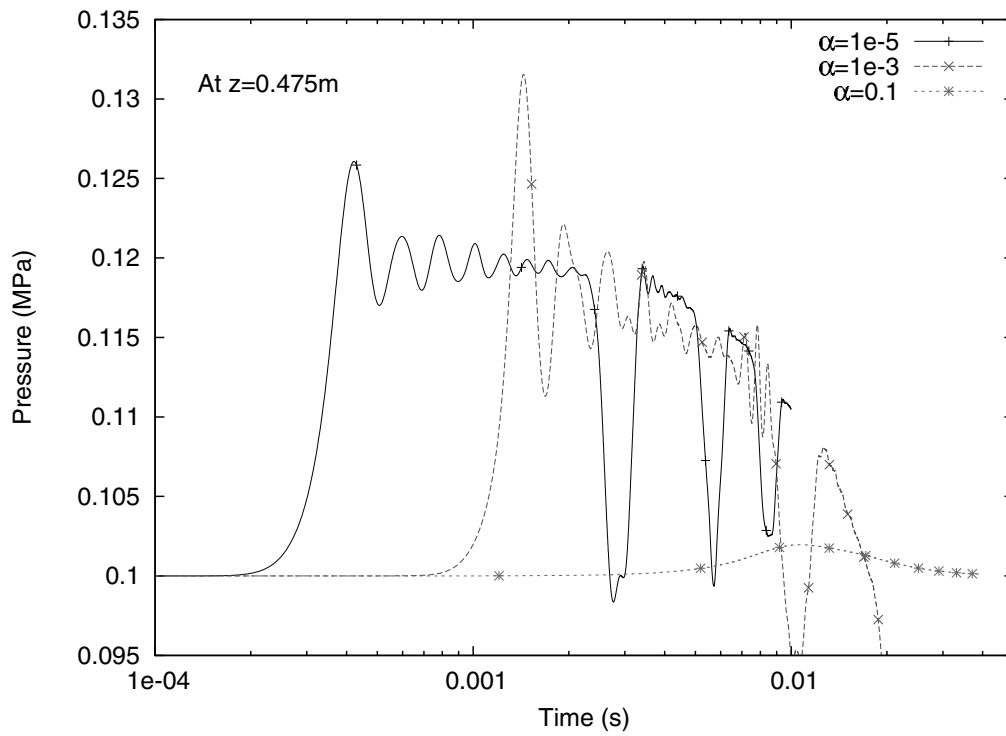
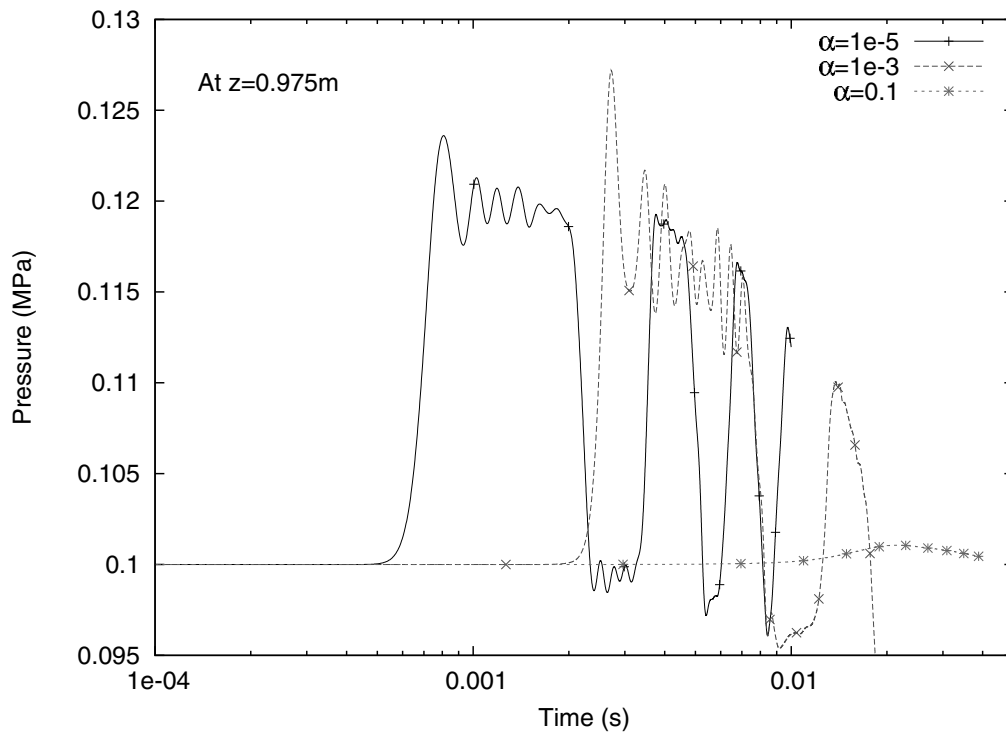


Figure 4.13: Geometry for the shock wave propagation test calculation.

Figure 4.14: Pressure histories at $z = 0.475\text{m}$ with various void fractions.Figure 4.15: Pressure histories at $z = 0.975\text{m}$ with various void fractions.

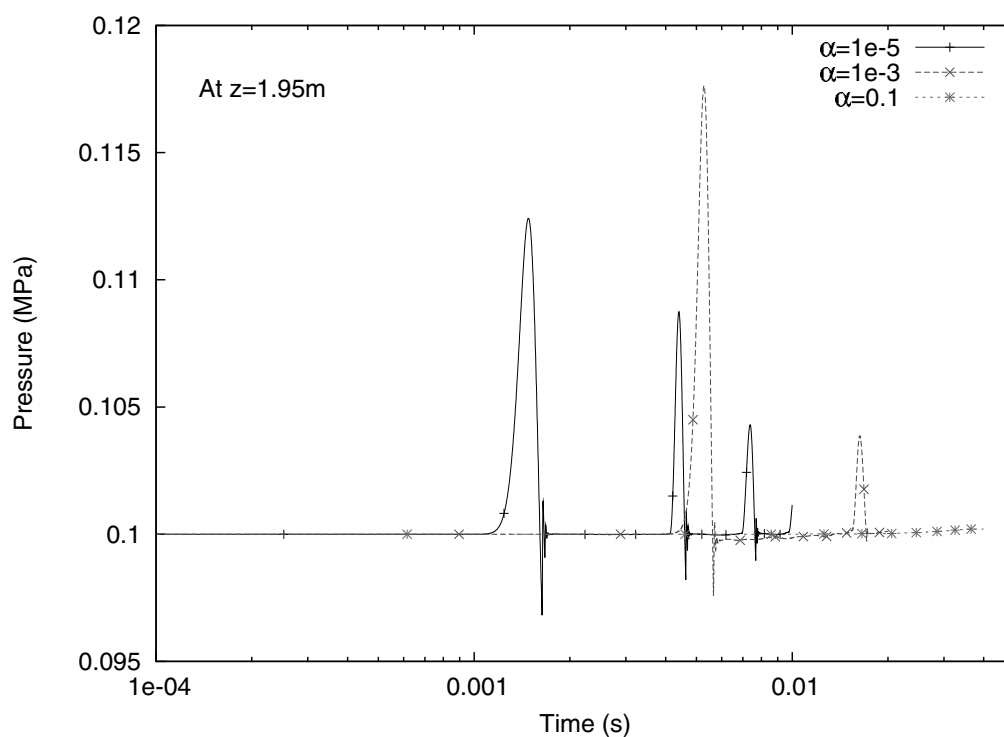


Figure 4.16: Pressure histories at $z = 1.95\text{m}$ with various void fractions.

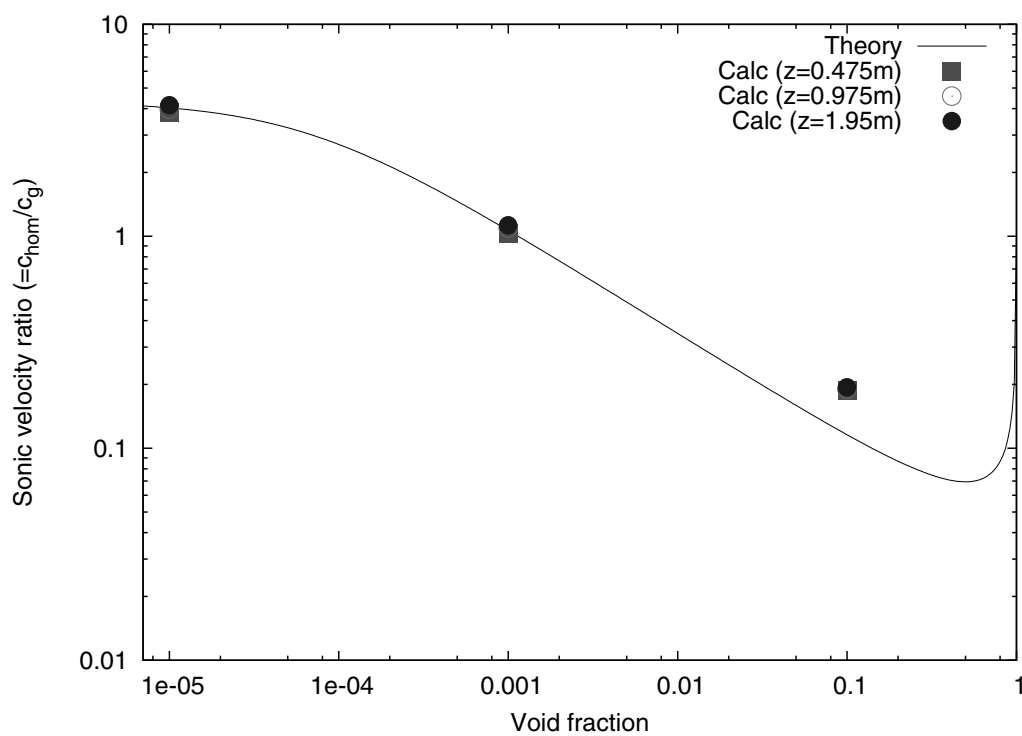


Figure 4.17: Dependence of two-phase sonic velocity on void fraction—comparison of homogeneous two-phase medium theory and JASMINE calculation.

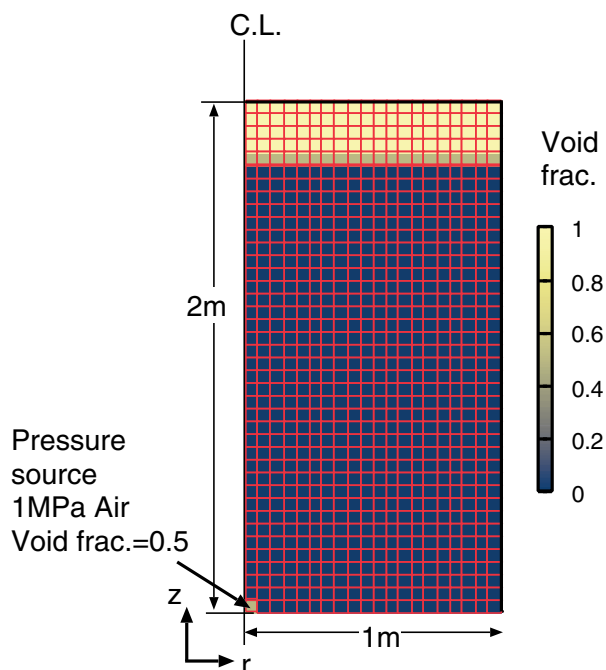


Figure 4.18: Geometry for the two-dimensional shock wave propagation test calculation.

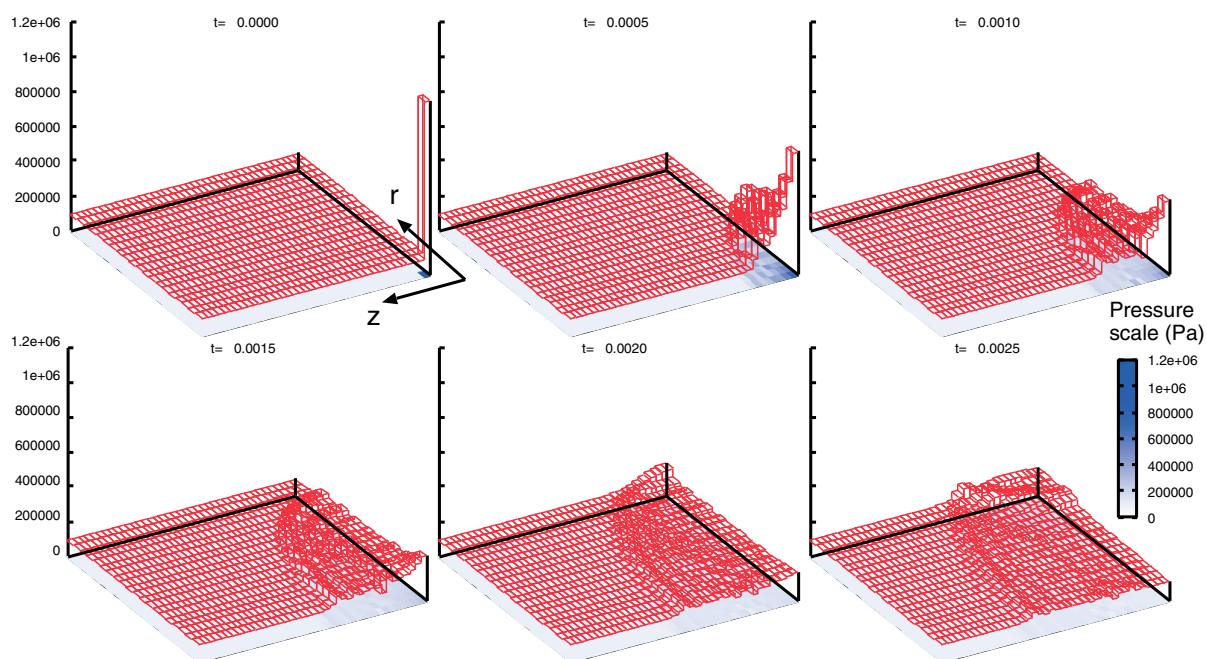


Figure 4.19: Pressure profiles obtained by the calculation, showing spherical propagation of the shock front and its interference with the reflected wave from the side wall.

Table 4.1: Conditions and results of FARO melt jet quenching experiments, and analytical conditions.

	L14	L28	L31
Melt			
Material	Corium ($T_{sol}/T_{liq} = 2830/2850(K)$, 80wt%UO ₂ -20wt%ZrO ₂)		
Released mass (kg)	125	175	92
Temperature (K)	3073	3053	2990
Jet diameter at inlet (mm)	92	44	48
Water			
Temperature (Subcool) (K)	537 (1)	424 (1)	291 (104)
Pool depth (m)	2.05	1.44	1.45
Water vessel diameter (m)	0.71	0.71	0.71
Cover gas			
Atmosphere	Steam	Steam	Argon
Initial pressure (MPa)	5.0	0.51	0.22
Cover gas volume(m ³)	1.26	3.53	3.49
Results			
Pressure rise at plateau (MPa)	2.5	1.2	0.04
Level swell (m)	~1.4	~0.6	~0.3
Agglomerated mass (kg)	20 (16%)	77 (44%)	0
Debris mean dia. ^{a)} (mm)	5.0	3.0	3.3
Analytical			
Grid (Water pool zone)	6×37(6×20)	8×25(6×14)	
Central column radius (m)	0.15	0.10	0.10
Time step (ms)		~0.5	
Jet initial velocity(m/s)	3.0	~3.0	~2.7
Jet flow-in duration(s)	0.80	5.2	2.5
Melt particle dia.(const.)(mm)	5.0	3.0	3.0
Jet break-up length model ^{b)}	Taylor type, $C_{ent} = 1$		
Surface temperature drop model	Use		
N_{pcr} ^{c)}	1000		
n_{hist} ^{c)}	1000		
F_{htint} ^{d)}	0.02		

a) mass median diameter b) see 2.2.1 c) see 2.2.3 d) see 2.3.2

4.2 Simulation of Premixing Experiments

Purpose

For the verification of the premixing-related model functions and the parameter tuning, we performed simulation of FARO experiments that were performed at JRC Ispra of EU[35, 36]. In those experiments, ~100kg of molten corium (mixture of UO₂ and ZrO₂) was dropped into a water pool. Data for the pressurization and water level swelling by steam generation during the melt jet break-up and quenching, particle size distribution of the quenched debris are available. We referred three experiments, L14, L28 and L31 with different subcools, pressures and jet sizes, and compared the calculation and experimental results.

Calculation conditions

The experimental conditions of the three experiments, and analytical conditions for the simulations are summarized in Table 4.1. Figure 4.20 shows the grids to simulate the FARO experimental geometry.

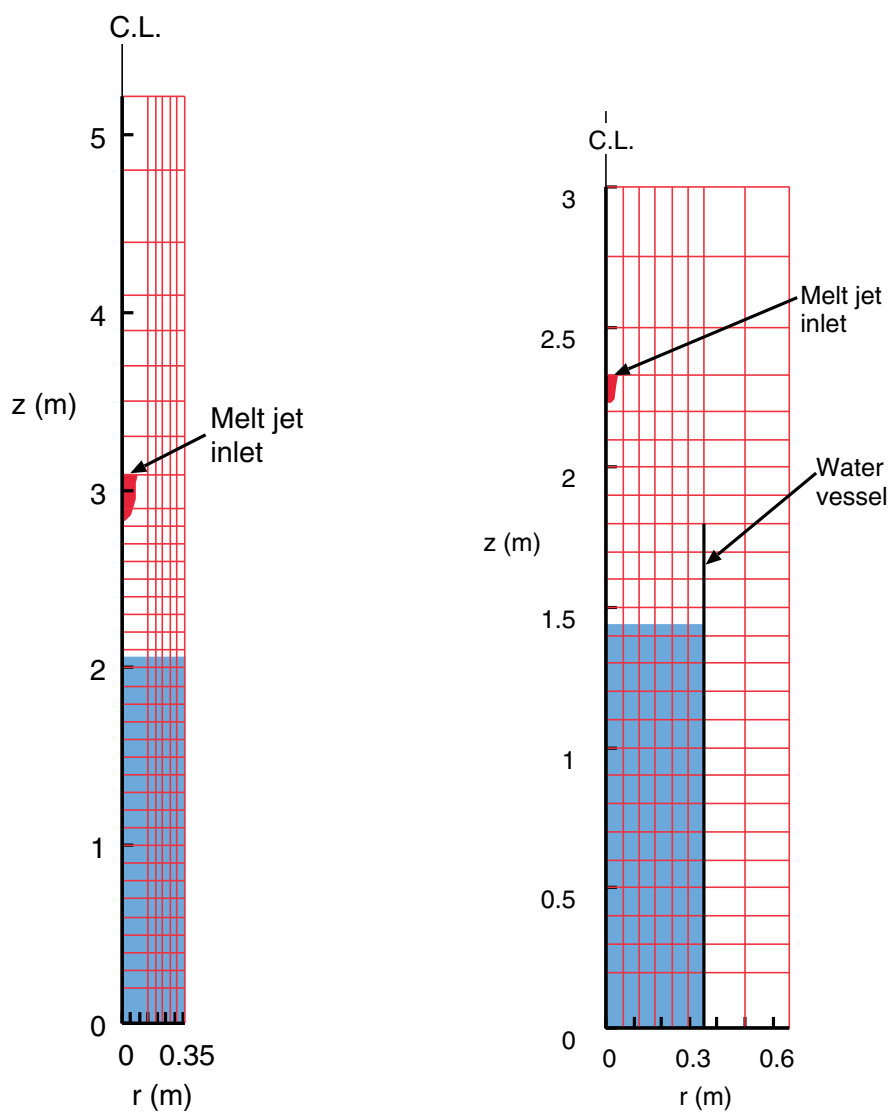


Figure 4.20: Grid geometry to simulate the experimental system of FARO-L14 (left), L28 and L31 (right).

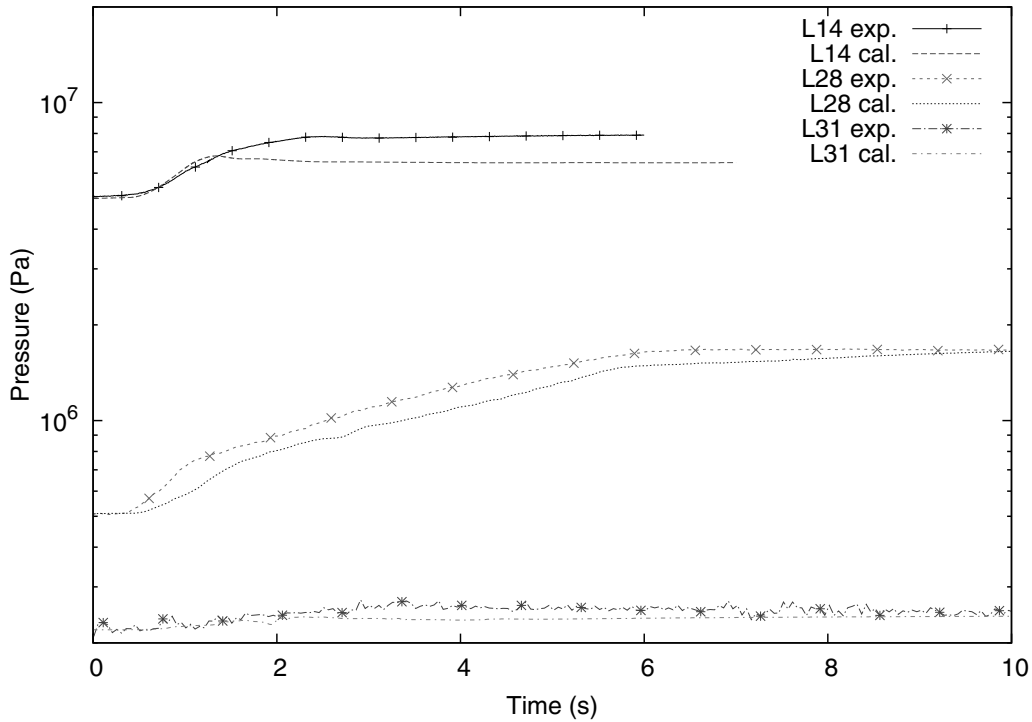


Figure 4.21: Comparison of calculation and experimental results: Pressure history.

Calculation results

Calculation results are compared with experimental data in Figs. 4.21–4.23. The pressure histories (Fig. 4.21) and the level swellings (Fig. 4.22) were roughly in reasonable agreement. In detail, we can see a trend of underestimating the pressure rise while overestimating the level swelling, especially for low pressure conditions (L28 and L31). This trend depicts the present limitation in the premixing modeling.

We consider that steam bubbles generated in the premixing zone escapes faster in reality than in the simulation especially in low pressure conditions. It seems that we need considerable work in two-phase flow constitutive models if we want to improve this situation.

Figure 4.23 shows the comparison on the mass fraction of agglomerated melt, that was found as a continuous lump at the bottom. The lump can be made either by direct arrival of the jet column without fragmentation during the fall or by re-agglomeration of once-fragmented melt droplets. The simulation results did not agree with experimental results.

These results show that ability of the present model in simulating the complicated premixing phenomena and long term cooling behavior is not in a satisfactory level. Nevertheless, we can use the present model with a certain level of confidence for the purpose of steam explosion simulations, in which mainly the “premixed” melt mass in the initial phase of premixing is needed. (see the next section.)

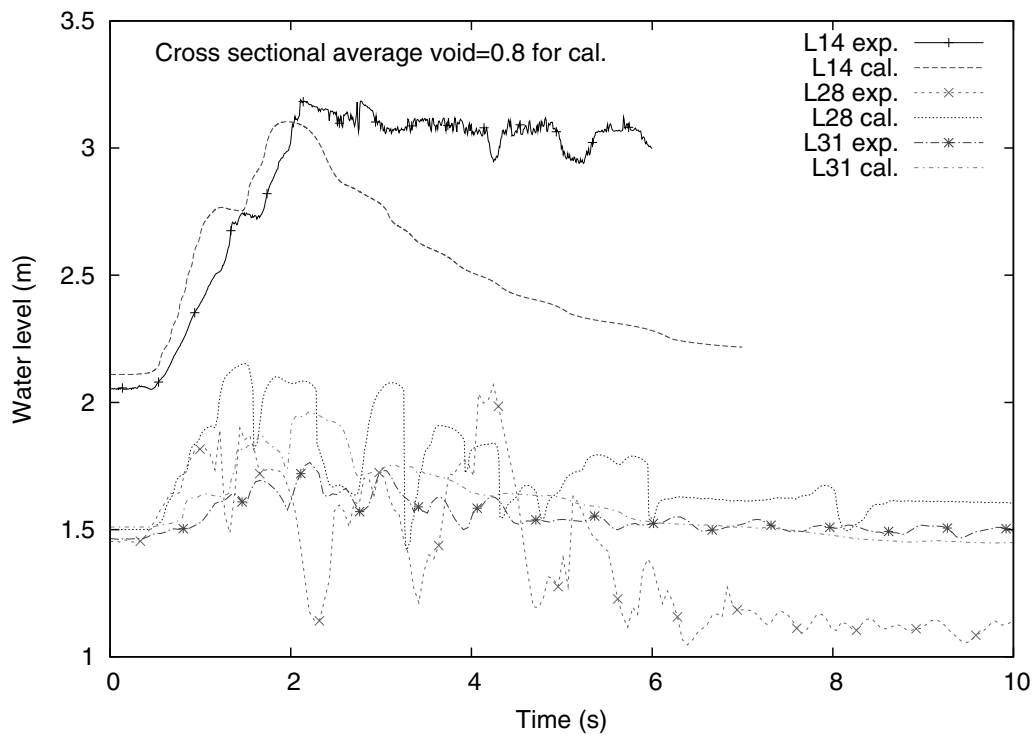


Figure 4.22: Comparison of calculation and experimental results: Water level swelling.

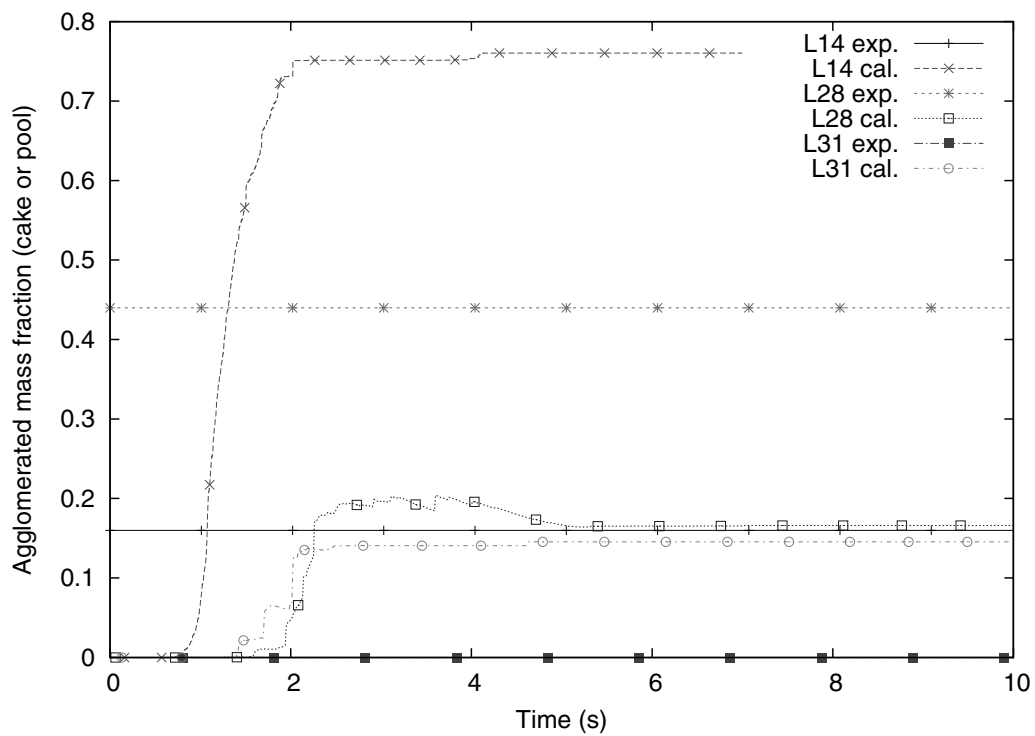


Figure 4.23: Comparison of calculation and experimental results: Agglomerated melt mass fraction.

4.3 Simulation of Explosion Experiments

Purpose

For the verification of the explosion-related model functions and the parameter tuning, we performed simulation of KROTOS experiments and a FARO experiment that were performed at JRC Ispra of EU[37, 38]. In KROTOS experiments, several kilograms of molten alumina or corium (mixture of UO_2 and ZrO_2) was dropped into a column of water, and a triggering for a steam explosion was given by a pressure pulse generated by releasing compressed argon gas. We referred three cases, 44, 42 and 37 from the KROTOS series experiments. We referred another experiment, FARO-L33, a steam explosion experiment in a larger scale, in which about 100kg of corium melt was dropped into a water pool, and a steam explosion was triggered by pressure pulses from a detonator. For those experiments, data for transient pressure histories at several locations showing shock wave propagation and escalation behavior, and particle size distribution of the fine fragments produced by the steam explosion are available.

Calculation conditions

In the calculation, we simulated the experimental condition as summarized in the Table 4.2. Figure 4.24 shows the grids to simulate the KROTOS and FARO experimental systems.

The calculation of the steam explosion needs two steps, premixing and explosion calculations. In the premixing calculation, the model was tuned so that experimentally observed premixing behavior was reasonably simulated. Namely, the jet break-up length correlation and its tuning factor were selected so that jet break-up length observed in a similar condition but without explosion was reproduced in the simulation. The melt particle diameter also was given in a similar way. For FARO-L33 experiment, the Taylor type jet break-up length correlation (see Section 2.2.1) should be valid, and it was applied. While, in KROTOS experiments, it is not the case due to a transient nature of the melt delivery.[37]

After confirming that reasonable premixing calculation results, i.e. agreement with experimentally observed overall void fraction at the time of triggering, were obtained, we used those results as the initial conditions for the explosion calculations.

In the explosion calculations, on the other hand, we set a consistent set of model parameters for all the cases independent of the melt material and other conditions, i.e. $C_{frag} = 0.35$, $d_{frag} = 50(\mu\text{m})$, $t_{triglife} = 1$ (ms) and $K_{ev} = 0.7$. It was demonstrated that as long as the premixing condition was given reasonably, the explosion results were simulated reasonably with the same set of the explosion model parameters. This set of explosion model parameters was obtained by tuning them to have agreement with KROTOS alumina experiments on the pressure pulses and the mass fractions of fine debris produced by the steam explosion.

A rationale of this tuning method is as follows. Figure 4.25 shows the difference between the alumina and corium cases of KROTOS experiments on the total, molten (not frozen), molten and premixed (in the zone where void fraction is below 0.75) masses of corium obtained by the premixing calculations. Alumina melt is kept molten through out the period of the premixing stage and does not cause too much steam generation in the KROTOS condition. Thus, an ideal premixing condition, i.e. most of the melt is molten and well-mixed with water, is realized. On the other hand, with corium melt, considerable amount of the melt is already frozen or enveloped in a highly voided zone at the time of triggering, and, only a small part of the melt can actually participate in the explosion process. This difference is caused by material physical properties and the initial temperature. Alumina has lower melting and initial temperature, lower density and a larger latent heat than corium. Then, it makes larger droplets and takes much longer to freeze than corium. Also, heat transfer to water is much slower than corium due to the lower temperature as well as smaller surface area per volume. This explains the well-

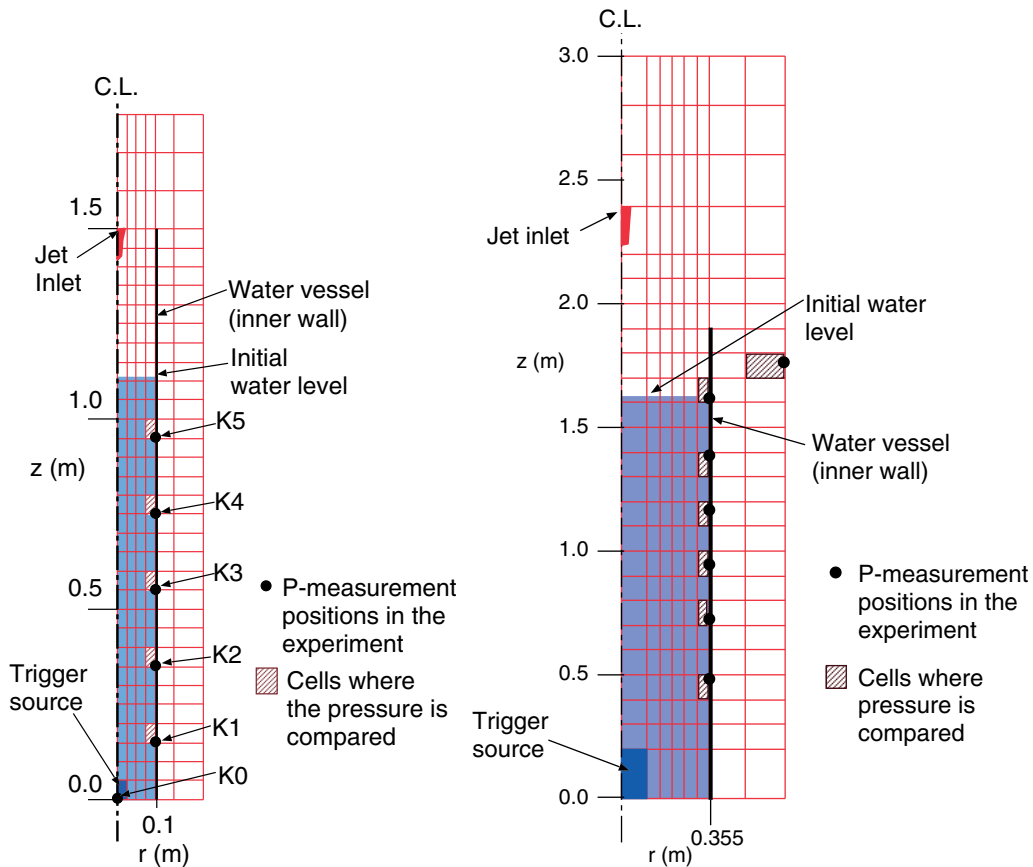


Figure 4.24: Grid geometry to simulate steam explosion experiments KROTOS series (left) and FARO-L33 (right).

known experimental observation that corium melt usually does not cause as strong explosions as alumina melt does. [39]

Considering the above, the alumina experiments are more suitable as references for the tuning of fragmentation model parameters due to the simple and ideal premixing condition. Application of the same parameter setting for corium cases should reasonably estimate weaker explosions if the difference in the premixing condition, i.e. more fraction of frozen melt and higher void fraction, is adequately simulated.

External triggering was simulated by placing a certain amount of high pressure gas in the center bottom cell. For the KROTOS experiments, the gas chamber used in the experiment was simulated by its specification (15cm^3 , 14MPa , $pV \sim 220\text{kJ}$). For FARO-L33, an equivalent volume and pressure of the gas (28.6cm^3 , 35MPa) was deduced from the detonator energy $\sim 1\text{kJ}$. Figure 4.26 shows the calculation result for propagation of the pressure pulse by the triggering device in pure water in the FARO-L33 geometry. It was confirmed that the calculated trigger pulse is in a reasonable agreement with experimental data[40].

Calculation results

Figures 4.27 and 4.28 show the comparison of calculated and experimentally observed pressure histories at various vertical locations for KROTOS alumina experiments. With the tuned explosion model parameters, the calculation results reasonably agreed with the experimental data. The influence of the water subcool was not significant. Figure 4.29 shows the calculation results for KROTOS-37, the corium experiment. It was reported that no propagating energetic

Table 4.2: Conditions and results of KROTOS-44, 42, 37 and FARO-L33 experiments, and analytical conditions (“K#” denote run numbers of KROTOS series).

		K44	K42	K37	L33
Melt	Material	Alumina ^{a)}		Corium ^{b)}	
	Released mass (kg)	1.50	1.54	3.22	100
	Temperature(K)	2673	2465	3018	3070
	Jet release dia. (mm)	30			48
	Free fall height(m)	0.44			0.77
Water	Temperature(Subcool) (K)	363(10)	293(80)	296(77)	294(124)
	Depth (m)	1.105			1.62
	Vessel diameter (m)	0.20			0.71
Cover gas	Atmosphere	Steam	Argon		
	Pressure (MPa)	0.10			0.41
	Cover gas volume(m ³)	0.290			3.496
Premixing results	Level swell (cm)	12	3	30	9
	Jet break-up length (m)	~0.3		~0.8	~1.1
Explosion results	Pressure peaks (MPa)	~50	~50	NA ^{c)}	~6
	Half height width (ms)	~1.5	~1	NA ^{c)}	~3
	Debris <0.106mm (%)	47	31	1.4	~8 ^{d)}
Analytical conditions	Time step (μ s)	~2			
	Jet initial velocity(m/s)	3.0			~2.9
	Jet flow-in duration(s)	0.270	0.255	0.191	2.6
	Melt Particle dia.(mm)	10		2	3
	Jet break-up length model ^{e)}	S: $C_{ent} = 2.5$		S: $C_{ent} = 1.7$	T: $C_{ent} = 1$
	Surface temperature drop model	Use			
	N_{per} ^{f)}	100			1000
	n_{hist} ^{f)}	500			1000
	External trigger	14.8MPa-15cm ³			35MPa-29cm ³
	Trigger time (s)	0.9		0.5	1.12
	C_{frg} ^{g)}	0.35			
	d_{frg} (μ m) ^{g)}	50			
	$t_{trigliffe}$ (ms) ^{g)}	1.0			
	p_{trig} (MPa) ^{g)}	0.2			0.5
	Fragmentation criterion	$T_{av} \geq T_{mp}$			
	K_{ev} ^{h)}	0.7			

a) $T_{melt} = 2300(K)$ b) $UO_2(80)-ZrO_2(20)$ (wt%), $T_{sol}/T_{liq} = 2830/2850(K)$

c) Reportedly “no propagating energetic explosions”[37].

d) Extrapolated from the size distribution reported in [41]. The ratio to the melt mass in the system at the triggering time, ~40kg, is ~20%.

e) S: Saito et al. correlation, T: Taylor type correlation (see 2.2.1)

f) see 2.2.3 g) see 2.2.4 h) see 2.3.2

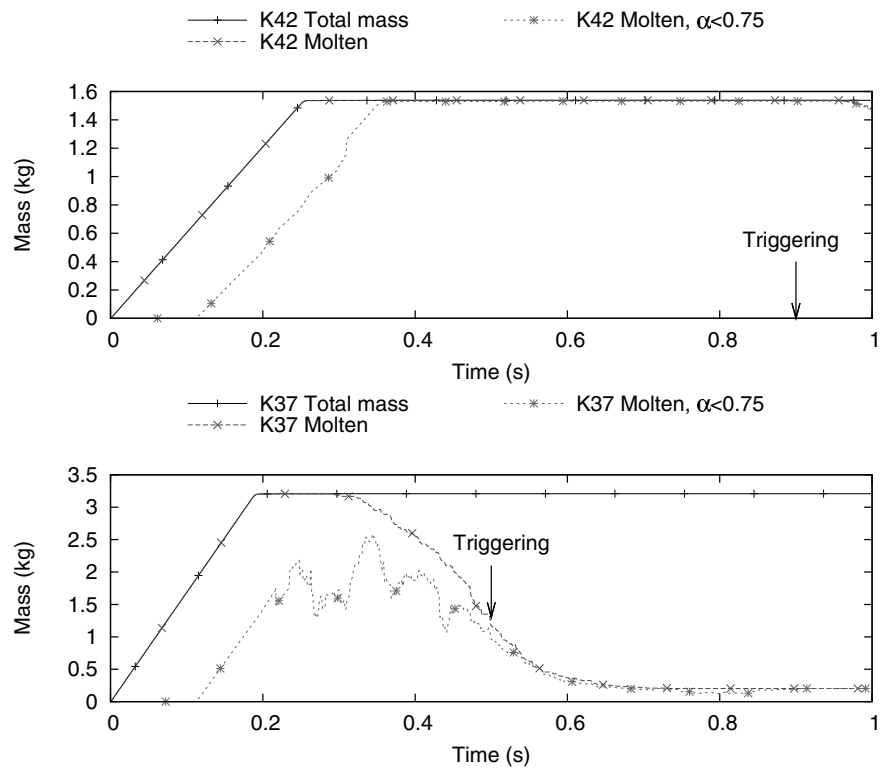


Figure 4.25: Difference of the premixing melt mass due to freezing and void in KROTOS alumina (K42, above) and corium (K37,below) experiments.

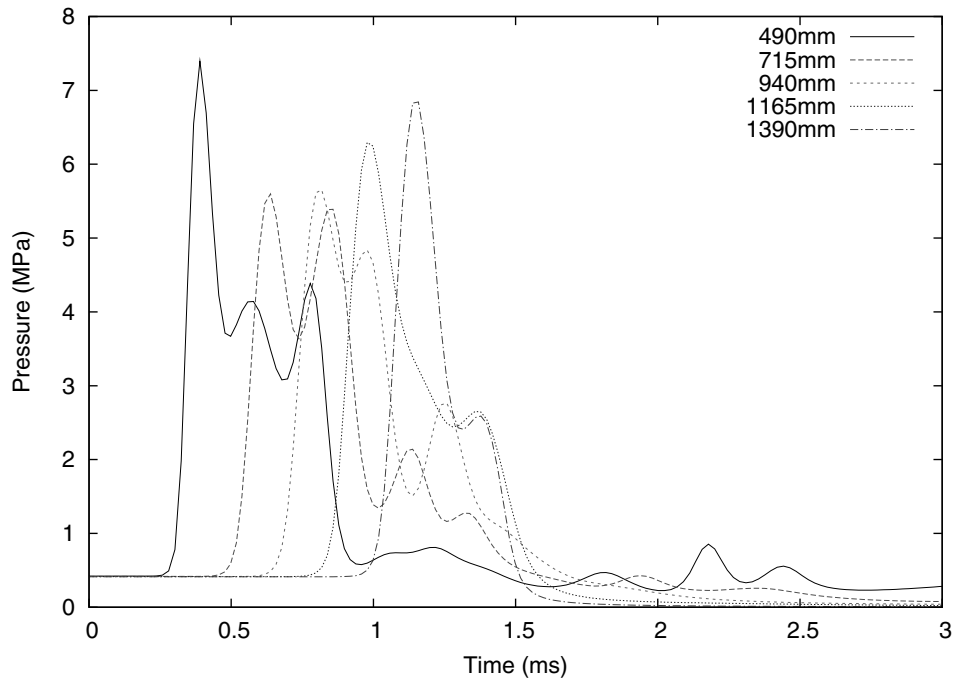


Figure 4.26: Simulation of FARO-L33 external trigger (propagation of the pressure pulse in pure water).

explosion was observed in the experiment.[37] In the calculation, the triggering pressure pulse escalated only near the bottom, K1–K2, and damped out later.

Figure 4.30 shows the comparison of calculated and experimentally observed pressure histories at various vertical locations for FARO-L33. The scale of the pressure pulse is reasonably simulated by the calculation.

Figures 4.31 and 4.32 show the evolution of the total fluid kinetic energy in the calculation in comparison with experimentally estimated kinetic energies. A good agreement was obtained for KROTOS alumina cases and FARO-L33. The calculation for KROTOS-37 showed very low kinetic energy, in agreement with the fact of no energetic explosion in the experiment.

Generally, very fine debris of the size smaller than 0.1 mm is produced by steam explosions. In the calculation, the fine debris produced by the explosion is modeled by fine fragments of uniform size, $50\mu\text{m}$. Figures 4.33 and 4.34 show comparison of the mass fraction of fine debris in experiments and in the calculations. Though rigorous comparison is not allowed due to difference in the classification of the debris size, the calculated debris mass fractions are comparable to those observed in the experiments.

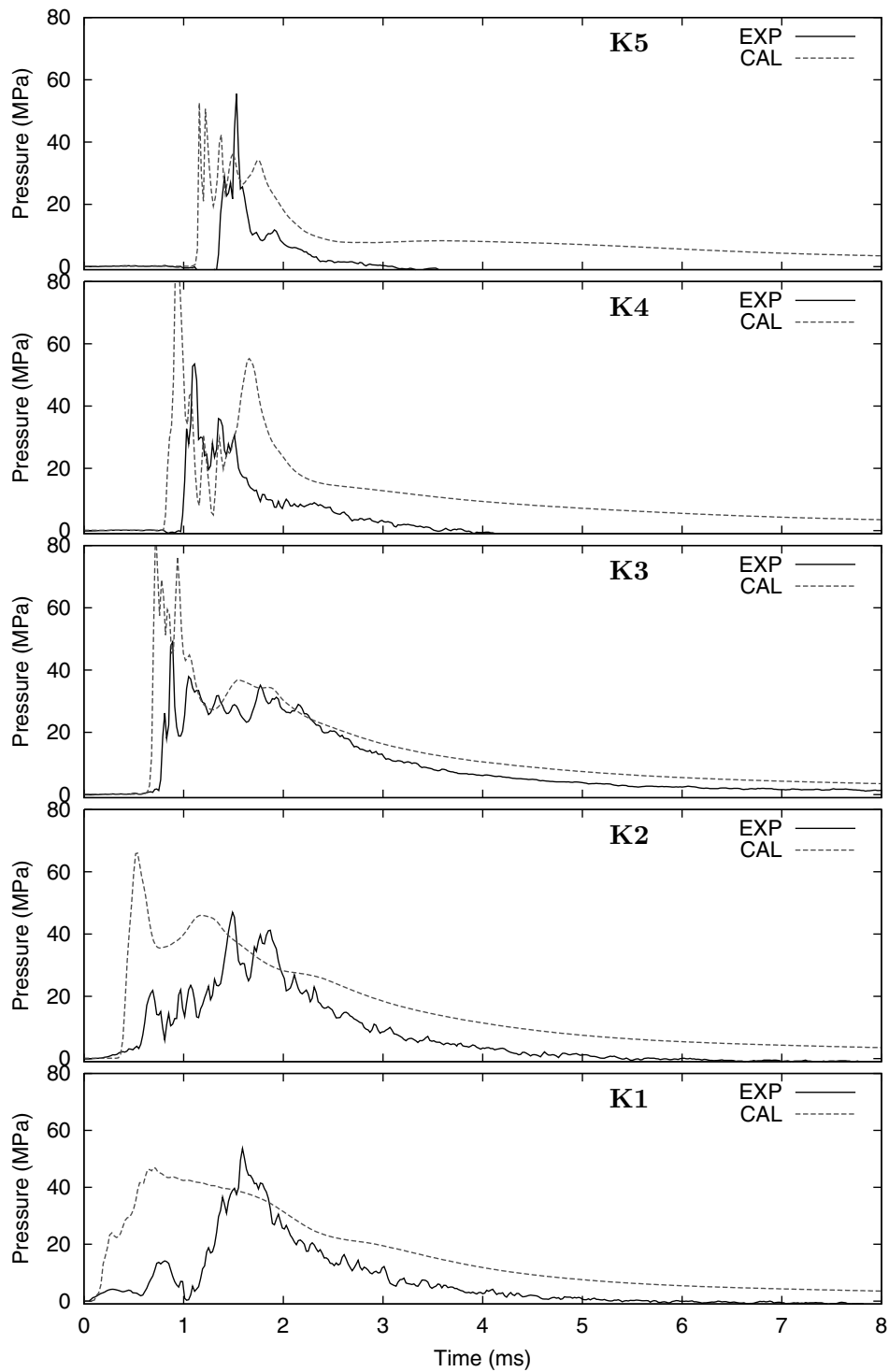


Figure 4.27: Comparison of calculation and experimental results: KROTOS 44 (alumina, saturation temperature) pressure histories at different vertical locations (K1–K5 refers locations of measurement, see Fig. 4.24).

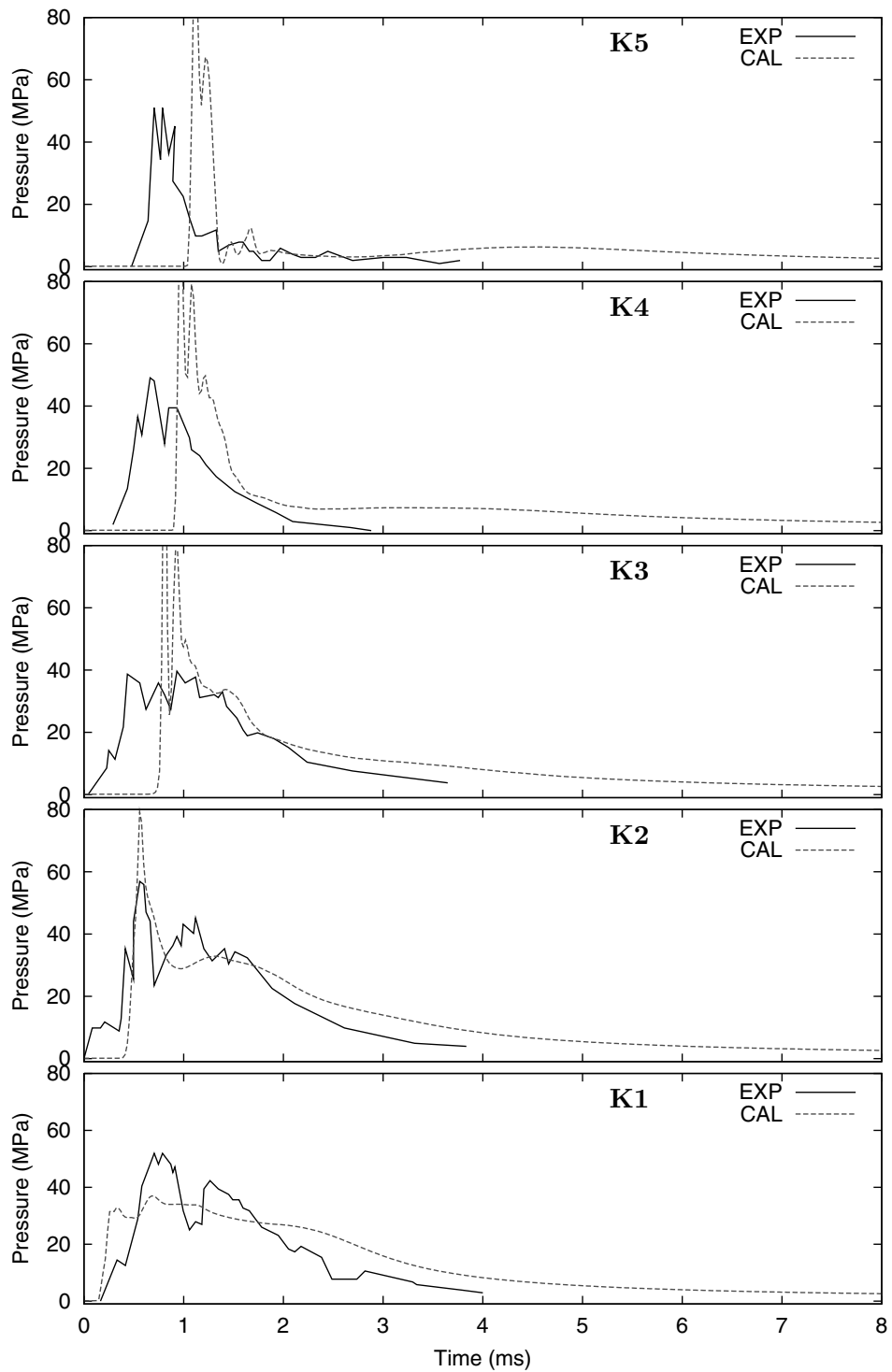


Figure 4.28: Comparison of calculation and experimental results: KROTOS 42 (alumina, sub-cooled condition) pressure histories at different vertical locations (K1–K5 refers locations of measurement, see Fig. 4.24).

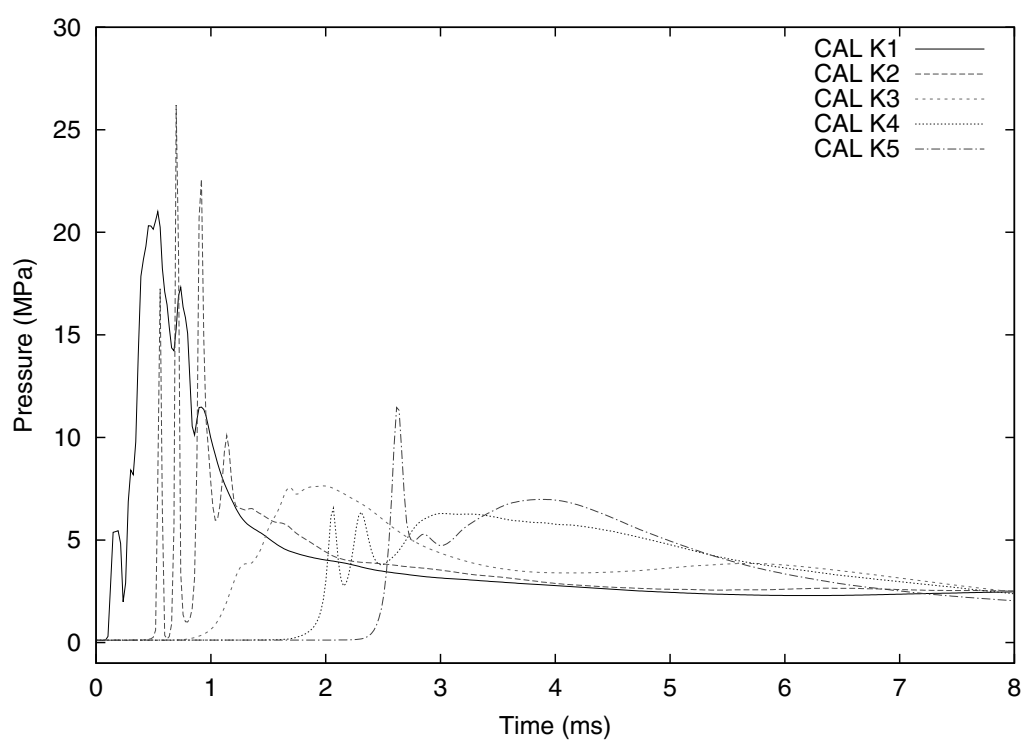


Figure 4.29: Calculated pressure histories for KROTOS 37 (corium, subcooled condition) at various vertical locations.

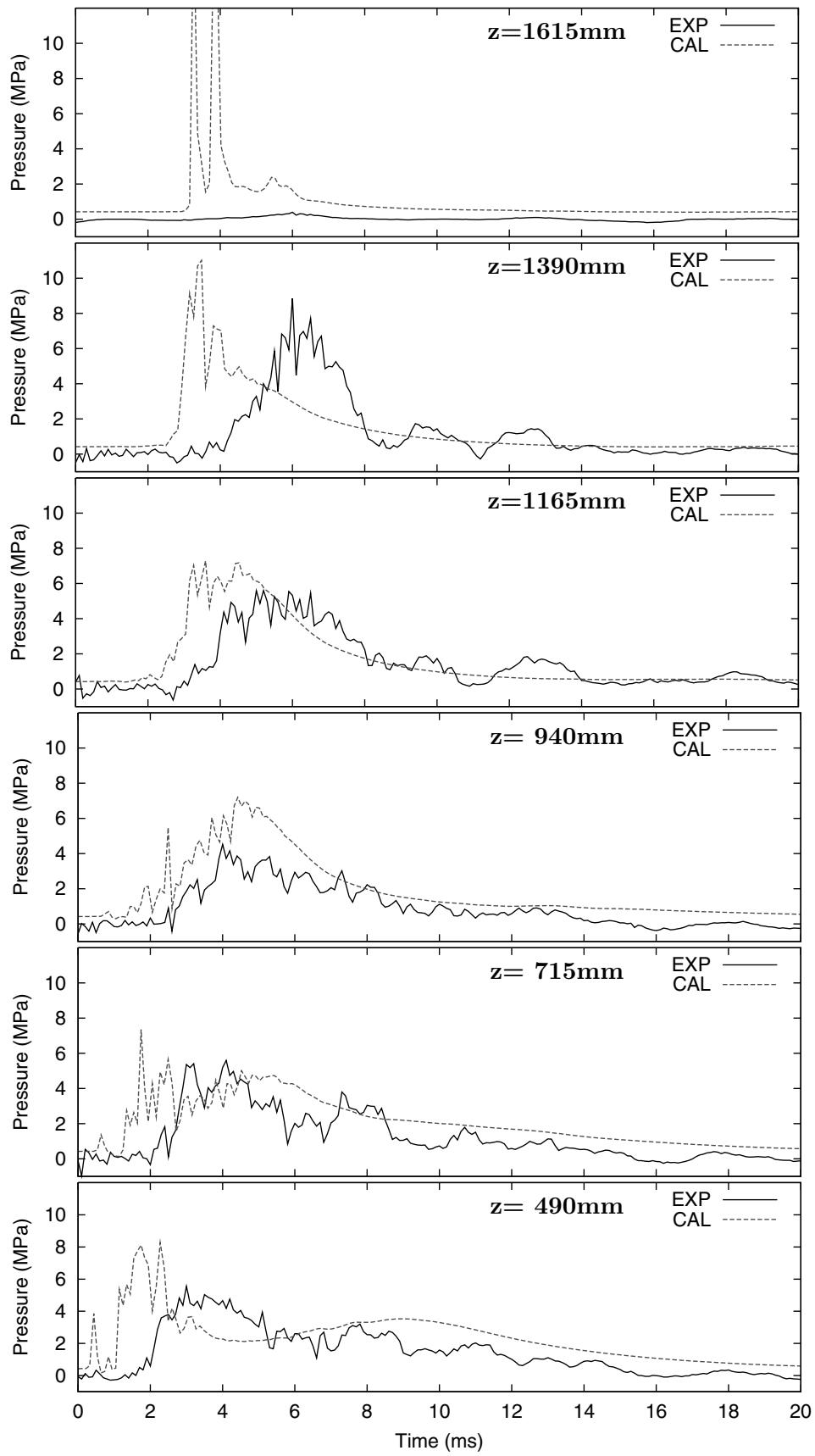


Figure 4.30: Comparison of calculation and experimental results: FARO-L33 (corium, subcooled, large scale) pressure histories at different vertical locations.

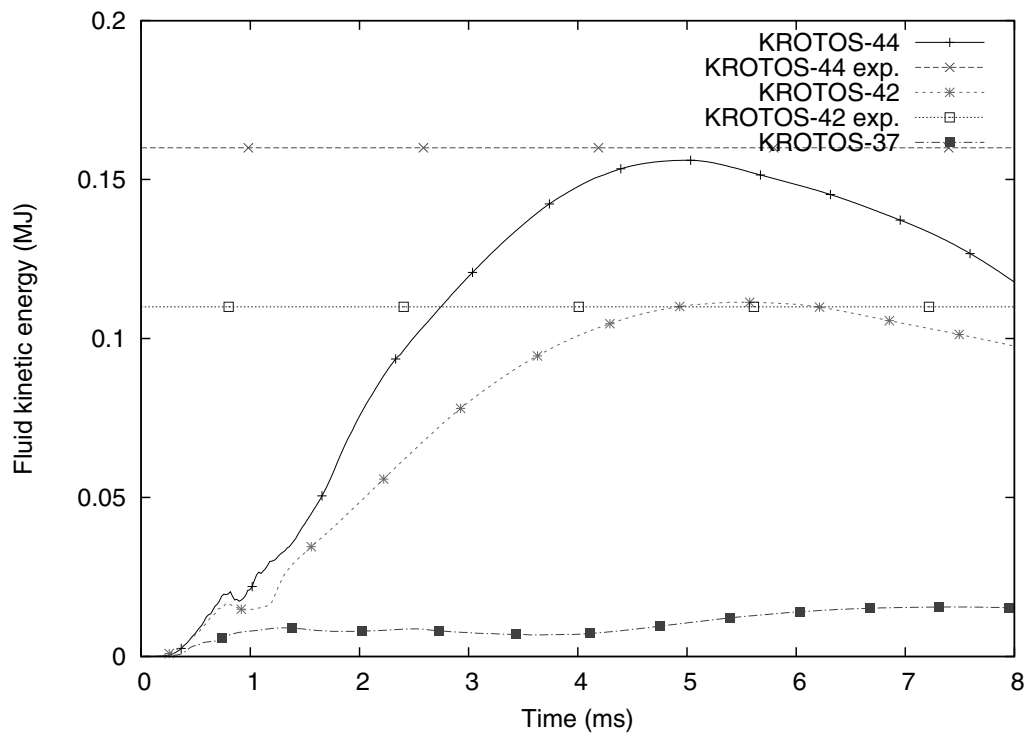


Figure 4.31: Comparison of calculation and experimental results: KROTOS total fluid kinetic energy (Experimental data is available for the final value; for KROTOS 37, only “no explosion” was reported).

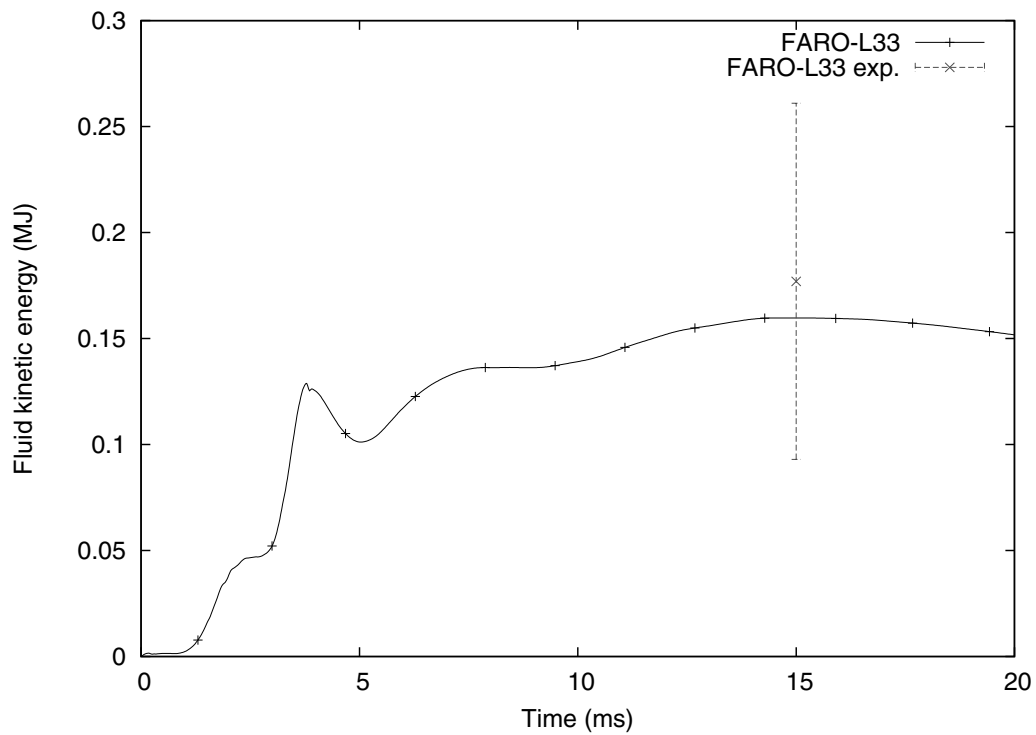


Figure 4.32: Comparison of calculation and experimental results: FARO-L33 total fluid kinetic energy (Experimental data is available for the final value).

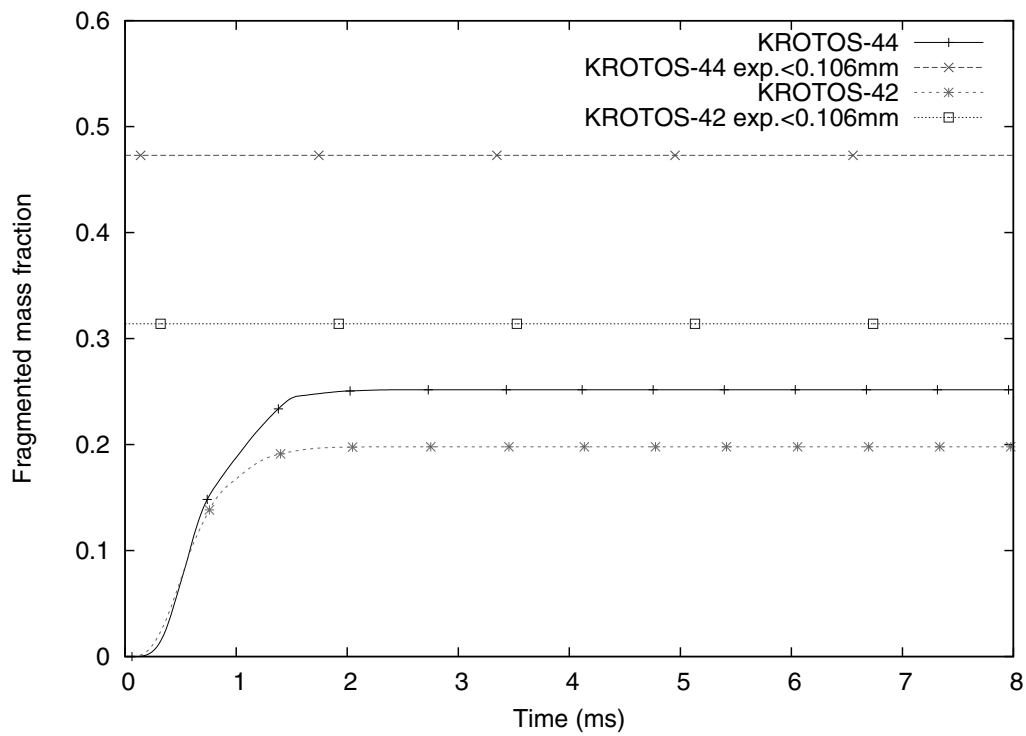


Figure 4.33: Comparison of calculation and experimental results: KROTOS fragmented mass (Experimental data is available for the final value).

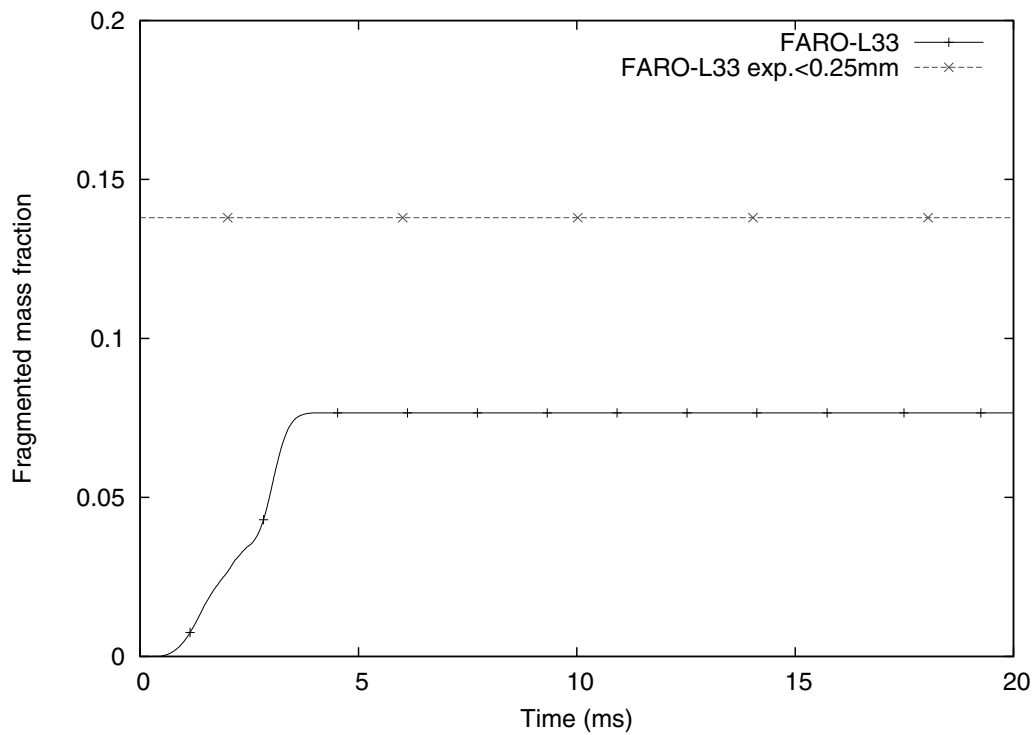


Figure 4.34: Comparison of calculation and experimental results: FARO-L33 fragmented mass (Experimental data is available for the final value).

4.4 Application for Plant Scale Simulation

Purpose

As an example for the application of JASMINE in plant scale, a simulation of PWR ex-vessel steam explosion is demonstrated.

Calculation conditions

Figure 4.35 shows the geometric conditions and the grid for the present analysis assuming a typical PWR cavity. The calculation condition is as follows.

- Water pool size: 4.1m deep, 2.75m radius
- Pressure vessel lower head: 2.2m radius, bottom position $z=5.0\text{m}$ (melt free fall height 0.9m)
- Pressure/water temperature: 0.2MPa, 342K (subcool 50K)
- Boundary condition: flow-out boundary at the top ($p=0.2\text{MPa}$, constant), Slip walls at bottom and side
- Melt material: $\text{UO}_2(80\text{wt}\%)\text{-ZrO}_2(20\text{wt}\%)$ corium, $T_{sol}/T_{liq} = 2830/2850\text{K}$, $T_{ini} = 2950\text{K}$ (superheat 100K)
- Melt jet diameter: 0.5m
- Melt release velocity: $\sim 5.5\text{m/s}$
- Triggering pressure source: bottom center, $p=10\text{MPa}$, $pV=1\text{MJ}$
- Triggering time: at the first peak of premixing mass, 0.7s
- Premixing model parameters: jet break-up length by Taylor type correlation with $C_{ent} = 1$, droplet diameter 5mm
- Explosion model parameters: $C_{frag} = 0.35$, $d_{frag} = 50(\mu\text{m})$, $t_{trigliffe} = 1$ (ms) and $K_{ev} = 0.7$ (as tuned in FARO/KROTOS simulation in the previous section)

Premixing calculation result and triggering time

The triggering time was chosen according to the premixing behavior. Figure 4.36 shows void and melt distribution profiles at different times in the premixing calculation. An oscillatory nature is observed, i.e. penetration and break-up of the melt jet, large vapor pocket generation causing worse contact of the water and melt, escape of the vapor and re-contact of the water with the melt.

The melt mass that effectively participates in the explosion process is the mass that is kept molten and resides where void fraction is not too high. So, the mass of the melt jet and particles (melt pool is excluded) whose temperature is below the melting point, and that exist in cells where void fraction is less than 0.75 is defined as “premixed mass”.

Figure 4.37 shows the history of the total mass, the molten mass and the premixed mass. The molten mass of the jet and particles are kept at almost constant level, about 5300kg, due to the balance of supply, freezing and merge to the pool. The premixed mass is oscillating reflecting the above mentioned oscillation of the void generation and escape. From our calculation experiences, the most energetic explosion is obtained by applying a triggering at the time when the premixed mass takes the first peak, about 0.7s from Fig. 4.37.

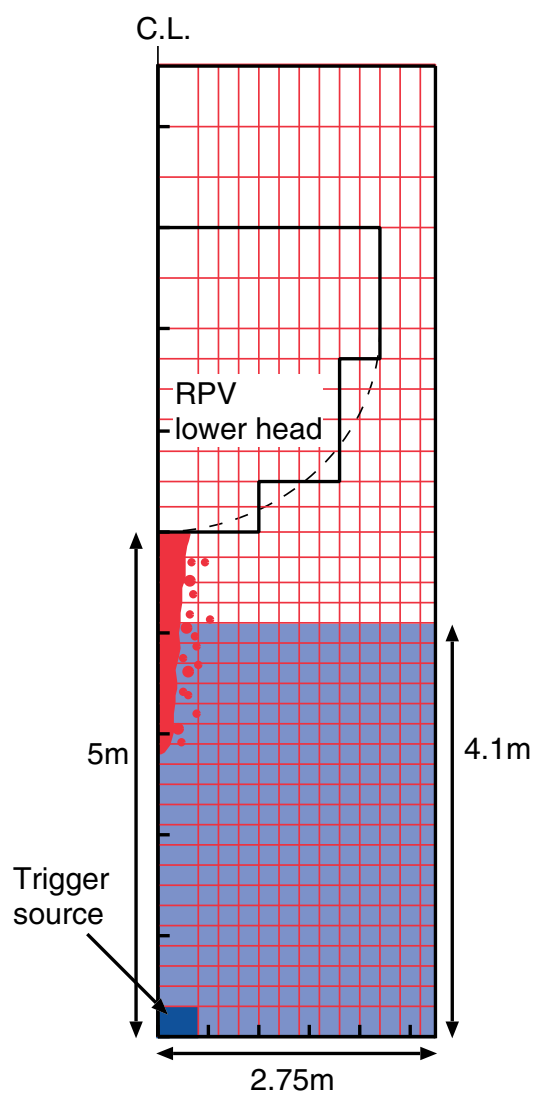


Figure 4.35: Grid geometry for the simulation of PWR ex-vessel steam explosion.

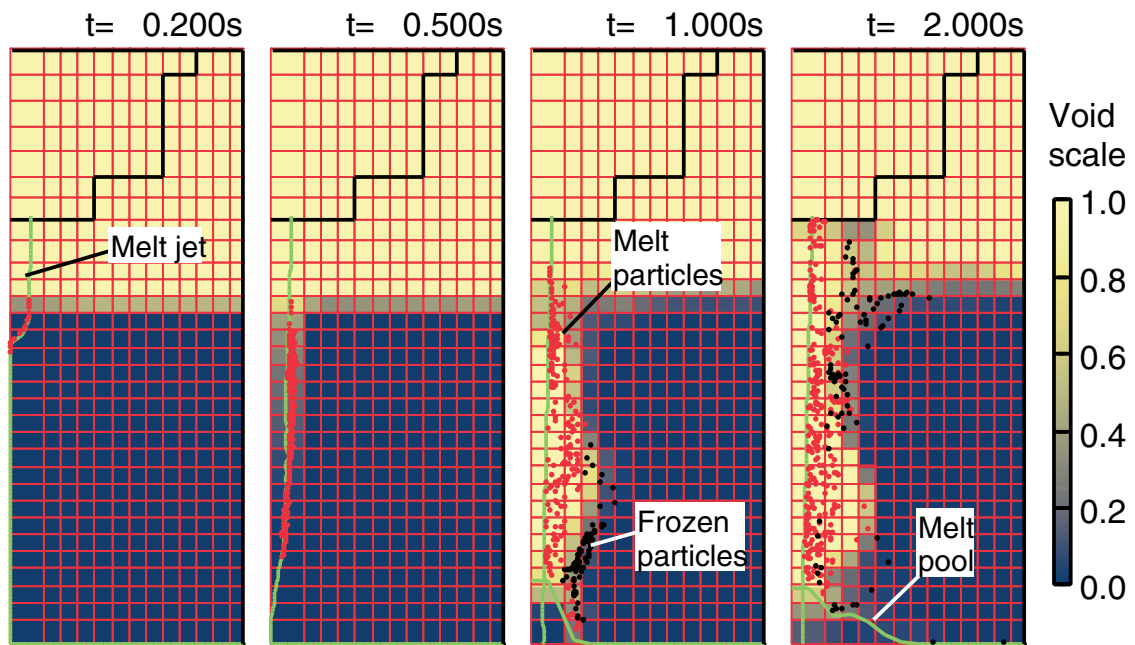


Figure 4.36: Profiles of the melt components (jet, pool and particles) and the void fraction in the premixing stage of PWR ex-vessel steam explosion simulation.

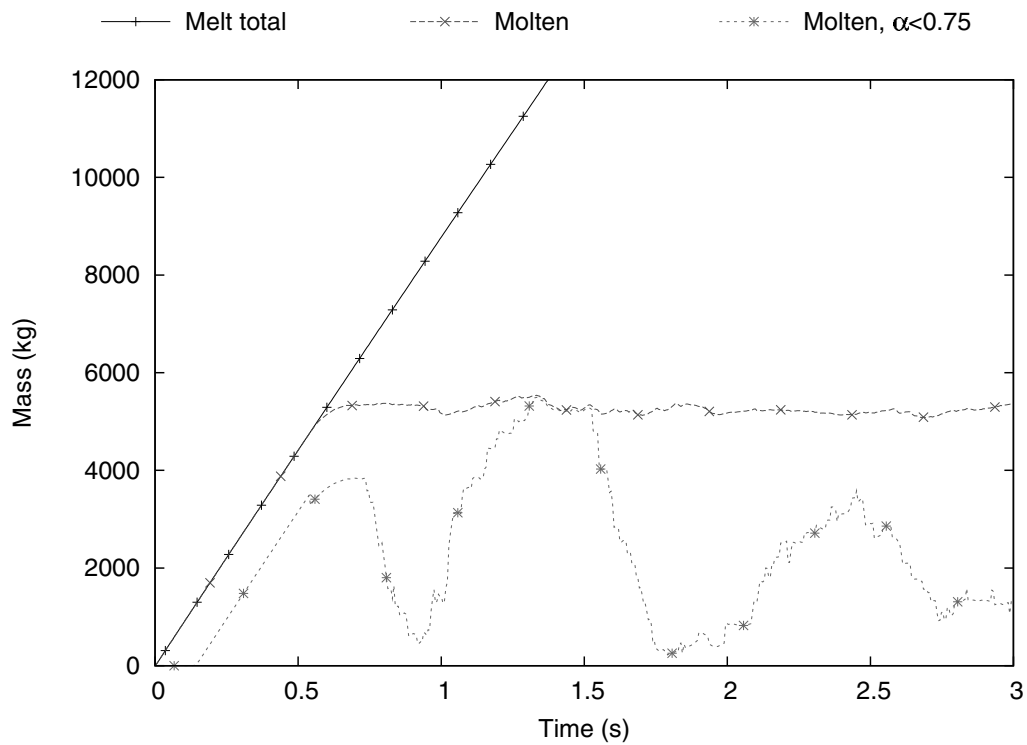


Figure 4.37: Calculated melt mass (total, molten and molten-premixed) in the premixing of PWR ex-vessel steam explosion simulation.

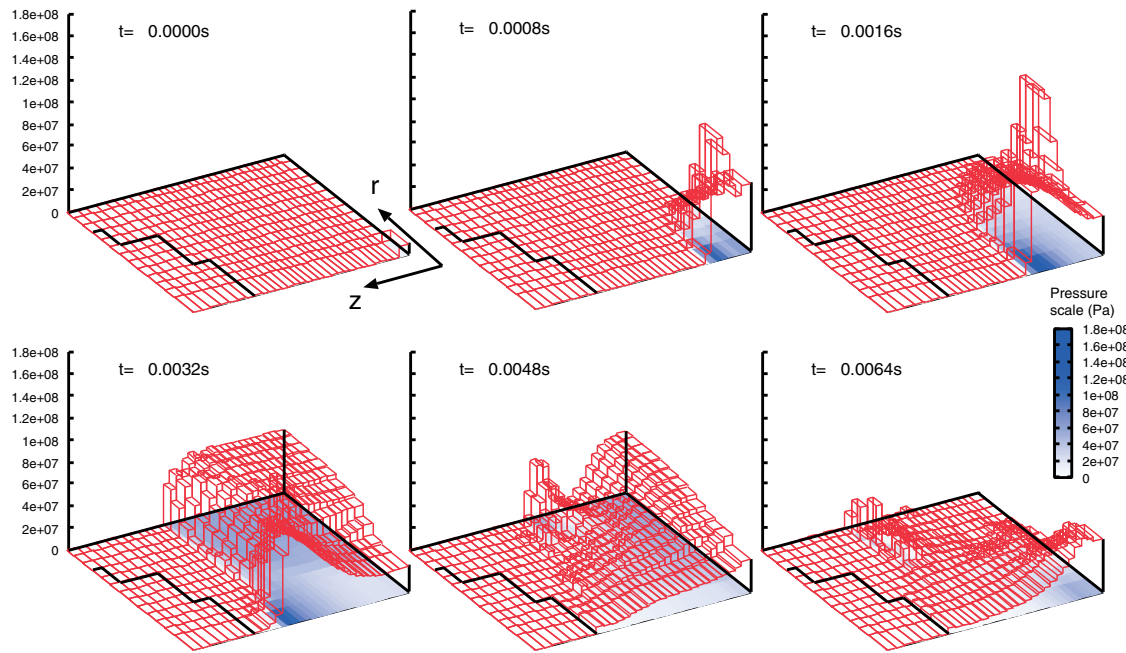


Figure 4.38: Profiles of the pressure wave propagation in the explosion stage of PWR ex-vessel steam explosion simulation.

Explosion calculation result

Figure 4.38 shows the pressure wave propagation obtained by the explosion calculation. Figure 4.39 shows the evolution of the total fluid kinetic energy. In this case, about 230MJ of the kinetic energy is reached at about 13ms after the triggering.

As output information of the explosion calculation, the impulse on wall structures can be also obtained by integrating the pressure in the cells adjacent to the wall. The impulse would be more useful for the evaluation of the integrity or damage of the walls than the kinetic energy of the fluid.[42, 43]

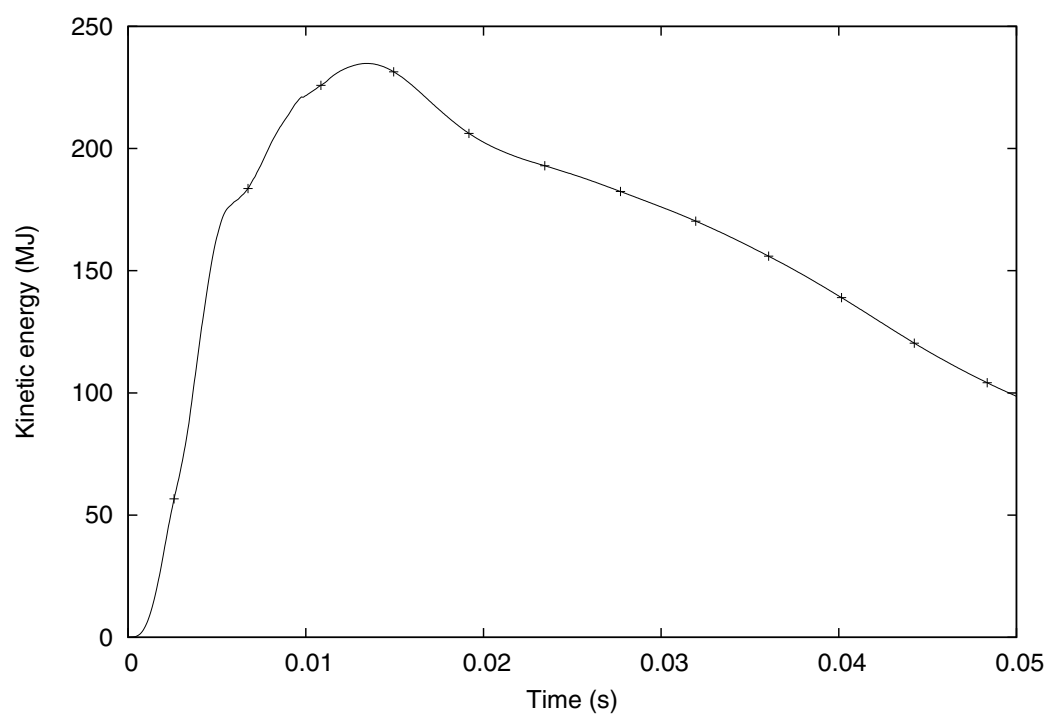


Figure 4.39: Calculated total kinetic energy of fluids in the explosion stage of PWR ex-vessel steam explosion simulation.

5 Summary

An FCI simulation code JASMINE was developed. The concept, models, numerical solution methods, verification and example calculations were described in this report. Also, some model details and practical information are collected in appendixes.

Some papers have already been published on application of JASMINE code for simulation of experiments[39], risk assessment for LWRs[42], and on a strategy for the application of FCI simulation codes for plant risk assessment[43]. Those papers also include helpful information for the usage of JASMINE code. Some of the model parameter setting have been modified from previous works. The setting described in this report is the latest one compatible with JASMINE version 3.3a.

Present limitations of the models and calculation methods, and known practical problems are summarized below.

Limitations, cautions and known problems:

- JASMINE code is, at present, applicable only for the assessment of steam explosion loads. The ability to simulate debris bed formation process and to assess long term coolability of the debris bed or melt pool is still poor.
- The present modeling and verification concept relies on the idea of limitation of the steam explosion energetics due to void and freezing. So, the status and improvement of modeling techniques and experimental data on those aspects should be watched carefully.
- Void fraction issue
 - The current ability of JASMINE code in evaluating void distribution in the premixing stage for long term is not good. We tried tuning related parameters conservatively, not to overestimate overall void fraction. To get more reliable simulation of void distribution in wide range of situations, it seems to need a fundamental improvement of 3D multiphase mixing modeling.
 - Influence of the void in the explosion process is considered with an intuitive attenuation factor, i.e. $1 \rightarrow 0$ for $\alpha = 0.3 \rightarrow 0.75$. However, such an effect of void on the fine fragmentation of the melt has not been experimentally confirmed at a fundamental level. Relevant experimental work is desirable for providing a reliable basis.
- Limitation by the numerical framework
 - As long as we use the conventional multiphase flow simulation method with spatially averaged volume fractions in relatively large cells, the void fraction in cells depends on the cell size. Water in small cells are more quickly heated-up and produce void than that in large cells due to the difference of heat capacity. It affects the attenuation of fragmentation by void.
 - At the prototypic range of melt temperature, $\sim 3000\text{K}$, radiation dominates the heat release and freezing of the melt. The radiation heat transfer may extend beyond the local cell when void fraction in the cell is large.¹ The present modeling of radiation

¹Thermal radiation is absorbed by water mostly in several millimeters of depth. However, steam is transparent to the radiation. Thus, the radiation from melt droplets in a cell filled with steam should travel to adjacent cells where is water.

- is limited within a single cell. Better radiation model considering heat deposition to surrounding cells would improve the results.
- Geometrical arrangement: The melt jet is only available in the central column of the analytical space. The one-dimensional modeling of the melt jet does not allow strong deformation of the jet leading edge (too much expansion in lateral direction causes a numerical problem).
 - Factors not modeled and that is relevant to the steam explosion process
 - Three dimensional effects: an explosion initiated not at the center of the pool (3D pressure wave dynamics)
 - Chemical effects: hydrogen generation and chemical reaction heat due to oxidation of metallic components in the melt[35, 44]
 - Leading edge effects in jet break-up
 - A care should be taken about extrapolation in scale, i.e. an application for plant scale (~ 10 tons) means an extrapolation by two orders of magnitude in the melt mass from the verification basis (~ 100 kg, in the FARO experiment). There can be unknown scale factor that causes additional uncertainty in such extrapolation.
 - Practical limitations
 - Inflexible physical property packages: The water and melt physical property packages are not flexible. The steam table package is totally hard coded; thus, usage of other kind of coolant fluid needs considerable code modification. Several kinds of melt property packages are already made available, as separate source files. Change of the melt property packages needs re-linking of the object file of the melt property package.
 - Redundancy in the output data: The binary output files, i.e. plot file for two-phase flow and melt dump file for the melt, include most of useful information. Other text format files are redundant though they may be convenient for a quick check of calculation results.
 - Restart function is only available when the melt model is used.
 - Coding style is old. (Fortran 77)

Acknowledgments

The authors acknowledge valuable suggestions and discussions of the late Mr. N. Yamano, supports by Dr. A. Ohnuki and Dr. H. Akimoto who developed and provided two-phase flow code ACE3D, an excellent work in modifying ACE-3D code for JASMINE by Mr. H. Kamo, and valuable discussions on FCI modeling and its applications with OECD/SERENA Phase-1 members. Part of the FARO/KROTOS experimental data was provided by European Commission for SERENA Phase-1 participants.

Appendix A Notation

Notation of major variables in this report is summarized here.

Alphabets

A	: cross section, surface or interface area
Bo	: Bond number
c_p	: specific heat
C	: constant, tuning parameter
$C_{damppar}$: damping factor for particle-particle collision
$C_{dampwal}$: damping factor for particle-wall collision
C_{ent}	: correction factor on the mass flux of droplet entrainment from the melt jet
C_{frag}	: tuning parameter for the fine fragmentation model
C_{vx}	: empirical constant on the entrainment x -velocity
C_{vzw}	: empirical constant for the weight in averaging melt jet and ambient fluid velocities to give the entrainment z -velocity
D, d	: diameter
\mathcal{D}	: diffusion coefficient
d_{bnd}	: boundary layer thickness around the melt jet
D_e	: diameter of melt droplets entrained from the melt jet surface
d_f	: fine fragment diameter
D_{med}	: mass median diameter of melt droplets
D_{smx}	: maximum stable diameter of melt droplets
D_p	: melt particle (droplet) diameter
e	: internal energy
f	: friction factor, function
F	: force, function
$F_{htint}, f_{higkill}, f_{hilkill}$: parameters for control of coolant evaporation in premixing stage
\mathbf{F}_{hy}	: hydrodynamic drag force on a particle
f_α	: function of the void fraction
Fr	: Froude number
g, \mathbf{g}	: gravitational acceleration
Gr	: Grashof number
h	: heat transfer coefficient, heat transfer rate, pool height
H	: height of the calculation domain, heat transfer coefficient
H_{pl}	: water pool depth
\dot{j}	: diffusional mass flux
K	: friction factor
K_{ev}	: parameter for control of coolant evaporation in explosion stage
l	: length
L_{brk}	: jet breakup length
M	: molecular weight
m_e	: mass flux of the entrainment from jet surface
m_p	: mass of a particle in a particle group
m_s	: mass flux falling on the pool surface
$n, n+1$: (superscript) old or new time step
n_g	: number of non-condensable gas components
n_{hist}	: step number criterion for release of real particle groups

N_p	: number of particles in a particle group
N_{pcr}	: criterion in number of particles for real particle-group generation
Nu	: Nusselt number
p	: pressure
p_s	: pseudo partial pressure of steam
Pr	: Prandtl number
q	: surface heat flux, heat input in a cell
Q	: heat
\dot{q}	: heat release rate
r_x, r_z	: half width of a particle group in the x and z direction
r_{xcr}	: criterion in x -direction size for real particle-group generation
R	: radius of the calculation domain, particle radius
Ra	: Rayleigh number
Re	: Reynolds number
t	: time
T	: temperature
u, v, w	: velocity components in x (r), y (θ) and z direction
v, \mathbf{v}	: velocity
V	: fluid volume in a cell, velocity, volume flux
$w(x)$: width of the calculation domain at position x ($\equiv x\Theta$)
We	: Weber number
\mathbf{x}_p	: position of the center of particle group ($\equiv (x_p, z_p)$)
x, z	: horizontal and vertical coordinates
z_{bnd}	: distance from the leading edge of the melt jet

Greek symbols

α	: void fraction, volume fraction
α_{pack}	: maximum packing ratio for particle (~ 0.6)
β	: volume expansion coefficient, an alternative independent variable ($\equiv \alpha T$)
Γ	: mass generation rate
δ	: boundary layer thickness, variance
Δh_{fg}	: latent heat of evaporation
Δt	: time step
$\Delta x, \Delta z$: grid size for x, z coordinate
Δx_{min}	: minimum x -direction grid size in the system
ϵ	: density ratio, emissivity
Θ	: Azimuthal width (angle) of the calculation domain
κ	: thermal diffusion coefficient
λ	: thermal conductivity
μ	: viscosity
ν	: kinetic viscosity
π	: Ludolphian number
ρ	: density
σ	: surface tension
σ_{SB}	: Stefan-Boltzmann constant
τ	: time, time constant

Suffixes

a	: non-condensable gas, ambient fluid
av	: average

<i>bnd</i>	: boundary layer
<i>c</i>	: continuous phase, core, center
<i>cr</i>	: critical, critical point
<i>d</i>	: dispersed phase
<i>e</i>	: entrainment
<i>f</i>	: fine fragment
<i>i</i>	: initial value
<i>i, j, k</i>	: dummy index for coordinates or components
<i>J</i>	: melt jet
<i>l</i>	: liquid water
<i>liq</i>	: liquidus point
<i>m</i>	: melt, dummy index for components
<i>mp</i>	: melting point
<i>p</i>	: melt particle
<i>P</i>	: melt pool
<i>r</i>	: relative, e.g. between melt and coolant
<i>rad</i>	: radiation
<i>s</i>	: steam
<i>sat</i>	: saturation
<i>sf</i>	: surface
<i>sol</i>	: solidus point
<i>sub</i>	: subcool
<i>sup</i>	: superheat
<i>v</i>	: vapor
<i>w</i>	: wall
∞	: infinity, far enough distance

Appendix B Particle Heat Conduction Models

B.1 Surface Temperature Drop of Melt Particles

The concept of the model is illustrated in Fig. B.1. A particle with uniform initial temperature T_c cooled at the surface is considered. A temperature profile of quadratic function is assumed in the thermal boundary layer,

$$T(r) = T_c - \frac{T_c - T_{sf}}{\delta^2} \{r - (R - \delta)\}^2, \quad (\text{B.1})$$

where T_{sf} denotes the surface temperature; δ denotes the boundary layer thickness.

The heat loss corresponding to the temperature drop in the boundary layer, Q , is expressed by

$$Q = \int_{R-\delta}^R 4\pi r^2 c\rho(T_c - T)dr, \quad (\text{B.2})$$

where c and ρ denote the specific heat and density, respectively. Substituting T with the assumed temperature profile, Eq. (B.1), gives

$$Q = \frac{4}{3}\pi R^3 c\rho(T_c - T_{sf}) \frac{\delta}{R} \left\{ 1 - \frac{1}{2} \left(\frac{\delta}{R} \right) + \frac{1}{10} \left(\frac{\delta}{R} \right)^2 \right\}. \quad (\text{B.3})$$

The surface heat flux, q , should satisfy the continuity,

$$q = -\lambda \left(\frac{dT}{dr} \right)_{r=R} = 2\lambda \frac{T_c - T_{sf}}{\delta}, \quad (\text{B.4})$$

and also the heat balance

$$4\pi R^2 q = \frac{dQ}{dt}. \quad (\text{B.5})$$

Assume that the surface heat flux q is kept constant during the period the surface temperature drops, i.e. both δ and T_{sf} in Eq. (B.3) change. By substituting

$$T_c - T_{sf} = \frac{\delta q}{2\lambda} \quad (\text{B.6})$$

obtained from Eq. (B.4) for $T_c - T_{sf}$ in Eq. (B.3), and by taking derivative of Eq. (B.3) in terms of t , we have

$$\frac{dQ}{dt} = \frac{4}{3}\pi R^2 \frac{q}{\kappa} \delta \left\{ 1 - \frac{3}{4} \left(\frac{\delta}{R} \right) + \frac{1}{5} \left(\frac{\delta}{R} \right)^2 \right\} \frac{d\delta}{dt}, \quad (\text{B.7})$$

where $\kappa = \lambda/(c\rho)$ is the thermal diffusion coefficient. By connecting Eq. (B.7) and Eq. (B.5), we have a differential equation for the evolution of thermal boundary layer,

$$\delta \left\{ 1 - \frac{3}{4} \left(\frac{\delta}{R} \right) + \frac{1}{5} \left(\frac{\delta}{R} \right)^2 \right\} d\delta = 3\kappa dt. \quad (\text{B.8})$$

We can get $T_c - T_{sf}$ by Eq. (B.6) with δ obtained by solving Eq. (B.8).

An expression for $T_{av} - T_{sf}$ is obtained by the definition of average temperature,

$$\frac{4}{3}\pi R^3 c\rho T_{av} = \frac{4}{3}\pi R^3 c\rho T_c - Q. \quad (\text{B.9})$$

Equations (B.3) and (B.9) gives

$$T_c = \frac{T_{av} - F_\delta T_{sf}}{1 - F_\delta}, \quad (\text{B.10})$$

where F_δ is a function of δ defined by

$$F_\delta = \frac{\delta}{R} \left\{ 1 - \frac{1}{2} \left(\frac{\delta}{R} \right) + \frac{1}{10} \left(\frac{\delta}{R} \right)^2 \right\}. \quad (\text{B.11})$$

Equations (B.6) and (B.10) lead an expression for the difference of the average and surface temperatures,

$$T_{av} - T_{sf} = \frac{\delta q}{2\lambda} (1 - F_\delta). \quad (\text{B.12})$$

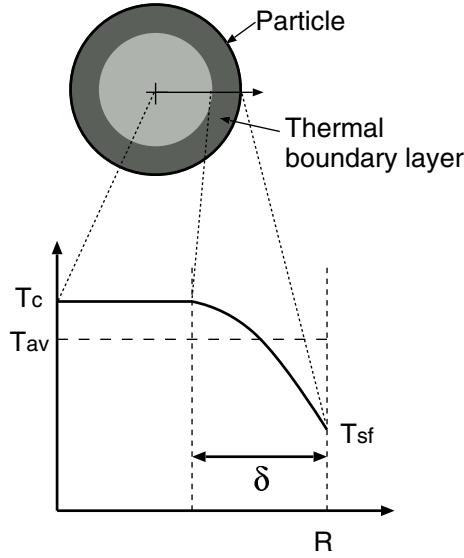


Figure B.1: The surface temperature drop model.

B.2 Fast Transient Heat Release from Fine Fragments

The concept of the model illustrated in Fig. B.2 is similar to the one for the surface temperature consideration of the melt particles (Appendix B.1). However, in the present model, the global cooling phase which comes after full development of the thermal boundary layer is also in the scope. Therefore, the present model consists of the following two phases.

- Phase I: Boundary layer development phase.
- Phase II: Global cooling phase.

In phase I, the model is basically the same as the one for the surface temperature model for melt particles. The heat loss is expressed by the boundary layer thickness, δ , by

$$Q = \frac{4}{3} \pi R^3 c \rho (T_{c0} - T_{sf}) \frac{\delta}{R} \left\{ 1 - \frac{1}{2} \left(\frac{\delta}{R} \right) + \frac{1}{10} \left(\frac{\delta}{R} \right)^2 \right\}. \quad (\text{B.13})$$

The assumed temperature profile in the boundary layer,

$$T(r) = T_{c0} - \frac{T_{c0} - T_{sf}}{\delta^2} \{ r - (R - \delta) \}^2, \quad (\text{B.14})$$

gives the heat flux at the surface by

$$q = 2\lambda \frac{T_{c0} - T_{sf}}{\delta}. \quad (\text{B.15})$$

In the present model, we assume constant surface temperature, $T_{sf} = \text{const.}$, instead of constant surface heat flux as we did in the previous section B.1. The constant surface temperature is valid typically for the interfacial heat conduction of two objects in sudden contact.

From the heat balance at the surface,

$$4\pi R^2 q = \frac{dQ}{dt}, \quad (\text{B.16})$$

and Eqs. (B.13) and (B.15), we obtain the differential equation for the boundary layer development,

$$\delta \left\{ 1 - \frac{\delta}{R} + \frac{3}{10} \left(\frac{\delta}{R} \right)^2 \right\} d\delta = 6\kappa dt. \quad (\text{B.17})$$

Non-dimensional form of the equations are obtained by normalizing δ , t and Q by

$$x = \frac{\delta}{R}, \quad \tau = \frac{\kappa t}{R^2}, \text{ and } \beta = \frac{Q}{Q_0}, \quad (\text{B.18})$$

where Q_0 is the total heat inventory

$$Q_0 = \frac{4}{3}\pi R^3 c\rho(T_{c0} - T_{sf}). \quad (\text{B.19})$$

The non-dimensional forms of Eqs. (B.13) and (B.17) are

$$\beta = x \left(1 - \frac{1}{2}x + \frac{1}{10}x^2 \right), \text{ and} \quad (\text{B.20})$$

$$x \left(1 - x + \frac{3}{10}x^2 \right) dx = 6d\tau. \quad (\text{B.21})$$

We can solve x by numerical integration starting with initial value $x_0 = \sqrt{12\tau_0}$ based on the first order analytical solution. During phase I process, the change of the non-dimensional parameters is $x = 0 \sim 1$, $\beta = 0 \sim \beta_1 (\equiv 3/5)$ and $\tau = 0 \sim \tau_1$. The non-dimensional time of the end of phase I, τ_1 , is 0.040 according to the numerical solution.

During phase II, the center temperature, T_c decreases from T_{c0} , while the boundary layer thickness is fixed at R . The additional heat loss during phase II is

$$\Delta Q = Q - Q_1 = \frac{8}{15}\pi R^3 c\rho(T_{c0} - T_c), \quad (\text{B.22})$$

where Q_1 is the heat loss at the end of phase I, which corresponds to β_1 . In this case, the surface heat flux balance, Eq. (B.16), leads the time evolution equation,

$$dT_c = -15(T_c - T_{sf}) \frac{\kappa}{R^2} dt. \quad (\text{B.23})$$

By normalizing the center temperature by

$$\theta = \frac{T_c - T_{sf}}{T_{c0} - T_{sf}}, \quad (\text{B.24})$$

we have normalized form of Eqs. (B.22) and (B.23),

$$\beta = \beta_1 + \frac{2}{5}(1 - \theta), \text{ and} \quad (\text{B.25})$$

$$d\theta = -15\theta d\tau. \quad (\text{B.26})$$

Equation (B.26) is solved analytically, with the initial condition $\tau = \tau_1$ and $\theta = 1$.

$$\theta = e^{-15(\tau - \tau_1)} . \quad (\text{B.27})$$

The non-dimensional parameters change by $\theta = 1 \rightarrow 0$, $\beta = \beta_1 \rightarrow 1$ and $\tau = \tau_1 \rightarrow \infty$ during phase II.

Let us define the non-dimensional time constant for the heat release from a fragment, τ_f , as non-dimensional time, τ , at which the heat loss fraction, β , equals $1 - e^{-1} \simeq 0.632$. The non-dimensional time constant, τ_f , is in phase II, and the value is about 0.046.

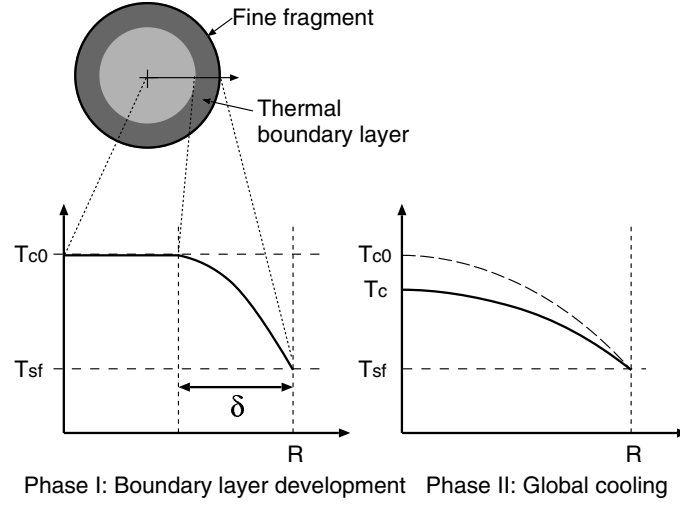


Figure B.2: The heat release model for fine fragments.

Appendix C Brief Description of CIP Method

C.1 Basic Concept of CIP Method

CIP—cubic interpolated pseudo particle—method was developed by Yabe and Aoki[31]. The basic concept of this scheme is cubic interpolation of discrete data and handling the advection term by moving the profile like in Lagrange method. Consider a one-dimensional hyperbolic equation

$$\frac{\partial f}{\partial t} + v \frac{\partial f}{\partial z} = 0, \quad (\text{C.1})$$

where advection velocity v is constant. Given a spatial profile of the function f and the velocity v at a certain time t , the value of f at a certain grid point z_i after a short moment Δt can be approximated as a result of advection.

$$f(z_i, t + \Delta t) \simeq f(z_i - v\Delta t, t) \quad (\text{C.2})$$

In the CIP method, the values of f between grid points are interpolated with a cubic polynomial

$$F_i(z) = \{(a_i X + b_i)X + f'_i\}X + f_i, \quad (\text{C.3})$$

where $X = z - z_i$, and f'_i is the spatial derivative of f at the point z_i . The constants a_i and b_i are derived by considering the continuity of f and f' at grid points i and $i + 1$ or $i - 1$ depending on the direction of the velocity,

$$a_i = \frac{-2\phi + f'_{i_2} + f'_i}{\Delta z^2}, \quad (\text{C.4})$$

$$b_i = \frac{3\phi - f'_{i_2} - 2f'_i}{\Delta z}, \quad (\text{C.5})$$

$$\phi = \frac{f_{i_2} - f_i}{\Delta z}, \quad (\text{C.6})$$

where $i_2 = i + 1$ when $v \leq 0$ or $i_2 = i - 1$ otherwise, and $\Delta z = z_{i_2} - z_i$. Note that the grid is defined such as $\dots z_{i-1} < z_i < z_{i+1} \dots$.

The controlling equation for the spatial derivative f' can be deduced from the original equation,

$$\frac{\partial f'}{\partial t} + v \frac{\partial f'}{\partial z} = -f' \frac{\partial v}{\partial z}. \quad (\text{C.7})$$

In linear case where v is constant, the right hand side vanishes and it becomes identical with the original equation.

Therefore, once the profile of the function and its derivative is given at t as f and f' , the profile at the next time step $t + \Delta t$ can be calculated using the constants a_i and b_i by

$$f_i^{new} = F_i(z_i - v\Delta t) = \{(a_i \xi + b_i)\xi + f'_i\}\xi + f_i, \quad (\text{C.8})$$

$$f'_i{}^{new} = F'_i(z_i - v\Delta t) = (3a_i \xi + 2b_i)\xi + f'_i, \quad (\text{C.9})$$

where $\xi = -v\Delta t$.

C.2 Improvement for Steep Steps—CIP1 Scheme

A steep edge of function f can be encountered at places such as leading or trailing edge of a melt jet, where the material suddenly begins or quits to exist. The basic scheme brings over- or under-shoot at such places, due to the feature of cubic polynomial interpolation. A simple counter measure for it is given in Ref.[31].

Assume that a certain grid point is located at the edge of the profile, i.e. one side is almost flat and the other side has a steep change. The interpolated function profile at the flat side is significantly different from the reality and causes unphysical over- or under-shoot. To prevent this feature, two different derivatives are considered on the front and the back side of such an “edge point”, and the use of derivative based on the interpolated profile is given up on the flat side, but give the derivative by finite difference between two points instead. This scheme is called CIP1[31]. An index n_p is introduced to put a flag on the point at the edge.

$$n_p = -1 \quad \text{if } \frac{|f_i - f_{i-1}|}{|f_{i+1} - f_i|} < \epsilon \text{ and } \frac{|f_{i-1} - f_{i-2}|}{|f_{i+1} - f_i|} < \epsilon \text{ (gap on the front side) or} \quad (\text{C.10})$$

$$n_p = 1 \quad \text{if } \frac{|f_{i+1} - f_i|}{|f_i - f_{i-1}|} < \epsilon \text{ and } \frac{|f_{i+2} - f_{i+1}|}{|f_i - f_{i-1}|} < \epsilon \text{ (gap on the back side) or} \quad (\text{C.11})$$

$$n_p = 0 \quad \text{otherwise.} \quad (\text{C.12})$$

The constant ϵ should be a small value like 0.05. The derivatives on both sides of the point i is taken differently as $f'_{i,1}$ (front) and $f'_{i,0}$ (back). They are initially set equal to f'_i and changed in case an edge is detected as follows.

$$f'_{i,0} = \frac{f_i - f_{i-1}}{z_i - z_{i-1}} \quad \text{if } n_p = -1, \quad (\text{C.13})$$

$$f'_{i,1} = \frac{f_{i+1} - f_i}{z_{i+1} - z_i} \quad \text{if } n_p = 1. \quad (\text{C.14})$$

$$(\text{C.15})$$

The improved scheme becomes as follows.

$$\text{if } \xi \geq 0, \quad i_2 = i + 1 \quad \text{and } i_3 = 1, \quad (\text{C.16})$$

$$\text{otherwise } i_2 = i - 1 \quad \text{and } i_3 = 0. \quad (\text{C.17})$$

$$\Delta z = z_{i_2} - z_i, \quad (\text{C.18})$$

$$\phi = \frac{f_{i_2} - f_i}{\Delta z}, \quad (\text{C.19})$$

$$a_i = \frac{-2\phi + f'_{i_2,1-i_3} + f'_{i,i_3}}{\Delta z^2}, \quad (\text{C.20})$$

$$b_i = \frac{3\phi - f'_{i_2,1-i_3} - 2f'_{i,i_3}}{\Delta z}, \quad (\text{C.21})$$

$$f_i^{new} = \{(a_i \xi + b_i) \xi + f'_{i,i_3}\} \xi + f_i, \quad (\text{C.22})$$

$$f_i^{new} = (3a_i \xi + 2b_i) \xi + f'_{i,i_3}. \quad (\text{C.23})$$

This CIP1 scheme is used in the melt jet model of JASMINE.

C.3 Non-Linear Equation

A non-linear hyperbolic equation with a source term g

$$\frac{\partial f}{\partial t} + \frac{\partial f v}{\partial z} = g \quad (\text{C.24})$$

is transformed into a non-conservation form

$$\frac{\partial f}{\partial t} + v \frac{\partial f}{\partial z} = g - f \frac{\partial v}{\partial z} \equiv G. \quad (\text{C.25})$$

Corresponding equation for the derivative is

$$\frac{\partial f'}{\partial t} + v \frac{\partial f'}{\partial z} = G' - f' \frac{\partial v}{\partial z}. \quad (\text{C.26})$$

These equations are solved in two steps, so called advection and non-advection phases.

- Advection phase:

$$\frac{\partial f}{\partial t} + v \frac{\partial f}{\partial z} = 0 \quad (\text{C.27})$$

$$\frac{\partial f'}{\partial t} + v \frac{\partial f'}{\partial z} = 0 \quad (\text{C.28})$$

- Non-advection phase:

$$\frac{\partial f}{\partial t} = G \quad (\text{C.29})$$

$$\frac{\partial f'}{\partial t} = G' - f' \frac{\partial v}{\partial z} \quad (\text{C.30})$$

Starting from values at the old time step, first, the advection phase is calculated by the method described in the previous section, and an intermediate result is obtained. Then, the non-advection phase is solved in any method such as finite-difference, and the final result for the new time step is obtained. The following equations are finite difference form of the non-advection phase, with intermediate values denoted by asterisk * and new time step values denoted by superscript *new*.

$$\frac{f_i^{new} - f_i^*}{\Delta t} = G_i \quad (\text{C.31})$$

$$\begin{aligned} \frac{f_i^{new} - f_i^*}{\Delta t} &= G_i - f_i^* \left(\frac{\partial v}{\partial z} \right)_i \\ &= \frac{(f_{i+1}^{new} - f_{i+1}^*) - (f_{i-1}^{new} - f_{i-1}^*)}{\Delta t(z_{i+1} - z_{i-1})} - f_i^* \left(\frac{\partial v}{\partial z} \right)_i \end{aligned} \quad (\text{C.32})$$

Appendix D Steam Table Package WRSTEAMTAB

WRSTEAMTAB is a rapid running steam table package that has table data generated by the formulas published in JSME (The Japan Society of Mechanical Engineers) steam table (1980 edition)[45, 46] and calculates physical properties at a given set of pressure and temperature by interpolation of the table. The calculation for the interpolation is much faster than direct calculation of the original formulas.

The steam table data consist of the values of density and enthalpy, and their derivatives in terms of temperature and pressure. The same cubic polynomial interpolation scheme as in the CIP method (Appendix. C) is used on the pressure-temperature plane. The table points are shown in Fig. D.1. Because of the utilization of the derivatives at each point, even a relatively coarse grid gives an adequate level of accuracy. Also, adoption of this interpolation method automatically brings the consistency of the derivatives that is necessary for the numerical solution of the two-phase flow model.

The table data covers the temperature range $274 < T_l < 787(\text{K})$ for water and $281 < T_g < 999(\text{K})$ for steam, and pressure range $10^3 < P < 10^8(\text{Pa})$. Extrapolation is provided at the edges of the table range either by linear extrapolation or ideal gas approximation to cover a wider range, $P \sim 2 \times 10^8(\text{Pa})$, $T_l \sim 800(\text{K})$ and $T_g \sim 3000(\text{K})$. Especially the high temperature range is needed for steam explosion modeling, which involves high temperature melt.

The two-phase flow model in JASMINE considers a two-phase medium even in the supercritical conditions. In other words, the conventional two-phase flow model is extended into the supercritical regime to cover the situation that may arise in the steam explosion simulation. To support this treatment, the saturation line is extended into the supercritical regime, and liquid/steam properties are given keeping a consistency, i.e. slightly smaller density and slightly higher enthalpy for steam than water. Both water and steam properties are made available near the saturation line so that superheated water (superheat $\sim 10\text{K}$) and supercooled steam (supercool $\sim 10\text{K}$) is managed numerically.

The accuracy of the saturation temperature, liquid density, liquid enthalpy, steam density and steam enthalpy are shown in Figs D.2–D.6. The very steep variation near the critical point is intentionally smoothed because it can be harmful for stable numerical solution. Then, the accuracy around that area is not good. However, an adequate accuracy is obtained in other areas.

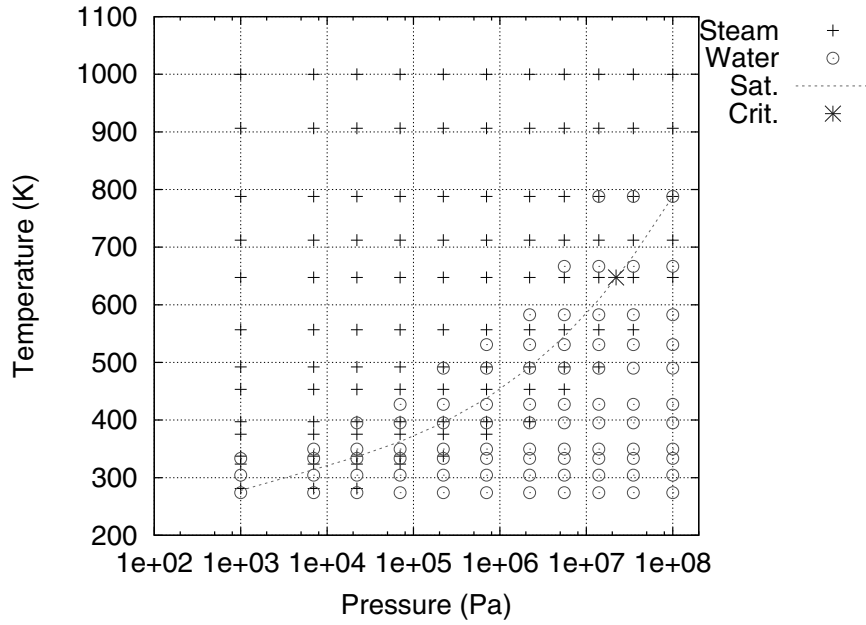


Figure D.1: The table data points for WRSTEAMTAB.

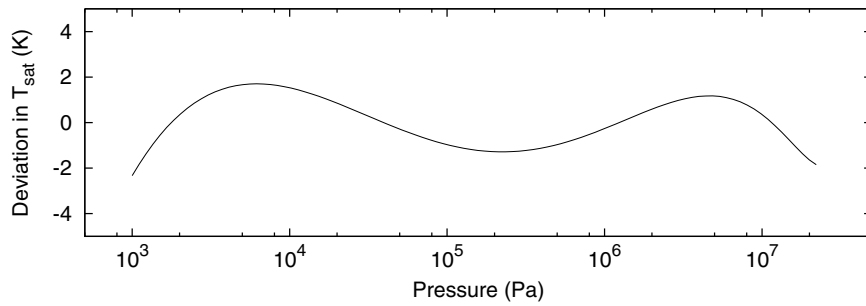


Figure D.2: Deviation of the calculated saturation temperature by WRSTEAMTAB from the JSME formula, $T_{sat}(\text{WRSTEAMTAB}) - T_{sat}(\text{JSME})$.

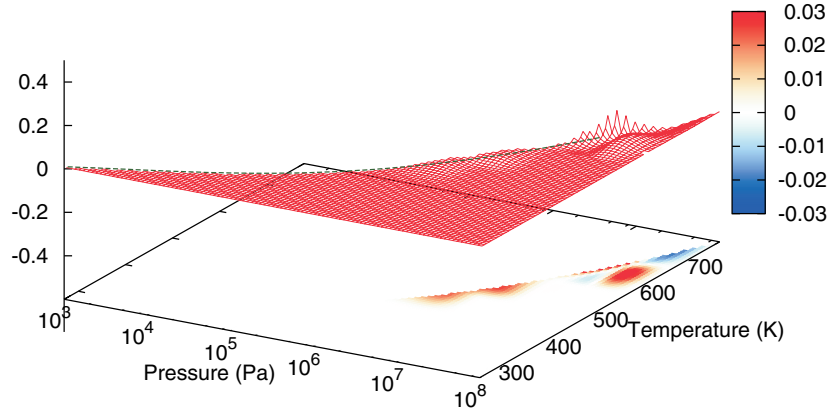


Figure D.3: Relative deviation of the calculated water density by WRSTEAMTAB from the JSME formula, $(\rho_l(\text{WRSTEAMTAB}) - \rho_l(\text{JSME}))/\rho_l(\text{JSME})$.

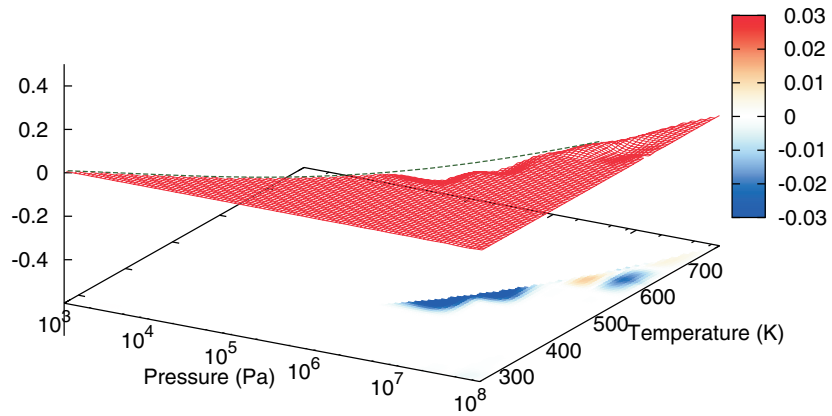


Figure D.4: Relative deviation of the calculated water enthalpy by WRSTEAMTAB from the JSME formula, $(h_l(\text{WRSTEAMTAB}) - h_l(\text{JSME}))/h_l(\text{JSME})$.

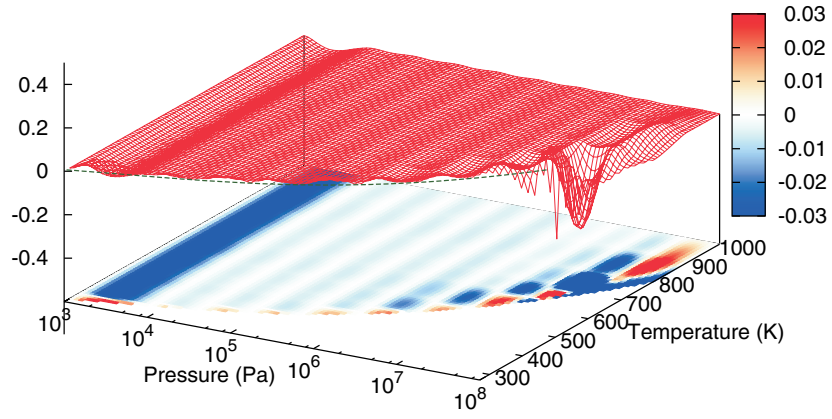


Figure D.5: Relative deviation of the calculated steam density by WRSTEAMTAB from the JSME formula, $(\rho_g(\text{WRSTEAMTAB}) - \rho_g(\text{JSME}))/\rho_g(\text{JSME})$.

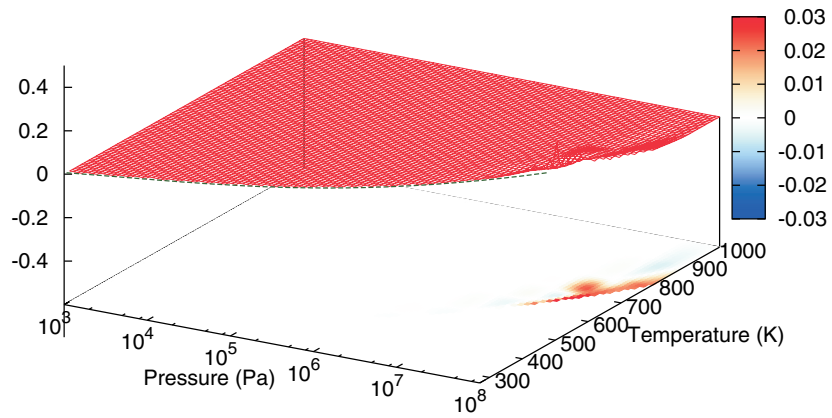


Figure D.6: Relative deviation of the calculated steam enthalpy by WRSTEAMTAB from the JSME formula, $(h_g(\text{WRSTEAMTAB}) - h_g(\text{JSME}))/h_g(\text{JSME})$.

Appendix E Input Preparation and Code Usage

E.1 Input File Format

The input file is prepared as a plain text file and read by the code line by line, then interpreted according to the order of the data. The interpreter has preprocessing functions to do with comments, inclusion of other files and echoing. In the following sections, the preprocessing functions and order of the data in the input file are described.

E.1.1 Preprocessing

Line length Maximum length of lines in the input file is 140 characters. The first 132 characters are interpreted as data and rest of the line is neglected as an ID field.

Comments Comment lines can be included in the input file. Any characters following double slashes “//” are ignored as comments.

```
//  this is a comment line.
  3      5      12.6  // anything after "//" is ignored.
```

Also, C-style commenting is available. That is, characters embraced by a pair of “/*” and “*/” is interpreted as a comment.

```
/* node */ 15 /* element */ 6
23.8 /*
  this is a comment.
  */ 56.7
```

Nesting of the “/* */” pair, as in the next example, is not allowed. The job is terminated if it is detected.

```
/*  /* this is an example of nesting. */ */
```

Directives There are directives that give instructions to the code about the processing of the input file. A directive is recognized by one of the following keywords at the head of a line.

- **#include <file name>** : To include a file at the position this directive appears. Nesting of including is not allowed.
- **#listoff** : To stop echoing the input data. (The input data is echoed into the list output unit.)
- **#liston** : To resume echoing the input data.

E.1.2 Input Variables and Their Ordering

An input file consists of following sections. The data are recognized according to the position (order) that they appears. In the followings, variable names, types, meanings, values to be given etc. are listed. Values given in () are default or recommended values.

Flag for the namelist options

The first section is a flag to instruct whether a namelist options (see below) are given or not.

Variable	Type	Description
iopt	Int	Flag on the usage of namelist options 0 = No use of namelist options 1 = Use of namelist options

Title

Title of the case is read as a 132-character string.

Variable	Type	Description
title	Char	Title of the case in a132 format

Namelist options

If iopt=1 is specified in the first section, a namelist “option” is read. The input format in this section conforms to the Fortran namelist input syntax. Variables defined in the namelist “option” is as follows.

Variable	Type	Description
cvm	Real	Coefficient of the virtual mass term for two-phase flow (0.0)
sdtim	Real	Time step for message (stdout) output (0.1[s])
sdstp	Int	Step interval for message output (1000)
editop	Int	List output selection (0) 0 = Primary variables only 1 = More variables 2 = All the available variables
idebug	Int	Flag to control debug information output (0) 0 = No output 1 = Output
idbeos	Int	Flag for EOS data output at bad convergence (0) 0 = No output 1 = Output (A file “out.db” is written.)
istdiff	Int	Flag to control the steam pseudo-diffusion model for smoothing of steam partial pressure field (1) 0 = No use 1 = Use
ddst	Real	Coefficient of steam pseudo-diffusion (0.1)
fhtint	Real	Fraction of the heat input from the melt that is directly deposited to gas-liquid interface for evaporation (0.02)
tlsupqcut	Real	Superheat of water at which deposition of heat from melt to bulk water is cut-off (0.5[K])
fhigkill	Real	Attenuation factor for the heat transfer coefficient between super-heated steam and gas-liquid interface for cells having heat input from melt (0.1)
fhilkill	Real	Attenuation factor for the heat transfer coefficient between sub-cooled water and gas-liquid interface for cells having heat input from melt (0.001)

fcondres	Real	Attenuation factor for the gas-liquid interface heat transfer when condensation takes place and the gas phase involves non-condensable gas, i.e. consideration on non-condensable gas accumulation near the interface (0.02)
fevapres	Real	Attenuation factor for the gas-liquid interface heat transfer when evaporation takes place and the gas phase involves non-condensable gas, i.e. consideration on non-condensable gas dilution near the interface (0.5)
dtminqvbd	Real	Lower limit for the denominator of qvbd/delt in the evaporation term, where qvbd[J] is the heat input from melt in a cell for one time step (1e-6[s]) (When time step is decreased in case of failure in conversion of Newton iteration, qvbd/delt increases and may make the situation worse. This is a measure to limit the increase of the source term and continue the calculation. Energy conservation is maintained.)
ihighil0	Int	Flag to control the heat transfer coefficient between water and gas-liquid interface (0) 0: Default; Recommended mode for premixing calculation 1: hig=hil=0 (no heat transfer) 2: Recommended mode for explosion calculation; Limited heat transfer, only to relax supercooled steam or superheated water (unstable state) or too high steam superheat ($T_g > (T_m + T_{sat})/2$)
taueqxplg	Real	Relaxation time of highly super heated steam when ihighil0=2 (1e-3[s])
irsarla0	Int	1: Set rsa=rla=0 (no heat transfer between non-condensable gas and water or steam) (0)
ici0	Int	1: Set cix=ciy=ciz=0 (no interface friction)(0)
fcfmist	Real	Attenuation factor of two-phase friction for droplet flow (1.0)
fcfbubb	Real	Attenuation factor of two-phase friction for bubbly flow (1.0)
ieqdia	Int	Control of bubble/droplet size model in two-phase flow (1) 0: Evaluation by local relative velocity and We (sensitive to velocity variation) 1: Use equilibrium size by balance of drag and gravity/buoyancy
nftran	Real	Power of interpolation function for two-phase friction in the transition regime, $\alpha = 0.3 - 0.75$; a larger value causes faster escape of bubbles from the pool (1.0–4.0)(1.0)
icimj	Int	n(> 0): Use separated (annular) flow model for columns 1–n from the center (0)

Time step section

Time step control variables are given in this section.

Variable	Type	Description
sttime	Real	Start time [s]
endtim	Real	End time [s]
deltmx	Real	Maximum time step [s]
deltmn	Real	Minimum time step [s]

Variable	Type	Description
edtim	Real	List output time step [s]
pltim	Real	Plot (binary) output time step [s]
httim	Real	History output time step [s]

Next, parameters for the time step control is given. The time step is increased or decreased according to the number of iterations necessary for conversion of the solution. The Courant limit is also checked and the time step is kept smaller than it.

Variable	Type	Description
itrinc	Int	Number of iterations; time step is increased when conversion is reached earlier than this number (5)
itrred	Int	Number of iterations; time step is decreased when conversion is not reached at this number (10)
fdtinc	Real	Increase factor of time step (1.20)
fdtred	Real	Decrease factor of time step (0.95)

Conversion check condition

The maximum iteration number and convergence criterion are given in this section. If the maximum iteration number for the pressure convergence is exceeded, the iteration is quited, the time step is reduced to 80% and the pressure convergence is re-tried. When the relative error of the pressure equation set becomes smaller than given criterion, it is considered that convergence is achieved.

Variable	Type	Description
maxitr	Int	Maximum limit iteration number (20)
epscnv	Real	Conversion criterion by the relative residual (1e-4)

History output section

Number of cells for which history output is made, nhstcell, is specified first. Then, the $x(r)$ and z direction indexes for those cells, (ihst(i),khst(i)), are given. The indexes are read by the following syntax.

```
read(iwkunt,*) (ihst(i),khst(i), i=1,nhstcell)
```

Variable	Type	Description
nhstcell	Int	Number of cells for which history output is made (max. 50)

Variable	Type	Description
ihst(i)	Int	$x(r)$ direction index of history output cells
khst(i)	Int	z direction index of history output cells

Water level output section

Number of $x(r)$ positions where water level is detected and written in the history output, nwlevel, is specified first. Then, $x(r)$ indexes for those positions are given. The indexes, iwlev(i), are read by the following syntax.

```
read(iwkunt,*) (iwlev(i), i=1,nwlevel)
```

Variable	Type	Description
nwlevel	Int	Number of $x(r)$ positions where water level is detected and written in the history output (max. 20)

Variable	Type	Description
iwlev(i)	Int	$x(r)$ indexes where water level output is made

The water level detection is made by the following two methods, and written as **leva** and **levb**, respectively.

- (a) Seek cells from the top at specified $x(r)$ position, and find a cell where $\alpha < \alpha_{lev}$ is first attained. Assume the z index of this cell is k_1 . Find the z position where $\alpha = \alpha_{lev}$, by linear interpolation between k_1 and $k_1 + 1$
- (b) Seek cells from the top at specified $x(r)$ position, and find a cell where $\alpha < \alpha_{lev}$ is first attained. Assume that there is the water surface in the cell, and find the z position of the water surface from α , the top and bottom positions of the cell.

The variable $\alpha_{lev}(\equiv 0.8)$ is the criterion to find the water surface.

System definition section

Definition of the analytical system is made in this section. The mesh number in every direction, number of non-condensable gas components and their indexes, usage of the melt model, coordinate system, boundary conditions and gravity control are given. For the boundary condition, wall, inlet with given velocity, or flow out with given pressure can be specified. Or, all the boundaries without specific definition are regarded as slip walls.

Variable	Type	Description
nx	Int	$x(r)$ direction mesh number
ny	Int	$y(\theta)$ direction mesh number (1)
nz	Int	z direction mesh number

Variable	Type	Description
ngas	Int	Number of the non-condensable gas components(max. 4)

if $ngas \geq 1$, the kinds of the gas components are given.

Variable	Type	Description
kindgs(1)	Int	The 1st gas component
kindgs(2)	Int	The 2nd gas component
...		(Repeat this ngas times.)
		Indexes for gas kinds:
		1 = air
		2 = hydrogen
		3 = helium
		4 = nitrogen
		5 = argon

Variable	Type	Description
igeom	Int	Selection of the coordinate (0) 0 = Cylindrical coordinate 1 = Cartesian coordinate
cyclic	Int	$y(\theta)$ boundary condition control (0) 0 = wall 1 = cyclic condition
nvgrav	Int	Gravity control 0 = z direction $g_z = -9.807(\text{m/s}^2)$ 1 = g_x, g_y and g_z are given in gravity components section later

Variable	Type	Description
igbcz(1)	Int	z direction boundary condition at the bottom ($k=0$) 0 = wall 1 = inlet condition 2 = flow out condition
igbcz(2)	Int	z direction boundary condition at the top ($k=nz+1$) 0 = wall 1 = inlet condition 2 = flow out condition

For the inlet boundary, constant velocity is given; for the flow out boundary, constant pressure is given.

The next section specifies walls defined inside the calculation domain. It is used to stop coolant flow in horizontal or vertical direction, useful for simulating vessel walls or structural walls. The number of the walls are first given and definition of the positions are to follow.

Note that the melt model does not know the walls defined here. Confinement of the zone where the melt can move is set later in the melt section.

Variable	Type	Description
nxwall	Int	Number of vertical internal walls ($x(r)$ direction stops) (max. 20)

Variable	Type	Description
ixwall(i)	Int	$x(r)$ index of internal wall i (cell boundary index)
kxwall(1,i)	Int	z index of the bottom of internal wall i (cell center index)
kxwall(2,i)	Int	z index of the top of internal wall i (cell center index)

Variable	Type	Description
nzwall	Int	Number of horizontal internal walls (z direction stops)(max. 20)

Variable	Type	Description
kzwall(i)	Int	z index of internal wall i (cell boundary index)
izwall(1,i)	Int	$x(r)$ index of the inner (left) end of internal wall i (cell center index)
izwall(2,i)	Int	$x(r)$ index of the outer (right) end of internal wall i (cell center index)

Mesh data section

Cell boundary positions are given for z , $x(r)$ and $y(\theta)$ coordinates. Though JASMINE only uses 2D cylindrical coordinate (r - z), θ direction cell size (of the only one grid) is needed. It defines the azimuthal slice size of the system.

Variable	Type	Description
z	Real	z direction cell boundary positions ($nz+1$ data)

Variable	Type	Description
rad	Real	$x(r)$ direction cell boundary positions ($nx+1$ data)

Variable	Type	Description
th	Real	$y(\theta)$ direction cell boundary positions ($ny+1$ data)

Gravity components section

This section is needed when $nvgrav = 1$ is specified.

Variable	Type	Description
gc	Real	Absolute value of the gravitational acceleration
gravx	Real	x (r) directional cosine
gravy	Real	y (θ) directional cosine
gravz	Real	z directional cosine

Cell variable data section

Fluid volume in cells and area of cell surfaces are initially set equal to the geometrical volume and area. (No obstacle objects) Volume fractions, pressures, temperatures and velocities in the cells are initially set uniform for the entire system, and modifications are made for specified rectangular zones later.

Variable	Type	Description
alpn0	Real	Initial value of steam volume fraction
pn0	Real	Initial value of pressure
tvn0	Real	Initial value of steam temperature
tlm0	Real	Initial value of water temperature

Variable	Type	Description
vvxr0	Real	Initial value of x (r) direction gas velocity
vvvt0	Real	Initial value of y (θ) direction gas velocity
vvz0	Real	Initial value of z direction gas velocity

Variable	Type	Description
vlxr0	Real	Initial value of x (r) direction water velocity
vlyt0	Real	Initial value of y (θ) direction water velocity
vlz0	Real	Initial value of z direction water velocity

Volume fractions and temperatures of non-condensable gases are given if $ngas \geq 1$. The following data is repeated for $ngas$ times.

Variable	Type	Description
alp0a	Real	Volume fraction of a non-condensable gas component
ta0	Real	Temperature of a non-condensable gas component

The partial pressure of a non-condensable gas component, P_a , is expressed by

$$P_a = \frac{\alpha_a}{(\alpha_s + \sum \alpha_a)} P \quad (\text{E.1})$$

where α_s is the steam volume fraction, α_a is the volume fraction of non-condensable gas component a , P is the total pressure.

Modification of the initial values for material distribution in cells can be made as follows, for arbitrarily defined rectangular zones.

Variable	Type	Description
nmatarea	Int	Number of rectangular zones for which material distribution is modified

If $nmatarea \geq 1$, the following specification is given for every rectangular zone.

Variable	Type	Description
is	Int	$x(r)$ index for the cell in one end of the diagonal of the rectangular zone (start point)
ks	Int	z index for the cell in one end of the diagonal of the rectangular zone (start point)
ie	Int	$x(r)$ index for the cell in another end of the diagonal of the rectangular zone (end point)
ke	Int	z index for the cell in another end of the diagonal of the rectangular zone (end point)

Variable	Type	Description
alpst	Real	Steam volume fraction in the zone
tv	Real	Steam temperature in the zone
tl	Real	Water temperature in the zone

Variable	Type	Description
alpgs(i)	Real	Volume fraction of non-condensable gas component i in the zone
tvgs(i)	Real	Temperature of non-condensable gas component i in the zone

These data for non-condensable gas components are given $ngas$ sets in the order of the gas index.

Boundary condition section

If $igbcz$ is not 0 in the system section, boundary conditions—inlet or flow out—are specified at the bottom and top of the analytical domain. The bottom boundary is specified first and the top boundary follows.

The method of boundary condition specification is as follows, and common for both the bottom and top.

The next variable is needed if $igbcz = 2$ (flow out condition). The size and volume of the boundary cell is calculated by this number. If $ibcgz = 1$ (inlet condition), this data is not read, and the boundary cell size is set as same as the adjacent cell inside of the system.

Variable	Type	Description
dz	Real	z direction size of the boundary cell

The following volume fractions, temperatures and velocities are necessary regardless of the value of $igbcz$.

If positive values are given for the volume fraction, pressure and temperatures, those values are set for all the cells along the boundary. If negative value(s) are given for one or more variable(s), cell dependent values are read from the next section for those variables. Velocities are always regarded cell dependent.

Variable	Type	Description
alpha	Real	Steam volume fraction
press	Real	Pressure
tempv	Real	Steam temperature
templ	Real	Water temperature

If a negative value is set for alpha, steam volume fractions for every cell along the boundary is read by the following. The reading format is the same as that for velocities.

Variable	Type	Description
alpha	Real	Steam volume fraction

It follows in the same way for pressure and temperatures.

Variable	Type	Description
press	Real	Pressure

Variable	Type	Description
tempv	Real	Steam temperature

Variable	Type	Description
templ	Real	Water temperature

Velocities are read as 2D data by the following format.

```

do 100 j = 1 , ny
  read(iwkunt,*) ( vel(i,j,k) , i = 1 , nx )
100 continue

```

If the boundary is the inlet (bottom), $k = 0$, or if it is the outlet (top), $k = nz$. The velocities read here override those read in the cell data section. In case of inlet boundary, the velocities read here become the inlet velocities.

Variable	Type	Description
vvz	Real	Gas velocity

Variable	Type	Description
vlz	Real	Water velocity

If non-condensable gas exists, i.e. $ngas \geq 1$, their volume fractions and temperatures are also needed for the boundary condition. If positive values are given for them, they are regarded uniform along the boundary. If negative values are given, it is regarded cell dependent and read from the following sections.

Variable	Type	Description
alp0a	Real	Gas volume fraction
ta0	Real	Gas temperature

This section is repeated for $ngas$ times.

Melt input section

The next part is the input data for the melt model. The first is the switching flag of the usage of the melt model.

Variable	Type	Description
imelt	Int	Flag for the usage of the melt model (1) 0 = Not use 1= Use

The following melt model related input data are necessary to be filled even though $imelt=0$ is specified. The first section is about the mesh and boundary.

Variable	Type	Description
prmpp_iedg	Int	$x(r)$ index (coolant flow cell boundary index) of the right (outer) end of the zone in which the melt components (pool and particles) move
prmj_ktop	Int	z index (coolant flow cell boundary index) of the melt jet inlet position, that is also the top end of the zone of melt components movement
prmj_nsub	Int	Number of sub-division of the z direction coolant flow cells for the finer grid for melt jet (4)

The next section specifies the melt jet inlet condition.

Variable	Type	Description
prmj_tempini	Real	Initial melt jet temperature (const.)
prmj_nini	Int	Number of the time dependent data for the velocity and diameter of the melt jet (max. mjetini=500)

Time dependent melt jet velocity and diameter data follows. They are read by the following format.

```
read(iwkunt,*) (prmj_ini(i), i=1,prmj_nini)
```

So, prmj_nini pieces of values are necessary for each of the time, velocity and diameter.

Variable	Type	Description
prmj_tini(i)	Real	Time (s) at which the melt jet inlet velocity and diameter is given

Variable	Type	Description
prmj_vini(i)	Real	Melt jet inlet velocity at times specified in prmj_tini(i)

Variable	Type	Description
prmj_dini(i)	Real	Melt jet inlet diameter at times specified in prmj_tini(i)

The melt jet inlet velocity and diameter are interpolated or extrapolated for time by the following scheme.

- For time between prmj_tini(1) and prmj_tini(prmj_nini) : linear interpolation between the pair of data just before and after the time wanted
- For time before prmj_tini(1): the value at prmj_tini(1)
- For time after prmj_tini(prmj_nini): the value at prmj_tini(prmj_nini)

A function to put melt particle groups at arbitrary positions at arbitrary times is equipped. One data set for this purpose includes position, attributes, the time to start throwing-in, the frequency and interval of throwing-in. The number of the data sets is to be given first.

Variable	Type	Description
nparin	Int	Number of the data sets for arbitrary particle group throwing-in

Then, nparin sets of data are given. One data set includes data for the following variables. Care should be taken not to give physically inconsistent particle group size, particle diameter and number of particles in the group, e.g. too densely packed group.

Variable	Type	Description
x	Real	x (r) position (coordinate) of the center of the group
z	Real	z position (coordinate) of the center of the group
vx	Real	x (r) direction velocity
vz	Real	z direction velocity
rgx	Real	1/2 size of the group in x (r) direction
rgz	Real	1/2 size of the group in z direction
dp	Real	Particle diameter
tav	Real	Average temperature of the particle (the same temperature is assumed for the particle surface)
np	Real	Number of particles in the group
tstart	Real	Time to start throwing-in the particle group
frequency	Int	Total frequency of throwing-in the particle group
tint	Real	Interval of throwing-in

Next, parameters for the constitutive equations in the melt model are given.

Variable	Type	Description
prmj_brkmdl	Int	Selection of the jet break-up length model (0=Saito et al. (local water density, in effect under the water level), 1=Saito-type2 (cross section averaged two-phase density for ambient fluid density, cut-off if it is less than 1/1000 of melt density), 2=Saito-type3 (ambient fluid density defined according to cross section averaged void fraction α_{av} : max. two-phase density in the radial profile (\sim water density) if $\alpha_{av} < 0.5$; cross section averaged two-phase density if $0.75 < \alpha_{av}$ with cut-off if it is less than 1/1000 of melt density; linear interpolation between them), 3=JAERI model (the same ambient fluid density with Saito-type3, use Taylor type or Saito type according to Bo_J , with limitation in the valid range for Saito type correlation) (3)
prmj_sacvx	Real	C_{vx} (5.0)
prmj_sacvzwt	Real	C_{vzwt} (0.5)
prmj_sacent	Real	C_{ent} (1.0)
prmj_saedia	Real	D_e 2–6mm for corium, \sim 10mm for alumina; should be given according to experimental results, or a certain range is surveyed parametrically (involving values causing maximum explosion load)
prmj_sacfrc	Real	C_{frc} (1.0)

Variable	Type	Description
prmpa_mergecrt	Real	Criterion for matching (relative difference) for merge of particle groups (0.2)
prmpa_cdamppar	Real	Damping factor for collision of two particle groups (0.5)
prmpa_cdampwal	Real	Damping factor for collision of a particle group and a wall (0.1)
prmpa_crnump	Real	Criterion for the number of particles for production of a particle group (10–5000)

prmpa_crhist	Int	Criterion for the number of steps for production of a particle group (1000)
prmpa_ccfrf	Real	Correction factor for particle-fluid friction factor based on the solid sphere correlation (1.0)
prmpa_chtc	Real	Correction factor for particle-fluid heat transfer coefficient (also used for the melt pool heat transfer) (1.0)
prmpa_nattrad	Real	Exponent of the void attenuation factor for radiation heat transfer from melt particles; smaller values (< 1) let the radiation effect persistent till higher void fractions (1.0)
prmpa_coxd	Real	Correction factor for particle oxidation model (1.0, presently not implemented)
prmpa_mh2max	Real	Hydrogen production for unit mass of melt [kg/kg] ($2.4\text{e-}3$, presently not implemented)
prmpa_fhtstl	Real	Heat transfer degradation factor for settled particle groups (~ 0.1)
prmpa_dminpar	Real	The min. limit particle size in the secondary break-up of particles in the premixing stage ($1\text{e-}3[\text{m}]$)
prmpa_ivxran	Int	Flag for the random factor for $x(r)$ velocity of particle groups at release (0=no random factor, 1=enable random factor) (1)
prmpa_ibrkcri	Int	Selection of temperature criterion for secondary break-up of particles (-1) 0: $T_{av} > T_{m.p.}$ (average temp. higher than melting point) 1: $T_{sf} > T_{sol.}$ (surface temp. higher than solidus point) 2: $T_{sf} > T_{sol.}$ or $T_{av} > T_{liq.}$ -1 : Suppress secondary break-up
prmpa_inotdrp	Int	Flag for suppression of the particle surface temperature drop model (1=suppress) (0)
prmpa_imrgtsf	Int	Flag for usage of surface temperature criterion for particle-pool merging; by enabling this, merge becomes less frequent and the surface area persists; if disabled, particle average temperature criterion is used (1=use) (0)
prmpa_ihtpack	Int	Flag for the collapse and heat transfer degradation for settled particle groups (see prmpa_fhtstl). (1=use) (1)
prmpa_inomerge	Int	Flag for disabling merge between particle groups (e.g. when tracking of a group is wanted) (1=disable) (0)

Variable	Type	Description
prmp_inoht	Int	Flag for disabling melt pool heat transfer model (1=disable) (0)
prmp_inotdrp	Int	Flag for disabling melt pool surface temperature drop model (1=disable) (0)
prmp_inopamb	Int	Flag for disabling the ambient (fluid) pressure term in the melt pool momentum equation (for stability) (1=disable) (1)

The followings are input data required for “explosion mode” calculations. When “explosion mode” is specified in a restart run, melt jet and melt pool components are converted into particle groups, and explosion related constitutive models are enabled.

Variable	Type	Description
prmf_ixpl	Int	Flag for “explosion mode” 0 : OFF 1 : ON 2 : ON (conversion of jet/pool into particle groups is suppressed) (restart after an explosion mode run does not have jet/pool components and this does not have effect)

The following data are read only when prmf_ixpl> 0 is specified.

Variable	Type	Description
prmf_ifrgmdl	Int	Selection of fragmentation model (0) 0 : Caracharios(1983) model 1 : Yuen(1994) model
prmf_cfrg	Real	Tuning factor for fragmentation model (0.35)
prmf_ifrgcri	Int	Flag for temperature criterion for fragmentation (0) 0: $T_{av} > T_{m.p.}$ (average temp. higher than melting point) 1: $T_{sf} > T_{sol.}$ (surface temp. higher than solidus point) 2: $T_{sf} > T_{sol.}$ or $T_{av} > T_{liq.}$
pmrf_ifrgatt	Int	Flag for the void attenuation factor for fragmentation (2) 0: Two-phase fluid-particle interaction scheme 1: Interaction with water, attenuation by $1 - \alpha$ 2: Interaction with water, cut-off in the range $\alpha = 0.3 - 0.75$
prmf_ikevmdl	Int	Flag for the model for partition of heat released from fine fragments to evaporation/bulk heating (0) 0 : Given by constant (=prmf_kevfrg) 1 : Original model (not tested)
prmf_ckeavfrg	Real	Fraction of heat from fine fragments assigned for evaporation (0.7) (used if prmf_ikevmdl=0)
prmf_cvicfrg	Real	Constant for the original model (not tested) (used if prmf_ikevmdl=1)
prmf_cqfrg	Real	Factor on the heat release rate of fine fragments (1.0)
prmf_ttriglife	Real	Period during which particle fragmentation is enabled after the local triggering (passage of pressure front) (1e-3[s])
prmf_ptrig	Real	Threshold for local triggering (cell pressure) (5e5–10e6[Pa], should be set higher than initial pressure and lower enough than pressure pulses by explosion)
prmf_nmtrig	Int	Number of possible triggering for a particle group (fragmentation is enabled for a given period after triggering, and this sequence is repeated for the frequency given here) (< 5) (1)
prmf_dfrg	Real	Size of fine fragments (50e-6[m])
prmf_dmminfrg	Real	The min. size of particles that can undergo fine fragmentation (too small particles are not fragmented further) (if 0 is specified, the same as fragment size is set) (0)

The recommended values for explosion model parameters given above are found as a result of test calculations. For users who try this tuning by themselves, some generic features of the parameters summarized below would give a perspective.

- `prmf_cfrg` : The peak of the pressure pulse changes.
- `prmf_ttriglife` : The width of the pressure pulse changes.
- `prmf_ckeefrg` : Smaller values for this parameter make less part of heat released from fine fragments goes to the evaporation, and pressurization. Thus, smaller pressure pulses and mechanical energy outputs arise for production of unit mass of fine fragments.

To fit the pressure pulse intensity and width (or mechanical energy output), tune `prmf_cfrg` and `prmf_ttriglife` to get better fit. When good agreement is obtained for the pressure pulse while the comparison of the fine debris mass (e.g. mass of debris finer than $\sim 0.1\text{mm}$ in experiments) and the calculated fragment mass is not good, tuning of `prmf_ckeefrg` should be tried. To keep the same size of the pressure pulse and to get more fragment mass, a larger value for `prmf_cfrg` and a smaller value for `prmf_ckeefrg` should be tried.

E.2 Running the Code

E.2.1 Normal Run

Instructions for arrangement of the source tree and compilation are given in electronic texts included in the distributed source package. Execution of JASMINE on a Unix-like environment is as follows.

```
jasmine.{PROP} -i input_file -o output_file -p plot_file -h hist_file \
                [-r restart_info_file]
```

We recommend to name the load module (executable file) “`jasmine.{PROP}`” where `{PROP}` is the name of the melt physical property package. This is a counter measure of the inflexible handling of the physical property packages, i.e. we need to make separate load modules for different melt physical property packages. The files specified in the command line are as follows.

input_file Input data file

output_file List output file for coolant two-phase flow

plot_file Plot (binary) output file for coolant two-phase flow

hist_file History output file for coolant two-phase flow

The input file can not be omitted. If the list output file is omitted (including `-o`), `./work/outlist` is used as default. If the plot output file is omitted (including `-p`), `./work/plotfile` is used as default. If the history output file is omitted (including `-h`), `./work/histfile` is used as default. To use these default output file names, it is necessary to have a work directory `./work` in advance.

The option `-r` specifies a restart calculation, as explained later.

E.2.2 Output Files

The output files include both the coolant two-phase flow data (output from ACE3D) and melt data (output from the melt package). The ACD3D output file names can be given by the command line options as described above. Their contents are as follows.

List output (output_file) Cell variables, error messages and so on, are written in plain text. The format of the list is an $x(r) \times z$ table for every variable.

Plot output (plot_file) Major variables for the two-phase flow are written in a binary (unformatted) file. Post process programs included in the JASMINE package, i.e. `readplot` and `mkrmdat`, can read out the data from the plot file for specified time or step. The data in the plot file can be cut out for visualization by the post process tools or for restart calculations.

History output (hist_file) History of the total mass and energy of every component, water level, etc. and major cell variables for cells specified in the input file are written in a column formatted text file., i.e. one line for one output step. Lines other than data are headed by `#`. The data in this file can be read and plotted by any plotting tool like *gnuplot*[47]. Note that this file has large number of columns, i.e. $\sim 22 + 2N_{watlev} + 12N_{hist}$ (N_{watlev} and N_{hist} are the number of columns for water level output and the number of cells for history output, respectively); thus, some software may fail in reading and plotting the data.

Message output Short messages to show progress of the calculation or warnings are printed on the screen if not redirected into a file.

The outputs from the melt package are written in files whose names are hard coded, as follows.

Jet list output (out.j) List of melt jet variables in a text file, written at the same timing with the two-phase flow list output.

Pool list output (out.p) List of melt pool variables in a text file, written at the same timing with the two-phase flow list output.

Particles list output (out.par) List of particle group variables in a text file, written at the same timing with the two-phase flow list output.

Fragments list output (out.frg) List of fragment group variables in a text file, written at the same timing with the two-phase flow list output.

Melt history output (out.mlt) History of general information for the melt model, i.e. total melt mass, internal energy, mass fractions of jet, pool and particles, etc. in a column formatted text file. The output timing is the same with two-phase flow history output.

Melt-two-phase flow exchange output (out.m2f) List of data for exchanges between melt and two-phase flow models (volume, force and heat) in a text file, written at the same timing with the two-phase flow list output.

Melt dump (out.mdp) Major variables for the melt model are written in a binary (unformatted) file, written at the same timing with the two-phase flow plot output. This file is processed by the post process program, `mkrmdat`, for the preparation of a restart data for the melt model.

E.2.3 Restart Run

When a calculation is failed (mainly by getting into a too small time step due to bad convergence), the calculation can be restarted at some steps before the failure, possibly with modified input parameters or field variables.

For a restart run, a restart data file should be made from the two-phase flow plot file and the melt dump file generated by the previous calculation. The restart data file is read as an initial condition for the restart run. Also, arbitrary change of cell variables can be made at the start of the restart run. The procedure is described below.

1. **Make a new directory for the restart calculation data.**

It is because a restart run writes a new set of output files. If a restart run is executed in the same directory with the original calculation, some files (melt outputs) are overwritten and lost.

2. **Copy the original input file into the new directory.**

This becomes the input file for the restart run, and it may be modified as long as the consistency of the physical conditions are kept. Assume the file name is `in`.

3. **Make a restart data file.**

A post process program, `mkrsdat`, cuts data out of the two-phase flow plot and the melt dump files, and produces a “restart data file”. Assume that we execute the restart run in the current directory, the previous calculation data are in another directory named `../a1`, and that the names of the two-phase flow plot file and melt dump file are `p1` and `out.mdp`, respectively. First, do the following to see the steps of the data included in the plot and melt dump files.

```
mkrsdat ../a1/p1 ../a1/out.mdp
```

Assume that we want the data at the step 1234. Then, `-s` option specifies that, as follows.

```
mkrsdat ../a1/p1 ../a1/out.mdp -s 1234
```

The restart data file is a binary file and the name is set `rs.dat` by default. The detailed usage of `mkrsdat` command is printed by calling it without options or arguments.

4. **Make a restart instruction file.**

A restart instruction file is a text file where instructions needed in performing a restart run is written. The format is as follows.

```
//
// restart instruction file: example
//
//                                     Description
//                                     -----
//                                     // makes comments that is ignored
// restart data file
//   rs.dat                           restart data file name
// modifications
// ndatmod
//   8                                number of data modification items
// name   i k value                   instructions for data modifications
```

```

pn      3 3 2.4e5    variable name, cell index(i,k), value
alpstn  3 3 0.100
alpgsn1 3 3 0.100    volume fraction of a non-condensable gas
//                                alpgsn#, # is one digit int for gas no.
tvn      3 3 410.
tln      3 3 s        "s" means the saturation temperature
tvgsn1   3 3 410.    non-condensable gas 1 temperature
//
//                                the following data do not have cell no.
time     0.          time given at the start of restart run
step     1           step no. at the start of restart run

```

In case that we need to set the temperature in a cell at the saturation point, and, at the same time, we need to modify the pressure, volume fraction for steam or non-condensable gas in the cell, the modification of pressure or volume fraction should be made before the specification of saturation temperature. It is because the calculation of the saturation temperature needs those information. Assume the name of the file is `rsi`.

5. Execute the restart run.

Run JASMINE code by specifying the restart instruction file with `-r` option.

```
jasmine.{PROP} -i in -o output_file -p plot_file -h hist_file -r rsi
```

This restart function is helpful for effective debugging. When a calculation is failed, we can try a restart calculation from a few steps before the failure and with a smaller data output time step to find out the reason of the failure.

E.2.4 Restart Calculation in “explosion mode”

The basic procedure is the same as described in the previous section, E.2.3. Specifying `prmf_ixpl=1` in the input file makes the restart run an explosion mode calculation, that differs from the normal one in the following points.

- The melt jet and pool data are converted into particle groups. If we want another explosion mode calculation after an explosion model calculation, this conversion is not in effect because there is no melt jet or pool data. (`prmf_ixpl=2` explicitly specifies suppression of this conversion)
- Constitutive models for the explosion mode are used in the melt model calculation. Those are as follows.
 - No heat transfer, break-up or merge for the particle groups are considered.
 - Fine fragments are generated by hydrodynamic interaction of the melt particles and coolant, and the quick heat release from the fine fragments dominates the evaporation and heat-up of the surrounding coolant.

Additionally, the following modification in the input file and the cell data is necessary.

- Modify the followings in the input file: specify `ihighl0=2` (suppress evaporation or condensation due to the thermal equilibration between the gas and water); give a small enough value for `dtminqvbd`, e.g. $1e-8s \ll \text{normal } dt$.

- Set the external triggering in the restart instruction file: set pressure and non-condensable gas volume fraction for a certain cell where a high pressure bubble is assumed, with pV value matched with an experimental condition or in an adequate range. Note that we should also assume a high temperature for the gas not to cause troubles due to temperature drop of the expanding gas. If the triggering by pressurized non-condensable gas is planned, the non-condensable gas should be included from the premixing calculation.
- Set time steps adequate for the explosion mode: $\sim 2\mu s$ for the maximum time step for the calculation, $\sim 0.1ms$ for the output time step.

References

- [1] A.W. Cronenberg and R. Benz. Vapor explosion phenomena with respect to nuclear reactor safety assessment. NUREG/CR-0245, TREE-1242, Idaho National Engineering Laboratories, 1978.
- [2] M.L. Corradini, B.J. Kim, and M.D. Oh. Vapor explosion in light water reactors: a review of theory and modeling. *Progress in Nuclear Energy*, 22(1), pp.1–117, 1988.
- [3] R. Meignen, D. Magallon, K-H. Bang, G. Berthoud, S. Basu, M. Bürger, M. Buck, M.L. Corradini, H. Jacobs, O. Melikhov, M. Naitoh, K. Moriyama, R. Sairanen, J-H. Song, N. Suh, and T.G. Thefanous. Comparative review of FCI computer models used in the OECD-SEREBE program. *Proceedings of International Congress on Advances in Nuclear Power Plants (ICAPP'05), Seoul, Korea*, 2005. (CD-ROM:Paper 5087).
- [4] N. Yamano, Y. Maruyama, T. Kudo, A. Hidaka, and J. Sugimoto. Phenomenological studies on melt-coolant interactions in the ALPHA program. *Nuclear Engineering and Design*, 155, pp.369–389, 1995.
- [5] K. Moriyama, N. Yamano, Y. Maruyama, T. Kudo, and J. Sugimoto. Study of premixing phase of steam explosion with jasmine code in ALPHA program. *Proceedings of 4th International Conference on Nuclear Engineering, New Orleans*, volume 1B, pp.903–915, 1996.
- [6] A. Annunziato, C. Addabbo, A. Yerkess, R. Silverii, W. Brewka, and G. Leva. FARO test L-14 on fuel-coolant interaction and quenching– comparison report, volume I: Analysis of the results – OECD/CSNI international standard problem 39. NEA/CSNI/R(97)31/Part I, OECD/NEA/CSNI, 1998.
- [7] Y. Yang, K. Moriyama, Y. Maruyama, H-S. Park, and J. Sugimoto. Propagation calculation for steam explosion with JASMINE-pro code. *Proceedings of the 7th International Conference on Nuclear Engineering, Tokyo (ICONE7)*, 1999. ICONE-7235.
- [8] Y. Yang, S. Nilsuwankosit, K. Moriyama, Y. Maruyama, N. Nakamura, and K. Hashimoto. JASMINE-pro: A computer code for the analysis of the propagation process in a steam explosion–user’s manual. JAERI-Data/Code 2000-035, Japan Atomic Energy Research Institute, 2000.
- [9] D. Magallon, K-H. Bang, S. Basu, G. Berthoud, M. Bürger, M.L. Corradini, H. Jacobs, R. Meignen, O. Melikhov, K. Moriyama, M. Naitoh, J-H. Song, N. Suh, and T.G. Thefanous. Status of international programme SERENA on fuel-coolant interaction. *Proceedings of International Congress on Advances in Nuclear Power Plants (ICAPP'05), Seoul, Korea*, 2005. (CD-ROM:Paper 5382).
- [10] D. Magallon, K-H. Bang, S. Basu, G. Berthoud, M. Bürger, M.L. Corradini, H. Jacobs, R. Meignen, O. Melikhov, K. Moriyama, M. Naitoh, J-H. Song, N. Suh, and T.G. Thefanous.

- Results of phase-1 of OECD programme SERENA on fuel-coolant interaction. *The 1st European Review Meeting on Severe Accident Research (ERMSAR-2005)*, Aix-en-Provence, France, 2005.
- [11] A. Ohnuki, H. Kamo, and H. Akimoto. Development of multidimensional two-fluid model code ACE-3D for evaluation of constitutive equations. JAERI-Data/Code 96-033, Japan Atomic Energy Research Institute, 1996. [in Japanese].
 - [12] K. Moriyama, H. Nakamura, and Y. Maruyama. Analytical tool development for coarse break-up of a molten jet in a deep water pool. *Nuclear Engineering and Design*, 236, pp.2010–2025, 2006.
 - [13] K. Moriyama, Y. Maruyama, T. Usami, and H. Nakamura. Coarse break-up of a stream of oxide and steel melt in a water pool. JAERI-Research 2005-017, Japan Atomic Energy Research Institute, 2005.
 - [14] G.I. Taylor. The dispersion of jets of metals of low melting point in water. G.K. Batchelor, editor, *The scientific papers of Sir Geoffrey Ingram Taylor, vol.3 Aerodynamics and the mechanics of projectiles and explosions*, pp.304–305. Cambridge University Press, Cambridge, 1963.
 - [15] M. Saito, K. Sato, and S. Imahori. Experimental study on penetration behaviors of water jet into freon-11 and liquid nitrogen. *ANS Proc. National Heat Transfer Conference, Houston, U.S.*, volume 3, pp.173–183, 1988.
 - [16] H. Schlichting. *Boundary layer theory*, chapter XXI. McGraw Hill, 7 edition, 1979.
 - [17] JSME, editor. *JSME data book: Heat Transfer (4th edition)*, pp.68–70. JSME, 1994. [in Japanese].
 - [18] S.S. Kutateladze. Heat transfer in condensation and boiling. ACE-tr-3770, US AEC, 1952.
 - [19] N. Zuber et al. *Int. Development in Heat Transfer, Part II*, p.230. ASME, 1961. paper 27.
 - [20] P.J. Berenson. Film boiling heat transfer from a horizontal surface. *ASME Journal of Heat Transfer*, 83, pp.351–358, 1961.
 - [21] L.A. Bromley, N.R. Leroy, and J.A. Robbers. Heat transfer in forced convection film boiling. *Industrial and Engineering Chemistry*, 45, pp.2639–2646, 1953.
 - [22] C. Liu and T.G. Theofanous. Film boiling on spheres in single- and two-phase flows. part I: Experimental studies. *ANS Proceedings of National Heat Transfer Conference, Portland, U.S.*, pp.34–47, 1995.
 - [23] R.B. Bird, W.E. Stewart, and E.N. Lightfoot. *Transport Phenomena*, chapter 6.3. John Wiley & Sons, 1960.
 - [24] W.E. Ranz and W.R. Marshall. Evaporation from drops: part I. *Chemical Engineering Progress*, 48, pp.141–146, 1952.
 - [25] Sa. Kondo, K. Konishi, K. Morita, N. Shirakawa, A. Furutani, and D. J. Brear. Experimental study on simulated molten jet-coolant interactions. *Nuclear Engineering and Design*, 155, pp.73–84, 1995.
 - [26] M. Pilch and C. A. Erdman. Use of breakup time data and velocity history data to predict the maximum size of stable fragments for acceleration-induced breakup of a liquid drop. *International Journal of Multiphase Flow*, 13(6), pp.741–757, 1987.

- [27] C. Caracharios, M. Burger, and H. Unger. A transient two-phase model to describe thermal detonations based on hydrodynamic fragmentation. *Proc. Int. Meeting on LWR Severe Accident Evaluation, Cambridge*, 1983.
- [28] W.W. Yuen, X. Chen, and T.G. Theofanous. On the fundamental microinteractions that support the propagation of steam explosions. *Nuclear Engineering and Design*, 146, pp.133–146, 1994.
- [29] I. Huhtiniemi, H. Hohmann, R. Faraoni, M. Field, R. Gambaretti, and K. Klein. KROTOS 38 to 44: data report. TN I.96.37, European Commission Joint Research Centre, Italy, 1996.
- [30] D.R. Liles and J.H. Mahaffy. TRAC-PF1/MOD1: an advanced best-estimate computer program for pressurized water reactor thermal-hydraulic analysis. NUREG/CR-3858, LA-10157-MS, U. S. Nuclear Regulatory Commission, 1994.
- [31] T. Yabe and T. Aoki. A universal solver for hyperbolic equations by cubic-polynomial interpolation, I. one-dimensional solver. *Computer Physics Communications*, 66, pp.219–232, 1991.
- [32] S.V. Patankar. *Numerical heat transfer and fluid flow*, chapter 6. Hemisphere publishing corporation, 1980.
- [33] D.F. Fletcher. An improved mathematical model of melt/water detonations – i. model formulation and example results. *International Journal of Heat and Mass Transfer*, 34(10), pp.2435–2448, 1991.
- [34] R. Barrett, M. Berry, T.F. Chan, et al. *Templates for the solution of linear systems: Building blocks for iterative methods*. Society for Industrial and Applied Mechanics (SIAM), 1993.
- [35] D. Magallon, I. Huhtiniemi, and H. Hohmann. Lessons learnt from FARO/TERMOS corium melt quenching experiments. *Nuclear Engineering and Design*, 189, pp.223–238, 1999.
- [36] D. Magallon and I. Huhtiniemi. Corium melt quenching tests at low pressure and subcooled water in FARO. *Nuclear Engineering and Design*, 204, pp.369–376, 2001.
- [37] I. Huhtiniemi, D. Magallon, and H. Hohmann. Results of recent KROTOS FCI tests: alumina versus corium melts. *Nuclear Engineering and Design*, 189, pp.379–389, 1999.
- [38] D. Magallon and I. Huhtiniemi. Energetic event in fuel-coolant interaction test FARO L-33. *Proc. 9th International Conference on Nuclear Engineering (ICONE-9), Nice Acropolis, France*, 2001. (Paper no.285).
- [39] K. Moriyama, H. Nakamura, and Y. Maruyama. Simulation of alumina and corium steam explosion experiments with JASMINE v.3. *Proceedings of the 6th International Conference on Nuclear Reactor Thermal Hydraulics, Operations and Safety (NUTHOS-6), Nara, Japan*, 2004. (CD-ROM: Paper ID.264).
- [40] R. Silverii and D. Magallon. FARO LWR programme: test L-33 data report. Technical Note No.I.00.124, EU JRC Ispra, 2000.
- [41] A. Annunziato, C. Addabbo, and D. Magallon. FARO test L-33 quick look report. TN I.00.111, European Commission Joint Research Centre, Italy, 2000.

- [42] K. Moriyama, S. Takagi, K. Muramatsu, H. Nakamura, and Y. Maruyama. Evaluation of containment failure probability by ex-vessel steam explosion in Japanese LWR plants. *Journal of Nuclear Science and Technology*, 43(7), pp.774–784, 2006.
- [43] K. Moriyama and H. Nakamura. A strategy for the application of steam explosion codes to reactor analysis. *Proc. Technical Meeting on Severe Accident and Accident Management, Tokyo, Japan*, 2006. (CD-ROM).
- [44] D.H. Cho, D.R. Armstrong, and W.H. Gunther. Experiments on interactions between zirconium-containing melt and water (ZREX): hydrogen generation and chemical augmentation of energetics. *Proc. OECD/CSNI specialists Meeting on Fuel-Coolant Interactions, Tokai-mura, Japan (JAERI-Conf 97-011, NEA/CSNI/R(97)26)(Part II)*, pp.595–607, 1997.
- [45] The Japan Society of Mechanical Engineers, editor. *JSME Steam Tables*. The Japan Society of Mechanical Engineers, 1981.
- [46] K. Kobayashi, K. Namatame, M. Akimoto, M. Okazaki, S. Sasaki, K. Soda, and K. Sanokawa. Digital computer subroutine STEAM for JSME steam table. JAERI-M 6967, Japan Atomic Energy Research Institute, 1977.
- [47] <http://www.gnuplot.info>. Gnuplot is a portable open source plotting software.

国際単位系（SI）

表 1. SI 基本単位

基本量	SI 基本単位	
	名称	記号
長さ	メートル	m
質量	キログラム	kg
時間	秒	s
電流	アンペア	A
熱力学温度	ケルビン	K
物質の量	モル	mol
光の度	カンデラ	cd

表 2. 基本単位を用いて表されるSI組立単位の例

組立量	SI 基本単位	
	名称	記号
面積	平方メートル	m ²
体積	立方メートル	m ³
速度	メートル毎秒	m/s
加速度	メートル毎秒毎秒	m/s ²
波数	毎メートル	m ⁻¹
密度（質量密度）	キログラム毎立方メートル	kg/m ³
質量体積（比体積）	立法メートル毎キログラム	m ³ /kg
電流密度	アンペア毎平方メートル	A/m ²
磁界の強さ	アンペア毎メートル	A/m
（物質量の）濃度	モル毎立方メートル	mol/m ³
輝度	カンデラ毎平方メートル	cd/m ²
屈折率	（数の）1	1

表 5. SI 接頭語

乗数	接頭語	記号	乗数	接頭語	記号
10 ²⁴	ヨタ	Y	10 ⁻¹	デシ	d
10 ²¹	ゼタ	Z	10 ⁻²	センチ	c
10 ¹⁸	エクサ	E	10 ⁻³	ミリ	m
10 ¹⁵	ペタ	P	10 ⁻⁶	マイクロ	μ
10 ¹²	テラ	T	10 ⁻⁹	ナノ	n
10 ⁹	ギガ	G	10 ⁻¹²	ピコ	p
10 ⁶	メガ	M	10 ⁻¹⁵	フェムト	f
10 ³	キロ	k	10 ⁻¹⁸	アト	a
10 ²	ヘクト	h	10 ⁻²¹	ゼプト	z
10 ¹	デカ	da	10 ⁻²⁴	ヨクト	y

表 3. 固有の名称とその独自の記号で表されるSI組立単位

組立量	SI 組立単位			
	名称	記号	他のSI単位による表し方	SI基本単位による表し方
平面角	ラジアン ^(a)	rad		m・m ⁻¹ =1 ^(b)
立体角	ステラジアン ^(a)	sr ^(c)		m ² ・m ⁻² =1 ^(b)
周波数	ヘルツ	Hz		s ⁻¹
力	ニュートン	N		m・kg・s ⁻²
圧力，応力	パスカル	Pa	N/m ²	m ⁻¹ ・kg・s ⁻²
エネルギー，仕事，熱量	ジュール	J	N・m	m ² ・kg・s ⁻²
工率，放射束	ワット	W	J/s	m ² ・kg・s ⁻³
電荷，電気量	クーロン	C		s・A
電位差（電圧），起電力	ボルト	V	W/A	m ² ・kg・s ⁻³ ・A ⁻¹
静電容量	ファラド	F	C/V	m ⁻² ・kg ⁻¹ ・s ⁴ ・A ²
電気抵抗	オーム	Ω	V/A	m ² ・kg・s ⁻³ ・A ⁻²
コンダクタンス	ジーメン	S	A/V	m ⁻² ・kg ⁻¹ ・s ³ ・A ²
磁束	ウェーバ	Wb	V・s	m ² ・kg・s ⁻² ・A ⁻¹
磁束密度	テスラ	T	Wb/m ²	kg・s ⁻² ・A ⁻¹
インダクタンス	ヘンリー	H	Wb/A	m ² ・kg・s ⁻² ・A ⁻²
セルシウス温度	セルシウス度 ^(d)	℃		K
光学的長さ	ルーメン	lm	cd・sr ^(c)	m ² ・m ⁻² ・cd=cd
照射（放射能）	ルクス	lx	lm/m ²	m ² ・m ⁻⁴ ・cd=m ⁻² ・cd
（放射性核種の）放射能	ベクレル	Bq		s ⁻¹
吸収線量，質量エネルギー分与，カーマ線量当量，周辺線量当量，方向性線量当量，個人線量当量，組織線量当量	グレイ	Gy	J/kg	m ² ・s ⁻²
	シーベルト	Sv	J/kg	m ² ・s ⁻²

- (a) ラジアン及びステラジアンの使用は、同じ次元であっても異なった性質をもった量を区別するときの組立単位の表し方として利点がある。組立単位を形作るときいくつかの用例は表 4 に示されている。
- (b) 実際には、使用する時には記号 rad 及び sr が用いられるが、習慣として組立単位としての記号“1”は明示されない。
- (c) 測光学では、ステラジアンの名称と記号 sr を単位の表し方の中にそのまま維持している。
- (d) この単位は、例としてミリセルシウス度 m℃ のように SI 接頭語を伴って用いても良い。

表 4. 単位の中に固有の名称とその独自の記号を含むSI組立単位の例

組立量	SI 組立単位		
	名称	記号	SI 基本単位による表し方
粘着力のモーメント	パスカル秒	Pa・s	m ⁻¹ ・kg・s ⁻¹
表面張力	ニュートンメートル	N・m	m ² ・kg・s ⁻²
角速度	ニュートン毎メートル	N/m	kg・s ⁻²
角加速度	ラジアン毎秒	rad/s	m・m ⁻¹ ・s ⁻¹ =s ⁻¹
流密度，放射照度	ラジアン毎平方秒	rad/s ²	m・m ⁻¹ ・s ⁻² =s ⁻²
熱容量，エン트로ピー	ワット毎平方メートル	W/m ²	kg・s ⁻³
質量熱容量（比熱容量），質量エン트로ピー	ジュール毎平方メートル	J/K	m ² ・kg・s ⁻² ・K ⁻¹
質量エネルギー（比エネルギー）	ジュール毎キログラム	J/(kg・K)	m ² ・s ⁻² ・K ⁻¹
熱伝導率	ジュール毎キログラム	J/kg	m ² ・s ⁻² ・K ⁻¹
体積エネルギー	ワット毎メートル毎ケルビン	W/(m・K)	m・kg・s ⁻³ ・K ⁻¹
電界の強さ	ジュール毎立方メートル	J/m ³	m ⁻¹ ・kg・s ⁻²
体積電荷	ボルト毎メートル	V/m	m・kg・s ⁻³ ・A ⁻¹
電気変位	クーロン毎立方メートル	C/m ³	m ⁻³ ・s・A
誘電率	クーロン毎平方メートル	C/m ²	m ⁻² ・s・A
透磁率	ファラド毎メートル	F/m	m ⁻³ ・kg ⁻¹ ・s ⁴ ・A ²
モルエネルギー	ヘンリー毎メートル	H/m	m・kg・s ⁻² ・A ⁻²
モルエン트로ピー	ジュール毎モル	J/mol	m ² ・kg・s ⁻² ・mol ⁻¹
モル熱容量	ジュール毎モル毎ケルビン	J/(mol・K)	m ² ・kg・s ⁻² ・K ⁻¹ ・mol ⁻¹
照射線量（X線及びγ線）	クーロン毎キログラム	C/kg	kg ⁻¹ ・s・A
吸収線量率	グレイ毎秒	Gy/s	m ² ・s ⁻³
放射強度	ワット毎ステラジアン	W/sr	m ⁴ ・m ⁻² ・kg・s ⁻³ =m ² ・kg・s ⁻³
放射輝度	ワット毎平方メートル毎ステラジアン	W/(m ² ・sr)	m ² ・m ⁻² ・kg・s ⁻³ =kg・s ⁻³

表 6. 国際単位系と併用されるが国際単位系に属さない単位

名称	記号	SI 単位による値
分	min	1 min=60 s
時	h	1 h =60 min=3600 s
日	d	1 d=24 h=86400 s
度	°	1°=(π/180) rad
分	′	1′=(1/60)°=(π/10800) rad
秒	″	1″=(1/60)′=(π/648000) rad
リットル	l, L	1 l=1 dm ³ =10 ⁻³ m ³
トン	t	1 t=10 ³ kg
ネーパ	Np	1 Np=1
ベル	B	1 B=(1/2) ln10 (Np)

表 7. 国際単位系と併用されこれに属さない単位で SI 単位で表される数値が実験的に得られるもの

名称	記号	SI 単位であらわされる数値
電子ボルト	eV	1 eV=1.60217733 (49) ×10 ⁻¹⁹ J
統一原子質量単位	u	1 u=1.6605402 (10) ×10 ⁻²⁷ kg
天文単位	ua	1 ua=1.49597870691 (30) ×10 ¹¹ m

表 8. 国際単位系に属さないが国際単位系と併用されるその他の単位

名称	記号	SI 単位であらわされる数値
海里		1 海里=1852 m
ノット		1 ノット=1 海里毎時=(1852/3600) m/s
アール	a	1 a=1 dam ² =10 ² m ²
ヘクタール	ha	1 ha=1 hm ² =10 ⁴ m ²
バール	bar	1 bar=0.1 MPa=100 kPa=1000 hPa=10 ⁵ Pa
オングストローム	Å	1 Å=0.1 nm=10 ⁻¹⁰ m
バール	b	1 b=100 fm ² =10 ⁻²⁸ m ²

表 9. 固有の名称を含むCGS組立単位

名称	記号	SI 単位であらわされる数値
エルグ	erg	1 erg=10 ⁻⁷ J
ダイン	dyn	1 dyn=10 ⁻⁵ N
ポアズ	P	1 P=1 dyn・s/cm ² =0.1 Pa・s
ストークス	St	1 St =1 cm ² /s=10 ⁻⁴ m ² /s
ガウス	G	1 G ≐10 ⁻⁴ T
エルステッド	Oe	1 Oe ≐ (1000/4π) A/m
マクスウェル	Mx	1 Mx ≐10 ⁻⁸ Wb
スチルブ	sb	1 sb =1 cd/cm ² =10 ⁴ cd/m ²
ホト	ph	1 ph=10 ⁴ lx
ガリ	Gal	1 Gal =1 cm/s ² =10 ⁻² m/s ²

表 10. 国際単位に属さないその他の単位の例

名称	記号	SI 単位であらわされる数値
キュリー	Ci	1 Ci=3.7×10 ¹⁰ Bq
レントゲン	R	1 R = 2.58×10 ⁻⁴ C/kg
ラド	rad	1 rad=1 cGy=10 ⁻² Gy
レム	rem	1 rem=1 cSv=10 ⁻² Sv
X線単位		1 X unit=1.002×10 ⁻⁴ nm
ガンマ	γ	1 γ=1 nT=10 ⁻⁹ T
ジャンスキー	Jy	1 Jy=10 ⁻²⁶ W・m ⁻² ・Hz ⁻¹
フェルミ	fm	1 fermi=1 fm=10 ⁻¹⁵ m
メートル系カラット		1 metric carat = 200 mg = 2×10 ⁻⁴ kg
トル	Torr	1 Torr = (101 325/760) Pa
標準大気圧	atm	1 atm = 101 325 Pa
カロリ	cal	
マイクロン	μ	1 μ =1 μm=10 ⁻⁶ m

